半導体超格子の超高速トンネル分光

（課題番号　６２４６００２２）

昭和６３年度科学研究費補助金（一般Ｂ）
研究成果報告書

平成元年３月

研究代表者　　舛本泰章

（筑波大学物理学系）

昭和６３年度科学研究費補助金（一般研究Ｂ）

半導体超格子の超高速レーザー分光

（研究課題番号 ６２４６００２２）

研究組織

研究代表者　　舛本　泰章　（筑波大学物理学系 助教授）

研究経費

昭和６２年度	７，４００千円
昭和６３年度	５００千円
計	７，９００千円

<はじめに>

半導体ヘテロ界面を通しての電子・正孔系のトンネル過程の実時間領域での様相を明らかにする事を目的として、以下の３つの研究を推進してきた。

<垂直電場引加下でのGaAs-$Al_{0.29}Ga_{0.71}As$の非線型発光分光>　垂直電場引加下で、GaAs-$Al_{0.29}Ga_{0.71}As$の励起子発光、および、光電流の光非線型性を励起レーザー光を二つに分け、別々の周波数でON-OFF変調をかけ、和周波成分を選択的に検出する事により研究した。この研究により、垂直電場引加下で競合する二つの過程 ― 励起子生成と電子のトンネル過程 ― の競合の様子が初めて明らかになった。

<混晶量子井戸$Al_xGa_{1-x}As$-AlAsの光学的研究>　混晶量子井戸$Al_xGa_{1-x}As$の系は、ｘを変化させる事により、$Al_xGa_{1-x}As$井戸中のΓ点とAlAsバリア中のＸ点を交差させる事ができる。この交差に伴い、井戸中のΓ点電子がバリア中のＸ点へ、ヘテロ界面を通してトンネル過程がおこる事が期待できる。このΓ－Ｘ交差の光スペクトルへの反映を、研究する事をねらってルミネッセンスおよび、吸収飽和分光の研究を行った。この研究により、井戸厚が１００Å程度のときｘ＝０．２程度でΓ－Ｘ交差がおき、ルミネッセンスに顕著な変化が観測された。

<$Al_{0.34}Ga_{0.66}As$-AlAsの超高速ポンプ・プローブ法により層間Γ－Ｘ散乱の研究>　約２００fsの時間分解能をもつポンプ・プローブ分光計を作成し、$Al_{0.34}Ga_{0.66}As$-AlAsの最低エネルギー励起子の吸収飽和の時間特性から、層間Γ－Ｘ谷間散乱のダイナミクスを初めて研究した。吸収飽和の１．２ps程度での速い回復の様子から、層間Γ－Ｘ散乱が、１．２ps程度で行っていると結論した。この時間は井戸中のΓ電子のバリア層へのわずかなしみ出しに起因すると推論した。

LIST OF PUBLICATIONS

1) Y.Masumoto, H.Okamoto and S.Tarucha:
"Tunneling Dynamics of Photo-Generated Carriers in Semiconductor Superlattices"
Phys. Rev. B 33 5961 (1986).

2)* Y.Masumoto and M.Matsuura:
"Two-Dimensional Excitons in Semiconductor Superlattices"
Solid State Physics (Kotai Butsuri) 21 493 (1986).

3) F.Minami, K.Hirata, K.Era, T.Yao and Y.Masumoto:
"Localized Indirect Excitons in a Short-Period GaAs-AlAs Superlattice"
Phys. Rev. B 36 2875 (1987).

4)* Y.Masumoto:
"Ultrafast Spectroscopy of Semiconductor Quantum Wells"
Solid State Physics (Kotai Butsuri) Special Issue: Optical Properties of Solids and Electron-Lattice Interaction, p.137 (1987)(in Japanese).

5)* Y.Masumoto:
"Relaxation and Tunneling Dynamics of Photogenerated Carriers in Semiconductor Superlattices"
Rev. Laser Engineering 15 941 (1987) (in Japanese).

6) Y.Masumoto and F.Sasaki:
"Dynamical Tunneling Spectroscopy in Photo-Excited Semiconductor Superlattices"
J. Lumines. 38 285 (1987).

7) Y.Masumoto and F.Sasaki:
"Tunneling Spectroscopy in Photo-Excited Semiconductor Superlattices"
J. Lumines. 40 709 (1987).

8) Y.Masumoto, M.Yamazaki and H.Sugawara:
"Optical Nonlinearities of Excitons in CuCl Microcrystals"
Appl. Phys. Lett. 53 1527 (1988).

9) Y.Masumoto and T.Tsuchiya:
"Optical Change of $Al_xGa_{1-x}As$-AlAs Ternary Alloy Multi-Quantum-Well Structures around Two Γ-X Crossovers"
J. Phys. Soc. Jpn. 57 4403 (1988).

10) F.Sasaki and Y.Masumoto:
"Tunneling and Relaxation of Photogenerated Carriers in Semiconductor Superlattices"
Submitted to Phys. Rev. B.

11) Y.Masumoto and M.Adachi:
"Pulse Propagation in GaAs Quantum Wells"
in Ultrafast Phenomena VI ed. by T.Yajima, K.Yoshihara, C.B.Harris and S.Shionoya (Springer, 1988) p.315; Proc. 6th Int. Conf. Ultrafast Phenomena, Kyoto, 1988.

12) Y.Masumoto, T.Mishina, F.Sasaki and M.Adachi:
"Interlayer Γ-X Scattering in Staggered-Alignment $Al_{0.34}Ga_{0.66}As$-AlAs Ternary Alloy Multi-Quantum-Well Structures"
Submitted to Phys. Rev. Lett.

13) M.Adachi and Y.Masumoto:
"Pulse Distortion in GaAs Quantum Wells Studied by Light Gating Technique"
Submitted to Phys. Rev. B.

14) Y.Masumoto, T.Wamura and A.Iwaki:
"Homogeneous Width of Exciton Absorption Spectra in CuCl Microcrystals"
Submitted to Appl. Phys. Lett.

* Publications in Japanese

＜口答発表＞

佐々木史雄、舛本泰章、松浦悦之

ＧａＡｓ－ＡｌＧａＡｓ超格子中の励起子の電場解離過程

日本物理学会　（１９８７年３月）

土屋朋信、舛本泰章、松浦悦之

強光励起下での半導体超格子中の励起子

日本物理学会　（１９８７年３月）

江良皓、南不二雄、舛本泰章

銅ハライドのＵＶｐｓ分光

日本物理学会　（１９８７年３月）

舛本泰章

時間分解分光－量子井戸構造中のエキシトン

応用物理学会　（１９８７年３月）

佐々木史雄、舛本泰章

ＧａＡｓ－ＡｌＧａＡｓ超格子中の光励起担体のトンネル過程と励起子生成の競合

日本物理学会　（１９８７年９月）

舛本泰章、井手下知史、芝弘史、遠田厚

ＧａＡｓ－ＡｌＡｓ量子井戸中の励起子の非線形発光

日本物理学会　（１９８７年９月）

土屋朋信、舛本泰章

混晶量子井戸ＡｌＧａＡｓ－ＡｌＡｓのΓ－Ｘ谷間相互作用と光学的性質

応用物理学会　（１９８８年３月）

木下靖、舛本泰章、竹村謙一、下村理

低温高圧下におけるＧａＡｓ－ＡｌＡｓ半導体量子井戸構造のフォトルミネッセンス

日本物理学会　（１９８８年４月）

足立充宏、舛本泰章

ＧａＡｓ量子井戸中の光パルス伝幡

日本物理学会　（１９８８年４月）

土屋朋信、舛本泰章

混晶量子井戸ＡｌＧａＡｓ－ＡｌＡｓのΓ－Ｘ谷間相互作用と光学的性質

日本物理学会　（１９８８年４月）

舛本泰章、井手下知史、芝弘史、遠田厚

ＧａＡｓ－ＡｌＡｓ量子井戸中の励起子の非線形発光 Ⅱ

日本物理学会　（１９８８年４月）

佐々木史雄、舛本泰章

ＧａＡｓ－ＡｌＧａＡｓ超格子中の光励起担体のトンネル過程と励起子生成の競合 Ⅱ
日本物理学会　（１９８８年4月）

足立充宏、舛本泰章
ＧａＡｓ量子井戸中の光パルス伝播 Ⅱ
日本物理学会　（１９８８年１０月）

三品具文、佐々木史雄、舛本泰章
超高速時間分解ポンプ・プローブ法による半導体の研究
日本物理学会　（１９８８年１０月）

松永高治、三品具文、舛本泰章
Ｓｉ表面構造とレーザー第二高周波発生との相関
日本物理学会　（１９８８年１０月）

舛本泰章
ＣｕＣｌ微結晶中の励起子の光学的非線型性
日本物理学会　（１９８８年１０月）

木下靖、舛本泰章、竹村謙一、下村理
低温高圧下におけるＧａＡｓ－ＡｌＡｓ多重量子井戸の時間分解分光
日本物理学会　（１９８８年１０月）

佐々木史雄、舛本泰章
ＧａＡｓ－ＡｌＧａＡｓ超格子中の光励起担体のトンネル過程と励起子生成の競合 Ⅲ
日本物理学会　（１９８８年１０月）

井手下知史、舛本泰章
ＧａＡｓ－ＡｌＡｓ量子井戸中の励起子の非線形発光 Ⅲ
日本物理学会　（１９８８年１０月）

佐々木史雄、三品具文、足立充宏、舛本泰章
Ⅱ－Ⅵ族半導体のポンプ・プローブ分光
日本物理学会　（１９８９年3月）

和村哲郎、佐々木史雄、舛本泰章、川上養一、田口常正、平木昭夫
ZnSe-ZnS歪み超格子中の励起子の非線形吸収
日本物理学会　（１９８９年3月）

三品具文、佐々木史雄、足立充宏、舛本泰章
超高速ポンプ・プローブ法による混晶量子井戸超格子中の励起キャリアの動的過程の研究
日本物理学会　（１９８９年3月）

井手下知史、佐々木史雄、三品具文、足立充宏、舛本泰章

BiI_3の超高速ポンプ・プローブ分光

日本物理学会　（１９８９年３月）

舛本泰章

ＣｕＣｌ微結晶の光物性

日本物理学会　（１９８９年３月）

以降は、発表論文リストの論文（2），4)除く）から構成されていますが、一部（下記 4 件）は、著作権者（出版社、学会等）の許諾を得ていないため、筑波大学では電子化・公開しておりません。

なお、電子ジャーナルとして出版社から公開されており、契約している場合は全文を読むことができますので、下記のリンク先でご覧ください。

論文　5)　http://dx.doi.org/10.2184/lsj.15.941

論文　6)　http://dx.doi.org/10.1016/0022-2313(87)90131-1

論文　7)　http://dx.doi.org/10.1016/0022-2313(88)90400-0

論文　9)　http://dx.doi.org/10.1143/JPSJ.57.4403

PHYSICAL REVIEW B VOLUME 33, NUMBER 8 15 APRIL 1986

Tunneling dynamics of photogenerated carriers in semiconductor superlattices

Yasuaki Masumoto
The Institute for Solid State Physics, The University of Tokyo, Roppongi 7-22-1, Minato-ku, Tokyo 106, Japan

Seigo Tarucha and Hiroshi Okamoto
Musashino Electrical Communication Laboratory, Nippon Telegraph and Telephone Corporation, Midori-machi 3-9-11, Musashino-shi, Tokyo 180, Japan

(Received 2 December 1985)

The tunneling dynamics of photogenerated carriers in GaAs-$Al_{0.29}Ga_{0.71}As$ multiple-quantum-well structures is studied using picosecond spectroscopy with an electric field perpendicular to the well layers. Drastic changes, such as an increase in the photocurrent, a decrease in the exciton luminescence, and a change in the exciton lifetime, take place simultaneously for electric fields of $\sim 5.0\times10^3$ V/cm. These changes are ascribed to the onset of exciton dissociation and electron tunneling through the $Al_{0.29}Ga_{0.71}As$ barrier layers. The electron tunneling rate is determined to be 1/(430 ps) and is compared with calculations.

Recently, the dynamics of carriers in semiconductor superlattices has attracted growing interest. There are two directions of motion of the carriers in semiconductor superlattices. One is motion in the plane of heterostructures and the other is motion across the heterostructures. So far, the former has been studied extensively in two-dimensional carrier systems by means of transport experiments. However, the study of the latter has been relatively scarce and limited to current-voltage characteristics since the first observation of resonant tunneling of electrons.[1] Current-voltage characteristics could be used to clarify the energy levels in superlattices but not the dynamical aspects of tunneling. Therefore, new techniques have been required.

In this work, picosecond spectroscopy has been used to study the motion of photogenerated carriers in the direction of the superlattice. We probed the exciton luminescence in GaAs-$Al_{0.29}Ga_{0.71}As$ multiple-quantum-well structures (MQW) in an electric field applied in the direction of the superlattice. Exciton luminescence quenching and the change in the exciton lifetime have already been observed in a GaAs-$Al_xGa_{1-x}As$ MQW in an electric field.[2-4] It has been pointed out that these phenomena are possibly correlated with the field-induced separation of electrons from holes in a well or the tunneling of electrons or holes across the barrier potential. In the preceding study, definitive evidence of the tunneling was not produced. In addition, the electric field in the MQW was not accurately determined, so that the experimental data could not be compared with the calculation. This is because the electric field is screened, to some extent, by the excess photogenerated carriers. We have overcome this difficulty. We have determined the electric field in the MQW by the peak shift of the heavy-exciton luminescence. In addition, we found that the exciton lifetime is surely dominated by the tunneling of electrons across the $Al_{0.29}Ga_{0.71}As$ barrier above a certain critical electric field because the tunneling rate of electrons becomes faster than the decay rate of the exciton population, due to the other processes including radiative recombination. Then, the tunneling rate can be estimated by transient measurement of the exciton luminescence. The tunneling rate thus obtained is compared with the calculated one on the basis of the precise knowledge of the electric field in the MQW.

The sample is a *p-i-n* diode structure grown by molecular-beam epitaxy.[5] The main part consists of 100 alternate periods of undoped 120-Å GaAs well layers and undoped 58-Å $Al_{0.29}Ga_{0.71}As$ barrier layers. The MQW are surrounded by the *p*-type and *n*-type $Al_{0.54}Ga_{0.46}As$ cladding layers 1 μm thick. The MQW and cladding layers are sandwiched between the p^+-type GaAs cap layer (0.5 μm thick) and the *n*-type GaAs substrate. Electrical Ohmic contacts are made on both the p^+-GaAs cap layer and *n*-GaAs substrate. With the sample in a perpendicular electric field at 4.2 K, we made measurements of the photoconductivity, the photocurrent-voltage characteristics, the exciton luminescence, the exciton-luminescence–voltage characteristics, and the picosecond transient response of the exciton luminescence.

For all measurements except photoconductivity, a dye laser synchronously pumped by a cw mode-locked Nd^{3+}:YAG laser (Quantronix 416) (where YAG is yttrium aluminum garnet) is used as the excitation source. The dye laser gives 1–2-ps light pulses with a repetition rate of 82 MHz. The laser dyes Rhodamine 6G and DCM are used to generate 605-nm (2.05-eV) and 678-nm (1.83-eV) light pulses, respectively. The band-gap energies of $Al_{0.54}Ga_{0.46}As$, $Al_{0.29}Ga_{0.71}As$, and GaAs are 2.15 eV (X), 1.88 eV (Γ), and 1.519 eV (Γ), respectively.[6] Therefore, neither 605- nor 678-nm light excites the $Al_{0.54}Ga_{0.46}As$ cladding layers. The 605-nm light excites both the well layers and the barrier layers, while the 678-nm light excites only the well layers. No significant difference was found in the results, including the time-resolved result, whether the barrier layers were excited or not. Therefore, only the results for the 605-nm light excitation are presented in this paper. The laser beam is loosely focused on a *p-i-n* diode sample immersed in liquid helium. To reduce the electrical screening by photogenerated carriers, the excitation laser intensity is reduced to being as weak as possible for the picosecond time-resolved study. The excitation density is about 10 mW/cm^2. The luminescence spectra are recorded by using a 50-cm monochromator. The exciton luminescence is temporally analyzed by using a synchroscan streak camera with 140-μm slit width. Then the time resolution is 42 ps.

The energy shift of the heavy exciton can be used to

determine the electric field in the MQW as described below. We measured the photoconductivity spectra of the sample in the electric field by using the incandescent lamp. The result is shown in the inset of Fig. 1. In the photoconductivity spectra, the heavy excitons in the quantum wells produce a peak. The heavy-exciton peak shifts toward lower energy with the increase in the applied electric voltage. The shifts do not vary with further reduction of the excitation light level. The built-in voltage V_{bi} was determined to be 1.8 V from the curve of the current-voltage characteristics. The sample has no buffer layers. Therefore, the field is simply calculated to be $F=(V_{ext}+V_{bi})/d$, where V_{ext} is the externally applied voltage and $d=1.78$ μm is the total thickness of the MQW. Following the calculation of Bastard for an infinite well, the energy shift of the lowest transition between the electron and hole sublevels, ΔE, is proportional to the square of the electric field F as follows:[7]

$$\Delta E=-2.135\times10^{-3}(m_e^*+m_{hh}^*)e^2F^2L_z^4/\hbar^2 \ , \qquad (1)$$

where e is the charge of electron, the z axis is along the superlattice direction, L_z is the well layer thickness, and m_e^* ($=0.665m_0$) and m_{hh}^* ($=0.45m_0$) are effective masses of the electron and the heavy hole, respectively. The change of the exciton binding energy is neglected because it is smaller than ΔE by an order of magnitude.[8] In fact, Eq. (1) explains the energy shift of the excitons in a strikingly complete manner, as is shown in Fig. 1. Conversely, the electric field in the MQW can be determined from the peak shift of excitons.

Under the picosecond laser excitation, the exciton-luminescence energy shifts toward lower energy with an increase in the externally applied voltage as is shown in the inset of Fig. 2. Then, however, the peak shift is not so large as expected. We attribute this disagreement to the screening of the electric field by the high density of photogenerated carriers[3] because we observe that the peak shift is reduced with an increase in the excitation intensity. Therefore, we do not estimate the electric field from the applied voltage. Instead, we determine the electric field from the peak shift on the basis of Eq. (1). In Fig. 2, both the exciton-luminescence intensity and the photocurrent across the superlattices are plotted as a function of electric field thus estimated. A sudden change is observed at a field of $F_t\sim5.0\times10^3$ V/cm. At this value, the exciton-luminescence intensity decreases and the photocurrent increases. These facts indicate that the excitons dissociate at this field and that electrons or holes tunnel through the potential barriers and contribute to the photocurrent. At the field of $F_t\sim5.0\times10^3$ V/cm, the field gain for the electrons or holes amounts to 9 meV when they move by a superlattice period

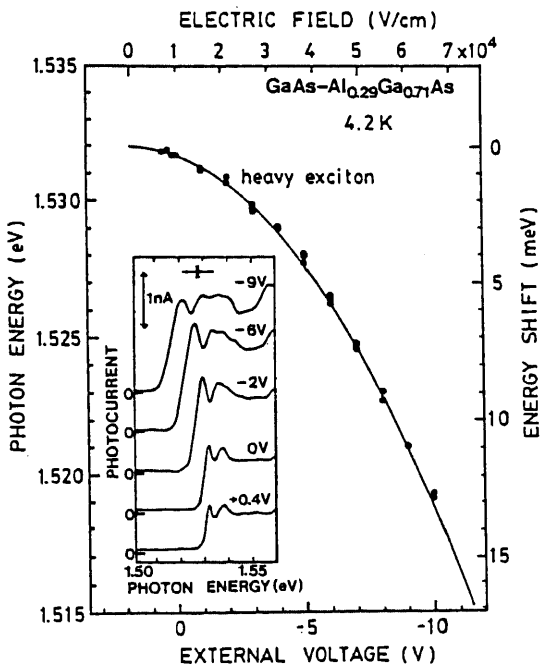

FIG. 1. Peak shift of the heavy excitons observed in photoconductivity spectra as a function of the applied electric voltage V_{ext}. Experimental data are shown by solid circles. The built-in voltage V_{bi} is +1.8 V. Electric field in the MQW is calculated to be $(V_{ext}+V_{bi})/d$. The solid line is the calculated one on the basis of Eq. (1). In the inset, photoconductivity spectra under the externally applied voltage are shown. The lowest-energy peak corresponds to heavy excitons.

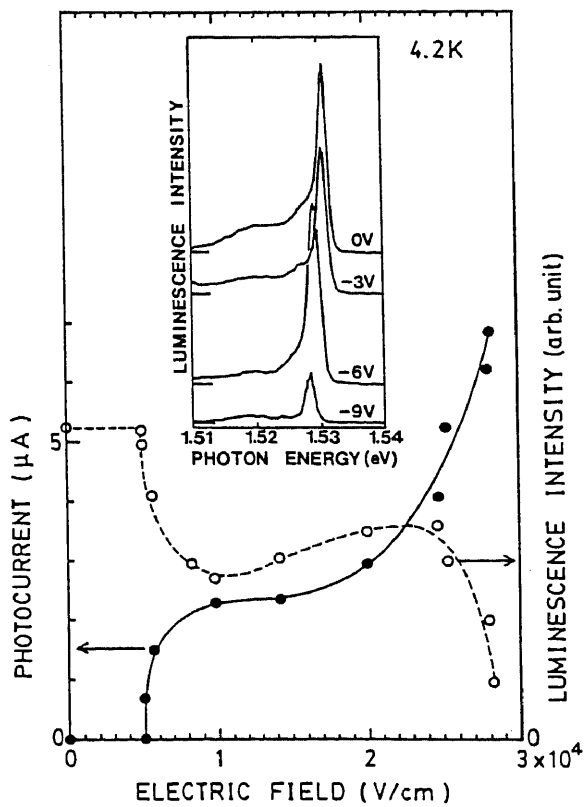

FIG. 2. Luminescence itensity of heavy excitons (○) and photocurrent (●) as a function of the electric field in the MQW. Solid and dashed lines are guides for the eyes. The inset shows heavy-exciton luminescence spectra under externally applied voltage. The peak shifts of heavy excitons indicate that applied voltages 0, −3, −6, and −9 V correspond to electric fields 5.0×10^3, 9.8×10^3, 2.5×10^4, and 2.8×10^4 V/cm, respectively.

(=178 Å). The field gain is almost equal to the exciton binding energy in 120-Å quantum wells (10 meV) derived from the magneto-optical measurements.[9] The field gain compensates for the binding energy. Therefore, it is quite reasonable for excitons to dissociate at a field of $F_t \sim 5.0\times10^3$ V/cm. Curves of photocurrent and luminescence intensity show a plateau between $\sim1.0\times10^4$ and $\sim2.0\times10^4$ V/cm. With the further increase in the electric field up to $\sim2.8\times10^4$ V/cm, the photocurrent increases and the exciton luminescence decreases.

The transient response of the exciton luminescence is shown in Fig. 3. At the field of $F_t\sim5.0\times10^3$ V/cm, the temporal profile of the exciton luminescence changes drastically. Below F_t, the exciton luminescence exponentially decays with a time constant of 1.52 ns. Above F_t, the exciton-luminescence decay seems to consist of two components. The fast decay has a time constant of 430 ps. The slow one has a long time constant which has not been determined in this experiment. We determine that the change of the temporal profile comes from the tunneling of the electrons or holes because the luminescence decrease and the photocurrent increase take place at the common electric field of $F_t\sim5.0\times10^3$ V/cm. Then, the fast decay of exciton luminescence is dominated by the tunneling of electrons or holes across the potential barriers. Therefore the tunneling rate can be estimated to be $1/(430\text{ ps})=2.3\times10^9\ s^{-1}$. At a field of $\sim2.8\times10^4$ V/cm, the slow-decay component of the exciton luminescence vanishes completely and the exciton luminescence exponentially decays with a time constant of 430 ps.

It is not easy to estimate the dissociation rate of excitons in the MQW. To estimate it, we must calculate the rates of at least two processes, the dissociation of excitons, and the tunneling of electrons or holes across the barrier potential. If the excitons are not in the quantum wells and are in the electric field F, the dissociation rate of excitons, w_1, is given by the following formula which also describes the ionization rate of hydrogen atoms.[10]

$$w_1=(16R^2/\hbar eFa_B)\exp(-4R/3eFa_B)\ , \tag{2}$$

where R (=4.2 meV) is the Rydberg energy and a_B (=136 Å) is the exciton Bohr radius. The dissociation rate reaches $2.8\times10^{13}\ s^{-1}$ at an electric field of $F_t\sim5.0\times10^3$ V/cm. The rate is much faster than the observed rate.

Compared with the above-mentioned dissociation rate, the tunneling rate of electrons or holes across the barrier potential is expected to be slow because the $Al_{0.29}Ga_{0.71}As$ barrier potential is much higher than the Coulomb barrier. The experimental results correspond exactly with this expectation. In the Wentzel-Kramers-Brillouin approximation, the tunneling rate of electrons or heavy holes across the barrier potential w_2 is estimated to be[11]

$$w_2=(\pi\hbar/2m^*_{e(\mathrm{hh})}L_z^2)\exp[-(2/\hbar)\sqrt{2m^*_{e(\mathrm{hh})}(U-E)}\,d_b]\ , \tag{3}$$

if the Coulomb interaction between the electrons and heavy holes is neglected. Here, E is the band discontinuity, U is the confinement energy of the lowest sublevel, and d_b (=58 Å) is the barrier thickness. The factor $2m^*_{e(\mathrm{hh})}L_z^2/\pi\hbar$ is the classical period of the electron (heavy-hole) motion in the quantum well,[11] because the z component of the velocity of electrons (heavy holes) in the lowest sublevel is $\hbar k/m^*_{e(\mathrm{hh})}=\pi\hbar/m^*_{e(\mathrm{hh})}L_z$. Equation (3) is the expression in the case of zero applied electric field. However, this equation approximately holds under the condition $eFd \ll U-E$, even when the electric field is applied.

The rate calculated on the basis of Eq. (3) is not altered much when the confinement energy U is neglected because U is smaller than the band discontinuity E by an order of magnitude. Therefore U is neglected for simplicity. If the band-gap discontinuity split of 85:15 is correct,[12] the conduction-band discontinuity E_c is 307 meV and the valence-band discontinuity E_v is 54 meV. Then, the tunneling rate of electrons is $3.9\times10^9\ s^{-1}$ and that of holes is $2.7\times10^8\ s^{-1}$. On the other hand, the tunneling rate of electrons is $1.8\times10^{10}\ s^{-1}$ and that of holes is $4.3\times10^5\ s^{-1}$, if the band-gap discontinuity split of 57:43 ($E_c=206$ meV, $E_v=155$ meV) is correct.[13] In both the cases, tunneling of electrons dominates the field dissociation rate of excitons across the barrier potential. The calculated tunneling rates are faster than the experimental value. However, disagreement is within an order of magnitude, although the calculation is the simplest one.

The simple calculation well explains the experimental characteristics that the tunneling rate is not affected by the electric field between 5.0×10^3 and 2.8×10^4 V/cm. In fact, unlike the earlier experiments,[2,3] the condition $eFd \ll U-E$ holds in our experiment. Nevertheless, excitons are stripped of electrons and electrons tunnel across barrier potentials critically at the field $F_t\sim5.0\times10^3$ V/cm, because the field gain can compensate for the binding energy of excitons. It is not easy to consider the tunneling of electrons through both the Coulomb barrier and the barrier potential. In fact, there is no available theoretical study of this problem. The slow-decay component observed between $\sim5.6\times10^3$ and $\sim2.8\times10^4$ V/cm may be due to nongeminate excitons made of stripped electrons and holes. With

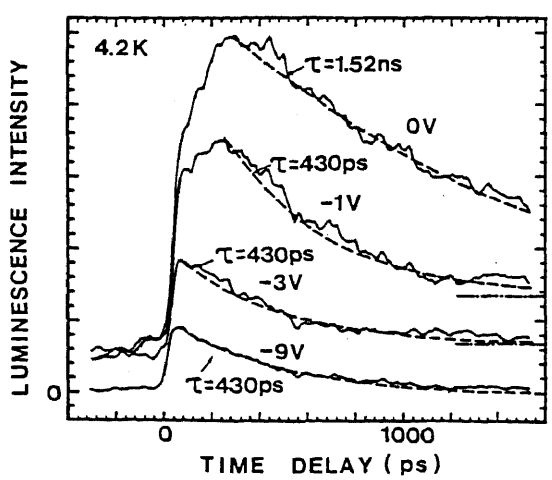

FIG. 3. Temporal profile of the heavy-exciton luminescence intensity in the perpendicular electric field. The estimated electric fields in the MQW are 5.0×10^3, 5.6×10^3, 9.8×10^3, and 2.8×10^4 V/cm for the applied voltages of 0, −1, −3, and −9 V, respectively. Dashed lines show exponential decay with respective time constant τ. Dash-dotted lines show long-lived component. The background observed before 0 ps comes from the stray of 6-ns-lived luminescence which is peculiar to the synchroscan streak camera.

the increase in the electric field, the slow-decay component decreases and the photocurrent increases. We may attribute this change to the onset of successive tunneling of electrons through many barriers. However, these processes remain to be clarified by future study.

In summary, the tunneling dynamics of photogenerated carriers in GaAs-$Al_{0.29}Ga_{0.71}As$ multiple-quantum-well structures have been studied in an electric field perpendicular to the well layers. Drastic changes, such as an increase in the photocurrent, a decrease in the exciton luminescence, and a change of the exciton lifetime take place simultaneously at the critical electric field of -5.0×10^3 V/cm. The changes are ascribed to the dissociation of excitons and the tunneling of electrons through the $Al_{0.29}Ga_{0.71}As$ potential barriers. These processes take place when the field gain can compensate for the exciton binding energy. The tunneling rate of the electrons is determined to be 1/(430 ps), slower than the simple estimation.

Note added. A recent work by Polland *et al.* [Phys. Rev. Lett. 55, 2610 (1985)] covers similar ground treated in the present work. Contrary to the present results, they have observed that the lifetime of excitons is prolonged with an increase in the electric field. The contradiction probably comes from a difference in the quantum-well structures, especially with respect to the thickness of barriers.

The authors wish to thank Professor M. Matsuoka for valuable discussions and continuous encouragement. The picosecond laser system used in this work was developed by one of the authors (Y.M.) in collaboration with Professor M. Matsuoka and Dr. M. Baba, whom the authors wish to thank. This work was supported in part by Scientific Research Grant-in-Aid No. 59460024 and Scientific Research Grant-in-Aid No. 60222017 for Special Project Research on "Alloy Semiconductor Electronics" from the Ministry of Education, Science and Culture of Japan.

[1]L. L. Chang, L. Esaki, and R. Tsu, Appl. Phys. Lett. 24, 593 (1974).

[2]E. E. Mendez, G. Bastard, L. L. Chang, L. Esaki, H. Morkoc, and R. Fisher, Phys. Rev. B 26, 7101 (1982).

[3]J. A. Kash, E. E. Mendez, and H. Morkoc, Appl. Phys. Lett. 46, 173 (1985).

[4]Y. Horikoshi, A. Fischer, and K. Ploog, Phys. Rev. B 31, 7859 (1985).

[5]H. Iwamura, T. Saku, and H. Okamoto, Jpn. J. Appl. Phys. 24, 104 (1985).

[6]H. C. Casey, Jr. and M. B. Panish, *Heterostructure Lasers* (Academic, New York, 1978), Part A, Chap. 4.

[7]G. Bastard, E. E. Mendez, L. L. Chang, and L. Esaki, Phys. Rev. B 28, 3241 (1983).

[8]D. A. B. Miller, D. S. Chemla, T. C. Damen, A. C. Gossard, W. Wiegmann, T. H. Wood, and C. A. Burrus, Phys. Rev. Lett. 53, 2173 (1984); Phys. Rev. B 32, 1043 (1985).

[9]S. Tarucha, H. Okamoto, Y. Iwasa, and N. Miura, Solid State Commun. 52, 815 (1984).

[10]L. D. Landau and E. M. Lifshitz, *Quantum Mechanics (Non-relativistic Theory)*, 3rd ed. (Pergamon, New York, 1977), Chap. 10.

[11]D. Bohm, *Quantum Theory* (Prentice-Hall, Englewood Cliffs, 1951), Chap. 12.

[12]R. Dingle, in *Festkörperprobleme*, edited by H. J. Queisser, Advances in Solid State Physics, Vol. XV (Pergamon, New York, 1975), p. 21.

[13]R. C. Miller, D. A. Kleinman, and A. C. Gossard, Phys. Rev. B 29, 7085 (1984).

Localized indirect excitons in a short-period GaAs/AlAs superlattice

F. Minami,* K. Hirata, and K. Era
National Institute for Research in Inorganic Materials, Tsukuba, Ibakaki 305, Japan

T. Yao
Electrotechnical Laboratory, Tsukuba, Ibaraki 305, Japan

Y. Masumoto
Institute of Physics, University of Tsukuba, Tsukuba, Ibaraki 305, Japan
(Received 31 December 1986)

We have studied the optical properties of a short-period superlattice composed of 20.4-Å GaAs and 14.7-Å AlAs layers. The superlattice behaves as an indirect-gap material. A slow and nonexponential decay of the luminescence can be interpreted as the emission from the Λ indirect excitons localized at the GaAs/AlAs interfaces. The temperature dependence of the exciton decay time can be explained in terms of a transition by phonon-assisted tunneling, followed by a nonradiative transition.

Recent advances in crystal growth techniques, such as the molecular-beam-epitaxy (MBE) method, have made it possible to produce semiconductor crystals consisting of alternating layers of two different semiconductors, i.e., superlattice structures. These superlattices are expected to form a new device and have been extensively studied, especially the GaAs/AlAs system. A number of experiments on GaAs/AlAs superlattices of large layer thickness have been carried out and analyzed successfully by means of the Kronig-Penney model.[1] There have been a few works on ultrathin layered GaAs/AlAs superlattices. However, considerable confusion exists in the interpretation of the electronic structure of these superlattices, especially of the short-period superlattices with nearly equal GaAs and AlAs layer thickness and with periods ranging from ~ 10 to ~ 60 Å. Some groups have claimed that these short-period superlattices behave as indirect-gap materials,[2,3] while others have concluded that these materials are direct gap.[4–7] In order to clarify the electronic structure of short-period superlattices, we have studied the optical properties of a superlattice composed of 20.4-Å GaAs and 14.7-Å AlAs layers. Special attention is given to the dynamics of photoexcited carriers. The experimental results indicate that our sample behaves as an indirect-gap material and that the emission near the band edge is due to localized indirect excitons.

The GaAs/AlAs sample used in this study consisted of 250 periods of 20.4-Å GaAs/14.7-Å AlAs grown by MBE at 550 °C on a (100) semi-insulating GaAs substrate. The Al content in the sample was 42%, which is near the direct-indirect crossover value of $\sim 40\%$ in the $Al_xGa_{1-x}As$ alloy system.[8–10] In order to make absorption measurements, the GaAs substrate was removed by preferential etching over a region of 1×1 mm^2, leaving only the MBE-grown film. The cw photoluminescence and excitation measurements were made by a DCM dye laser pumped by an argon-ion laser. For time-resolved spectra, the sample was excited by a cavity-dumped mode-locked cw dye (DCM) laser synchronously pumped by a mode-locked argon-ion laser. The transmitted light and luminescence were monitored by a double monochromator equipped with a cooled photomultiplier. Lifetime measurements were made by the time-correlated single-photon counting technique. The sample was immersed in liquid helium. At elevated temperatures, it was exposed to an atmosphere of helium gas.

The absorption spectrum at 4.2 K is presented in Fig. 1. The absorption coefficient $\alpha(\hbar\omega)$ was obtained from the optical density by taking into account multiple reflections. The spectrum shows the characteristic behavior of indirect-gap materials: No feature due to discrete-state exciton absorption is observed and an absorption tail is seen at low energies. From the kink in the curve, the direct gap E_g is measured as ~ 1.975 eV. We estimated the indirect gap E_{gi} roughly as ~ 1.88 eV through the relation $\alpha(\hbar\omega) \propto (E_{gi} - \hbar\omega)^2$.[2] The luminescence and excitation spectra at 4.2 K are also shown in Fig. 1. A relatively sharp line, labeled by I_{ex}, is observed at ~ 1.873 eV and dominates the near-gap emission. On the basis of the spectral position and time dependence shown later, we believe that the I_{ex} line comes from the decay of localized indirect excitons. Although weak and broadband emissions are observed at lower energies, here we confine our attention to the I_{ex} line. The excitation spectrum monitored at the I_{ex} line shows a well-defined peak at the direct-gap energy. This also indicates that the sample is indirect gap. Further, this conclusion is borne out by the temporal behavior of the I_{ex} emission described below. These results support the conclusions of Refs. 2 and 3, while they are in conflict with those made in Refs. 4–7.

Figure 2 shows the time evolution of the I_{ex} emission at 4.2 K. The emission decays slowly and nonexponentially. This temporal behavior can be interpreted well in terms of the emission from indirect excitons localized by disorder

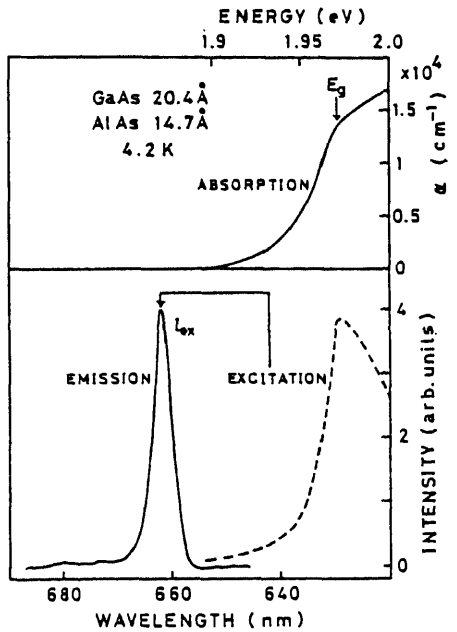

FIG. 1. Absorption, cw luminescence, and excitation spectra for the short-period GaAs/AlAs superlattice. The direct gap is denoted by E_g. The excitation spectrum was monitored at the I_{ex} line.

in the sample. In the presence of potential fluctuations, no-phonon radiative transitions of indirect excitons are allowed because these fluctuations break the k-selection rule. Reflecting the random nature of the scattering potential, the radiative decay rate is not well defined, but has a probability distribution. The no-phonon transitions of indirect excitons in such a case have been studied by

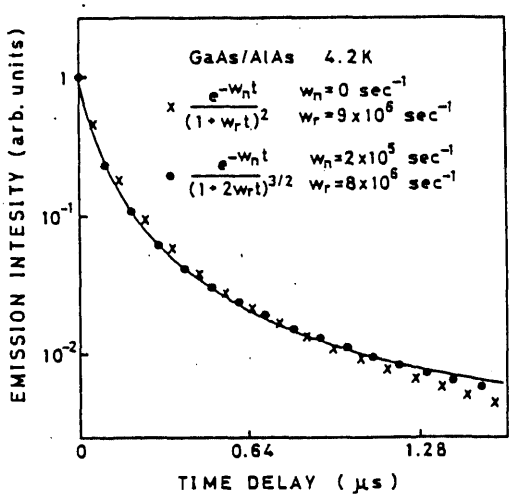

FIG. 2. Temporal evolution of the I_{ex} emission at 4.2 K. The solid line shows the experimental curve. Crosses represent Eq. (1) with $w_r=9\times10^6$ sec^{-1} and $w_n=0$ sec^{-1}. Circles represent Eq. (2) with $w_r=8\times10^6$ sec^{-1} and $w_n=2\times10^5$ sec^{-1}.

Klein *et al.*[11] According to their theory,[11,12] the time response of the emission from localized indirect excitons is given as

$$I(t)\propto e^{-w_n t}/(1+w_r t)^2\ , \tag{1}$$

for indirect excitons not at the zone boundary, or

$$I(t)\propto e^{-w_n t}/(1+2w_r t)^{3/2}\ , \tag{2}$$

for indirect excitons at the zone boundary, where w_r is the average radiative decay rate due to random potential scattering, and w_n is the total decay rate due to all other processes. The experimental data fit the time dependence predicted from this model. Theoretical curves derived from Eqs. (1) and (2) are also shown in Fig. 2. The best fits were obtained for $w_r=9\times10^6$ sec^{-1} and $w_n=0$ sec^{-1} in the case of Eq. (1), and for $w_r=8\times10^6$ sec^{-1} and $w_n=0.2\times10^6$ sec^{-1} in the case of Eq. (2).

A better fit is obtained to Eq. (2). From this result, however, one cannot conclude immediately that the I_{ex} emission is due to the zone-boundary excitons, because the theory of Klein *et al.* was developed for indirect excitons in an alloy system where scatterers are uniformly distributed. In superlattices potential fluctuations are considered to come from the inhomogeneity of the interface and scatterers to be distributed in the interface planes. In such a case, the summation in Eq. (6) of Ref. 11 must be performed over the position vectors L of the scatterers in the interfaces spanned by the exciton. The exciton in the present system encompasses only a few interface planes. The phase factor $e^{i\mathbf{k}\cdot\mathbf{L}}$ in this equation then does not have many different values for indirect excitons at wave vector k normal to the interface (i.e., on the Λ line). The theory should thus be modified for these excitons since the assumption of the uniform distribution of phase, used in Ref. 11, is no longer a good approximation. By modifying the model of Klein *et al.*, it can be deduced that the decay of indirect excitons on the Λ line follows Eq. (2) rather than Eq. (1).[13] In the superlattices, therefore, excitons both at the zone boundary and on the Λ line should decay as predicted by Eq. (2).

To determine the origin of the I_{ex} emission, it is necessary to know which points of the Brillouin zone are likely candidates for positions of the band extrema. Since it is well established that the topmost of the valence bands lies at Γ, we will search for the location of the conduction-band minimum. Following Ref. 3, we take the $Al_{0.42}Ga_{0.58}As$ alloy bands as unperturbed states and treat the superlattice potential as a perturbation. In the parent alloy the minimum of the conduction band occurs at the X point.[10] In the superlattices, the $X(001)$ point is folded back to the Γ point due to the superlattice potential, and through the coupling with other Γ states, it is lower than the unmixed $X(100)$ and $X(010)$ points. This point is then expected to become the lowest state of the conduction band. Actually, in the alloy the conduction-band minimum is not at X, but displaced from it by the "camel's-back" effect. This camel's-back structure would be reflected in the band structure of the superlattice. The conduction-band minimum is then expected to lie on the

Λ line.[3] On the basis of this consideration and the time dependence obeying Eq. (2), we think that the I_{ex} emission is attributable to indirect excitons on the Λ line, i.e., the camel's-back excitons near the Γ point.

The one-photon transition to the lowest Γ state of the conduction band is considered to be weakly allowed, since this Γ state is derived from the X point of the parent alloy and is only slightly modified by the superlattice potential.[3] Further, it can be shown that the decay of this "pseudodirect" exciton follows Eq. (2). Thus one may think that there is no camel's-back structure near the Γ point and the I_{ex} emission is due to the pseudodirect exciton consisting of a Γ hole and an electron at the Γ point which has the folded-X character of the $Al_{0.42}Ga_{0.58}As$ alloy. However, this is not our case. At the Γ point, the superlattice potential makes a more appreciable contribution to the radiative decay rate than the interface disorder does, and this nonstochastic contribution should be included in the decay rate w_n. This assignment then is not consistent with the result that w_n is much smaller than the average radiative decay rate w_r, which is a measure of the magnitude of interface disorder.

There is another possibility that the I_{ex} emission is due to excitons bound to neutral donors or acceptors. However, this assignment is very unlikely, because, by contribution to nonradiative Auger recombination, the bound excitons can decay exponentially with lifetimes less than 20 nsec even in indirect-gap materials.[12,14] Further evidence that the emission is not from excitons bound to impurities is provided by the temperature dependence of the emission. Since the bound exciton has a binding energy of a few meV, thermal dissociation of the bound exciton to the free indirect exciton should occur above ~20–30 K. The free-exciton emission should then dominate the bound-exciton emission at high temperatures. However, the experimental result shows that I_{ex} emission is predominant above 60 K. This possibility therefore is ruled out.

The temperature dependence of the decay of the I_{ex} line is shown in Fig. 3. There is a concomitant decrease in the emission intensity. At low temperatures, the emission shows a slow and nonexponential decay. With the increase of temperature, the decay becomes faster and approaches an exponential form. A changeover to exponential decay occurs above ~11 K. The temperature dependence of the decay time is shown in Fig. 4. Here we have defined the decay time as the slope of the exponential decay curve above ~11 K. In the figure we also show the temperature dependence of the steady-state luminescence intensity. The parallel decreases in the decay time and the emission intensity show that nonradiative processes are dominant above ~11 K. The decay time (or luminescence intensity) does not exhibit Arrhenius-type behavior. A reasonable fit is obtained to an expression of the form $\tau \propto e^{-T/T_0}$, with $T_0 \sim 10$ K. This temperature dependence is familiar in amorphous materials, such as As_2S_3 (Ref. 15) and a-Si:H (Ref. 16), and believed to be a characteristic of localized systems with a "mobility edge."[17] Further, this dependence has recently been observed in several mixed crystals and is considered to be associated with the mobility edge.[18] We thus think that the e^{-T/T_0} dependence in our sample indicates the existence of a mobility edge and excitons localized in the Anderson sense.[19] In this picture, the temperature dependence is explained as follows. At low temperatures only the processes which lower the energy are possible and the localization is fast and irreversible. The localized excitons then dominate the emission. They respond to the potential fluctuations and decay nonexponentially. The temperature dependence can be understood as a result of thermal delocalization of excitons. As the temperature is raised, the exciton mobility increases via phonon-assisted tunneling and the probability of reaching nonradiative recombination centers increases. As nonradiative processes are dominant, the decay becomes exponential and the radiative efficiency drops off.

Finally we make a short mention of the latest work on the same subject performed by Finkman *et al.*[20] From the temporal response of photoluminescence, they concluded that the lowest excited state of the short-period superlattices is an X-point (zone-boundary) exciton. On the

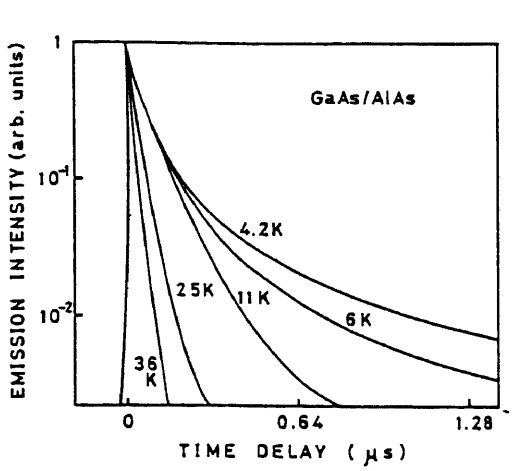

FIG. 3. Luminescence decay curves of the I_{ex} line for different temperatures.

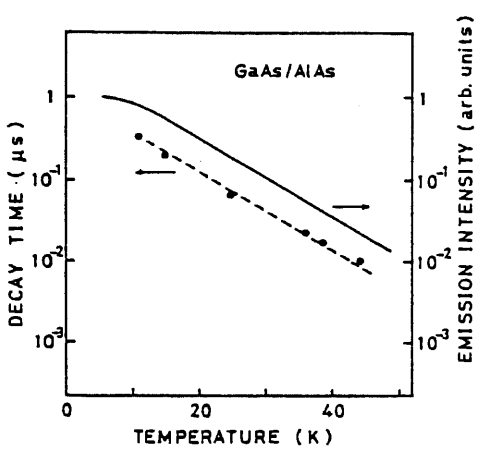

FIG. 4. Temperature dependence of the decay time and of the cw luminescence intensity of the I_{ex} line.

other hand, we suggest that it is an indirect exciton on the Λ line. Since the existing theories predict that the conduction-band minimum is at the Γ point[4–6] or on the Λ line,[3] we think our assignment is more reasonable. According to Ref. 20, however, there seems to exist a theory predicting that the unmixed X minima are the lowest. A full understanding of this state must involve a more complete investigation including, for example, the effect of uniaxial stress.

In conclusion, we have studied the optical properties of the short-period superlattice consisting of 20.4-Å GaAs and 14.7-Å AlAs layers. The superlattice behaves as an indirect-gap material. The emission at 4.2 K shows a slow and nonexponential decay. This behavior can be interpreted by the decay of indirect excitons on the Λ line made partially allowed by disorder at the GaAs/AlAs interfaces. The decay time of the excitons exhibits a e^{-T/T_0} temperature dependence, which is explained in terms of phonon-assisted tunneling of excitons to nonradiative centers.

We are grateful to Professor J. Nakahara of Hokkaido University for valuable discussions on the temperature dependence of the emission.

---

*Present address: Research Institute of Applied Electricity, Hokkaido University, Sapporo 060, Japan.

[1]For example, R. C. Miller, D. A. Kleinman, and A. C. Gossard, Phys. Rev. B 29, 7085 (1984).

[2]J. Van der Ziel and A. C. Gossard, J. Appl. Phys. 48, 3018 (1977); Phys. Rev. B 17, 765 (1978).

[3]W. Andreoni and R. Car, Phys. Rev. B 21, 3334 (1980).

[4]A. Ishibashi, Y. Mori, M. Itabashi, and N. Watanabe, J. Appl. Phys. 58, 2691 (1985).

[5]E. Caruthers and P. J. Lin-Chung, Phys. Rev. B 17, 765 (1978).

[6]J. N. Schulman and T. C. McGill, Phys. Rev. B 19, 6431 (1979).

[7]T. Nakayama and H. Kamimura, J. Phys. Soc. Jpn. 54, 4726 (1985).

[8]B. Monemar, K. K. Shih, and G. D. Pettit, J. Appl. Phys. 44, 2604 (1976).

[9]R. Dingle, R. A. Lorgan, and J. R. Arthur, in *GaAs and Related Compounds*, edited by C. Hilsum (IOP, London, 1977), p. 210.

[10]A. Baldereschi, E. Hess, K. Maschke, H. Neumann, K. R. Schulze, and K. Unger, J. Phys. C 10, 4709 (1977).

[11]M. V. Klein, M. D. Sturge, and E. Cohen, Phys. Rev. B 25, 4331 (1982).

[12]M. D. Sturge, E. Cohen, and R. A. Logan, Phys. Rev B 27, 2362 (1983).

[13]F. Minami (unpublished).

[14]R. J. Nelson, in *Excitons*, edited by E. Rashba and M. D. Sturge (North-Holland, Amsterdam, 1982), p. 319.

[15]R. A. Street, T. M. Searle, and I. G. Austin, in *Amorphous and Liquid Semiconductors*, edited by J. Stuke and W. Brenig (Taylor and Francis, London, 1974), p. 947.

[16]R. W. Collins, M. A. Paesler, and W. Paul, Solid State Commun. 34, 833 (1980).

[17]R. A. Street, Adv. Phys. 30, 593 (1981).

[18]J. Nakahara, S. Minomura, H. Kukimoto, F. Minami, and K. Era, J. Phys. Soc. Jpn. (to be published).

[19]N. F. Mott and E. A. Davis, *Electronic Processes in NonCrystalline Materials* (Oxford University Press, New York, 1979).

[20]E. Finkman, M. D. Sturge, and M. C. Tamargo, Appl. Phys. Lett. 49, 1299 (1986).

Optical nonlinearities of excitons in CuCl microcrystals

Yasuaki Masumoto, Makoto Yamazaki, and Hideyuki Sugawara
Institute of Physics, University of Tsukuba, Tsukuba, Ibaraki 305, Japan

(Received 16 March 1988; accepted for publication 10 August 1988)

Nonlinear optical properties of excitons in CuCl microcrystals in NaCl host crystals were studied by the absorption saturation method. Prominent absorption saturation of excitons was observed together with a blue shift. Optical nonlinearity was found to increase with an increase in the size of the CuCl microcrystals. The observed nonlinearities are very large compared with those in bulk CuCl crystals and GaAs quantum wells.

Recently optical properties of semiconductor microcrystals (quantum dots) have attracted much interest. This is because semiconductor microcrystals are expected to have novel optical properties in a way similar to semiconductor quantum wells. Also, semiconductor microcrystals are expected to have high optical nonlinearity. Therefore, they have a potential for becoming novel optoelectric devices which are useful in optical information processing. In this sense, the search for new materials including semiconductor microcrystals which have a high optical nonlinearity is important. So far, many authors have reported the quantum size effects for excitons in semiconductor microcrystals. Based on the classification made by Ekimov *et al.*, the quantum size effects are classified into two categories: electron or hole confinement and exciton confinement.[1] Hanamura expects high optical nonlinearity for excitons in semiconductor microcrystals where exciton confinement takes place.[2,3] The quantum size effect for excitons in CuCl microcrystals is a typical example of exciton confinement. Therefore, excitons in CuCl microcrystals are expected to give a high $\chi^{(3)}$ (the third-order nonlinear susceptibility). The purpose of this letter is to examine optical nonlinearity as a function of the size of CuCl microcrystals by means of nonlinear absorption, and to examine Hanamura's prediction.

Samples of CuCl microcrystals in NaCl host crystals are grown from high quality, zone-refined CuCl and vacuum-distilled NaCl. The transverse Bridgman method was used for the growth followed by various heat treatments. The heat treatment determines the size distribution of CuCl microcrystals. We determined the size of the CuCl microcrystals by the absorption peak energy of Z_3 excitons at 77 K following the method established by Itoh.[4] The molar fraction of CuCl was determined by the inductively coupled plasma optical emission spectroscopy. The spectroscopy analyzes chemically the concentration ratio of Cu and Na ions. The five samples used in this study are listed in Table I. For the transmission experiments, samples were directly immersed in bubble-free liquid nitrogen. We used an incandescent lamp for the weak-limit absorption experiments and a dye laser pumped by a nitrogen laser (600 kW, 10 ns) for the nonlinear absorption experiments. A dye solution, BBQ in dioxane, was used as the active medium. The pulse duration was 7 ns and the pulse energy was measured by using a pyroelectric energy detector (Gentec, ED100A and ED-X). The size of the excitation spot was measured under a microscope. The transmitted laser light was detected directly by a photomultiplier (Hamamatsu R453) with a calibrated set of neutral density filters. A boxcar integrator was used for averaging.

In the weak-limit absorption spectra, all the samples (1–5) show clear absorption peaks ascribed to Z_3 and $Z_{1,2}$ excitons at 77 K. The absorption peak positions of Z_3 excitons of samples 2, 3, 4, and 5 shift toward higher energies compared with the Z_3 exciton energy of bulk CuCl. Itoh studied both the Z_3 exciton energy and the size of CuCl microcrystals. The size was measured by means of small-angle x-ray scattering. On the basis of his study, the Z_3 exciton energy E_{ex} is best expressed by the formula

$$E_{ex} = E_{ex}(\text{bulk}) + (\pi\hbar)^2/[2M(a + 0.5a_{ex})^2],$$

where E_{ex} (bulk) means the Z_3 exciton energy of bulk CuCl crystals, $M(=2.3m_0)$ is the Z_3 exciton translational mass, a is the average radius of CuCl microcrystals, and $a_{ex}(=0.68$ nm) is the Z_3 exciton Bohr radius. The equation can give values of a from the values of E_{ex}. Thus the average radii of CuCl microcrystals in samples 2, 3, 4, and 5 as determined are shown in Table I. The shift of the Z_3 exciton absorption peak in sample 1 is much smaller than the absorption linewidth, so that the shift is not definitely obtained. Therefore, the radius of CuCl microcrystals in sample 1 is judged to be larger than 10 nm.

In Fig. 1, nonlinear absorption spectra around Z_3 excitons in CuCl microcrystals are shown. The absorption coefficient α is calculated by the formula $\alpha = -\ln(T)/fd$, where f is the volume fraction of CuCl in samples, d is sample thickness, and T is the transmittance of the laser light intensity. The absorption spectra under the lowest density laser exciton almost agree with the weak-limit absorption spectra. With the increase of the excitation density, the absorption peak decreases prominently together with a blue shift. These nonlinear absorption features are similar to those observed in semiconductor quantum wells.[5–8] The excitation intensity

TABLE I. List of samples. d is the sample thickness, f is the volume fraction of CuCl in samples, and E_{ex} is the Z_3 exciton energy at 77 K observed in the absorption spectra. Size means the average radius of CuCl microcrystals.

Sample No.	d(mm)	f(%)	E_{ex} (eV) at 77 K	Size (nm)
1	0.44	0.12	3.219	>10
2	0.34	0.12	3.223	5.7
3	0.60	0.12	3.225	5.0
4	0.55	0.12	3.236	3.3
5	0.52	0.12	3.240	3.0

 0003-6951/88/421527-03$01.00

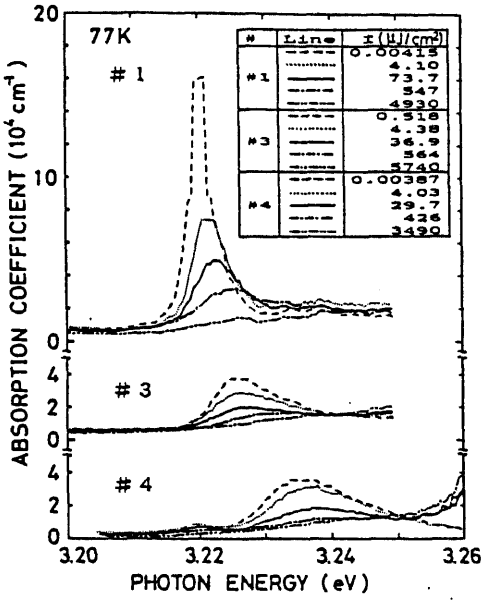

FIG. 1. Nonlinear absorption of Z_3 excitons in CuCl microcrystals in NaCl host crystals (1, 3, and 4). The sample temperature is 77 K. The excitation densities corresponding to various lines are shown in the inset table.

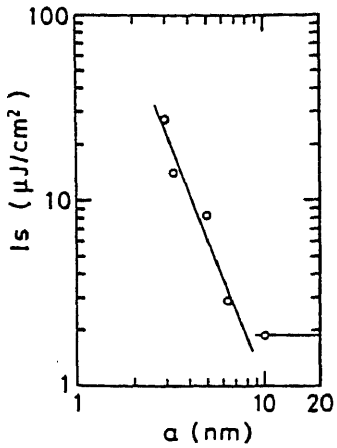

FIG. 3. Saturation density as a function of the average radius a of the CuCl microcrystals. A solid line shows the $a^{-2.6}$ dependence.

dependence of the absorption intensity is well described by the absorption saturation formula $\alpha = \alpha_1/(1 + I/I_s) + \alpha_2$ (shown in Fig. 2), where α_1 and α_2 are fitting parameters and I and I_s are the laser light density and saturation density, respectively. In Fig. 2, various symbols indicate experimental points and lines least-squares-fitted results. The experimental points are well expressed by the formula except in the highest power density region. The saturation density thus obtained is plotted as a function of the size of the CuCl microcrystals in Fig. 3. Here, the CuCl microcrystals are assumed to be spheres and the size means the radius of the spheres, a.[4] Figure 3 shows that the saturation density decreases with an increase of the size of the microcrystals. The relation between I_s and a is best expressed by $I_s \propto a^{-2.6}$. The saturation density I_s can be related to the third-order nonlinear susceptibility $\chi^{(3)}$, when we consider the low-density excitation limit. The relation is written by

$$\mathrm{Im}\chi^{(3)} = -\frac{\epsilon_0 n_0^2 c^2 \alpha_1 f d(\alpha_1 + \alpha_2)}{\omega I_s\{1 - \exp[-(\alpha_1 + \alpha_2) f d]\}},$$

where ϵ_0 is the dielectric constant in vacuum, n_0 the linear refractive index, and c the light velocity in vacuum.[9] The third-order nonlinear susceptibility $\chi^{(3)}$ increases with the increase of the size of CuCl microcrystals, because it is inversely proportional to I_s. The results almost agree with Hanamura's expectation of the a^3 dependence.

A more detailed analysis for sample 2 is shown in Fig. 4, where we derive the experimental changes in the absorption $\Delta\alpha(\omega)$ and the corresponding refractive index $\Delta n(\omega)$. The

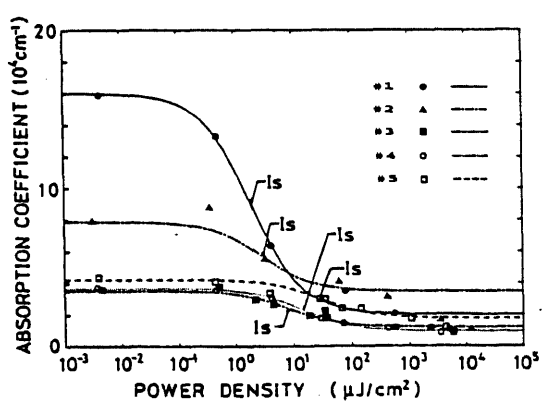

FIG. 2. Absorption coefficient α of Z_3 exciton absorption peak of samples (Nos. 1–5) as a function of laser power density I. Symbols show experimental values. Lines are least-squares fitted results by the equation $\alpha = \alpha_1/(1 + I/I_s) + \alpha_2$, where α_1 and α_2 are fitting parameters. Saturated density is shown by I_s.

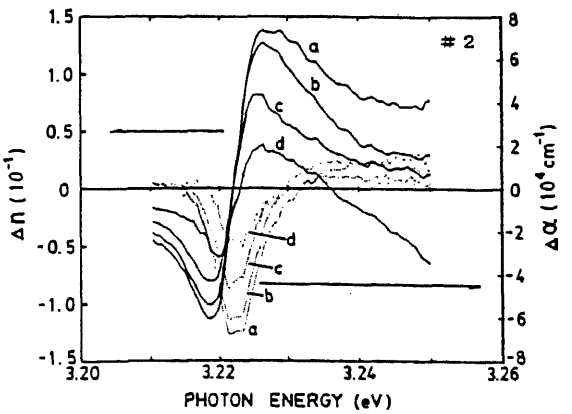

FIG. 4. Absorption change $\Delta\alpha(\omega) = \alpha(\omega, I) - \alpha(\omega, 3.1\times10^{-3}\,\mu\mathrm{J/cm^2})$ and the corresponding refractive index $\Delta n(\omega)$ for sample 2 (a = 5.7 nm). Dotted and solid lines show $\Delta\alpha(\omega)$ and $\Delta n(\omega)$, respectively. The excitation densities corresponding to a, b, c, and d are 11 800, 3430, 406, and 3.19 μJ/cm², respectively.

change in the refractive index $\Delta n(\omega)$ is obtained by the Kramers–Kronig transformation[10]:

$$\Delta n(\omega) = \frac{c}{\pi} P \int_0^\infty \frac{d\omega' \Delta\alpha(\omega')}{\omega'^2 - \omega^2}.$$

Practically, we used the data of $\alpha(\omega, I) - \alpha(\omega, 3.1\times10^{-3}\ \mu J/cm^2)$ for $\Delta\alpha(\omega)$. The change in the refractive index $\Delta n(\omega)$ is 4.0×10^{-2} under an excitation density of 3.2 $\mu J/cm^2$ (0.46 kW/cm^2) and increases to 1.4×10^{-1} under an excitation density of 11.8 mJ/cm^2 (1.7 MW/cm^2). The obtained $\Delta n(\omega)$ is larger than that observed in bulk CuCl by two orders of magnitude.[11] Figure 3 indicates that the saturation densities for samples 1 and 2 are 1.9 $\mu J/cm^2$ (270 W/cm^2) and 2.9 $\mu J/cm^2$ (420 W/cm^2), respectively. The saturation density is smaller than that reported in GaAs quantum wells,[7,12] indicating larger optical nonlinearity.

In conclusion, we experimentally demonstrated optical nonlinearity as a function of the size of CuCl microcrystals for the first time. Optical nonlinearity increases with an increase of the size of CuCl microcrystals. The observed nonlinearities are very high compared with those in bulk CuCl crystals and GaAs quantum wells. With a further increase of the size of CuCl microcrystals, a reduction of optical nonlinearity is expected. Testing the validity of this statement is necessary for a complete understanding of the optical nonlinearity due to excitons in CuCl microcrystals and remains to be studied in the future.

This work was supported in part by the Scientific Research Grant in Aid No. 62460022 from the Ministry of Education, Science and Culture of Japan.

[1]A. I. Ekimov, Al. L. Efros, and A. A. Onushchenko, Solid State Commun. 56, 921 (1985).
[2]E. Hanamura, Solid State Commun. 62, 465 (1987).
[3]E. Hanamura, Phys. Rev. B 37, 1273 (1988).
[4]T. Itoh, Solid State Phys. 23, 39 (1988) (in Japanese); T. Itoh, Y. Iwabuchi, and M. Kataoka, Phys. Status Solidi B 145, 567 (1988).
[5]N. Peyghambarian, H. M. Gibbs, J. L. Jewell, A. Antonetti, A. Migus, D. Hulin, and A. Mysyrowicz, Phys. Rev. Lett. 53, 2433 (1984).
[6]Y. Masumoto, S. Shionoya, and H. Okamoto, Opt. Commun. 53, 385 (1985).
[7]Y. Masumoto, S. Tarucha, and H. Okamoto, J. Phys. Soc. Jpn. 55, 57 (1986).
[8]D. Hulin, A. Mysyrowicz, A. Antonetti, A. Migus, W. T. Masselink, H. Morkoc, H. M. Gibbs, and N. Peyghambarian, Phys. Rev. B 33, 4389 (1986).
[9]The relation is obtained as follows. The equation, $\alpha = \alpha_1/(1 + I/I_s) + \alpha_2$, is expanded to be $\alpha = \alpha_1(1 - I/I_s) + \alpha_2$ in the weak limit of I. On the other hand, we can also obtain

$$\alpha = \alpha_1 + \alpha_2 + \frac{\mathrm{Im}\,\chi^{(3)}\omega I\{1 - \exp[-(\alpha_1 + \alpha_2)/d]\}}{\epsilon_0 n_0^2 c^2 f d(\alpha_1 + \alpha_2)}$$

by expanding Maruani's expression [see IEEE J. Quantum Electron. 18, 558 (1980)]. Then the I-dependent terms in both expressions are equated.
[10]D. A. B. Miller, C. T. Seaton, M. E. Prise, and S. D. Smith, Phys. Rev. Lett. 47, 197 (1981).
[11]The nonlinear refractive index Δn around the exciton resonance in bulk CuCl is estimated to be $\sim 3\times10^{-3}$ at an excitation density 400 kW/cm^2 at 3.2096 eV on the basis of the data by Kuwata [J. Lumin. 38, 247 (1987)].
[12]D. A. B. Miller, D. S. Chemla, D. J. Eilenberger, P. W. Smith, A. C. Gossard, and W. T. Tsang, Appl. Phys. Lett. 41, 679 (1982).

Tunneling and Relaxation of Photogenerated Carriers in Semiconductor Quantum Wells

Fumio Sasaki and Yasuaki Masumoto

Institute of Physics, University of Tsukuba, Tsukuba, Ibaraki 305, Japan

Abstract

The competition between tunneling (vertical transport) and relaxation (exciton formation) of photo-generated carriers in GaAs-$Al_{0.29}Ga_{0.71}As$ quantum wells in an electric field has been studied by using population mixing and time-correlated single photon counting techniques. In this study, a concept of a non-geminate exciton (NGE), which is made from a pair of an electron and a hole excited by different photons, is introduced to explain the experimental results. The nonlinear luminescence and photocurrent signals are qualitatively explained in terms of the competition between tunneling and relaxation. Furthermore, the heavy exciton luminescence shows two exponential decays when the electric field is 10~29kV/cm. The slow component is ascribed to the luminescence of NGE formed as a result of competition between tunneling and relaxation. Under the resonant electric field F_r=29kV/cm, where the electron sequential resonant tunneling occurs, the slow component diminishes because of increase of the electron tunneling rate.

The study of semiconductor quantum well structures under the electric field lies in one of the most attractive interdisciplinary fields of fundamental physics and application. Many interesting phenomena have been discovered concerning resonant tunneling[1-10]. In particular, relaxation and tunneling of photogenerated carriers in the semiconductor quantum wells are interesting and attractive in terms of the optical spectroscopy, because we can give artificially a variety of circumstances to photogenerated carriers by designing the semiconductor microstructures. In this work, we present the results of the study to reveal the competition between tunneling (vertical transport) and relaxation (exciton formation) of the photogenerated carriers. In the presence of the electric field along the quantum wells, some photo-generated electron-hole pairs are dissolved and fall into different wells. Then, some of them form excitons, while others move further to the next wells. The competition and the dynamical aspects of the above-mentioned processes are open problems and should be clarified. In this paper, we tried to solve the problems by means of population mixing[11,12] and time-correlated single photon counting techniques.

In the experiments, photoexcited GaAs-$Al_{0.29}Ga_{0.71}As$ semiconductor quantum wells were studied in an electric field along the quantum well growth (z direction) at 4.2K. Samples are GaAs-$Al_{0.29}Ga_{0.71}As$ quantum wells (100 alternate periods of 12nm-GaAs wells and 5.8nm-$Al_{0.29}Ga_{0.71}As$ barriers) embedded in the pin diode structure grown by molecular beam epitaxy.

For the photo-excitation source, a 7ps cavity-dumped dye laser synchronously pumped by a mode-locked Kr^+ laser was used. The excitation photon energy was 1.76eV which excites the GaAs wells selectively. Population mixing technique was adopted to study the heavy exciton

photoluminescence (I_{PL}) and the photocurrent (I_{PC}) as a function of the external electric voltage (V_{ext}). The technique is suitable to detect the small nonlinearity in the photoluminescence and the photocurrent. Two equally split laser beams were chopped at different frequencies, ω_1 and ω_2. By using an optical delay, both the laser beams were adjusted to hit the sample simultaneously. By using the lock-in technique, photoluminescence and photocurrent modulated at ω_1, ω_2, $\omega_1+\omega_2$ and $\omega_1-\omega_2$ frequencies were analyzed. In the population mixing experiment, the spectrally integrated intensity of the exciton luminescence was detected by using color filters and a photomultiplier (HAMAMATSU R1477). In the time-correlated single photon counting experiment, the exciton luminescence peak was temporally analyzed with spectral width of about 0.2nm.

Here we introduce a concept of non-geminate exciton (NGE) to interpret the nonlinearity in photoluminescence and photocurrent. Under sufficiently low density excitation, an exciton is formed from a geminate electron-hole pair which is generated by a single photon. The population of such geminate exciton (GE) is modulated at frequencies ω_1 and ω_2 in our experimental condition. On the other hand, an exciton can be formed from a non-geminate pair of an electron and a hole which are generated by different photons, if pair dissociation or exciton mutual collision is present. We call this exciton non-geminate exciton (NGE). The NGE formation gives $\omega_1+\omega_2$ and $\omega_1-\omega_2$ components as well as ω_1 and ω_2 components to photoluminescence and photocurrent[13]. In other words, by measuring the $\omega_1+\omega_2$ or $\omega_1-\omega_2$ component, we can detect the NGE signal selectively, because the $\omega_1+\omega_2$ and $\omega_1-\omega_2$ component sensitively reflect the nonlinearity.

The detection of the population mixing components gives us the knowledge about the competition between tunneling and relaxation, as described below. When an electron-hole pair is dissolved from an exciton by the electric field, it undergoes two processes, NGE formation and tunneling. Then, the NGE photoluminescence intensity (I_{PL}^{NGE}) is expressed by the branching ratios of two processes, and described by

$$I_{PL}^{NGE} = \frac{1/\tau_f}{1/\tau_t + 1/\tau_f} n_e \quad , \qquad (1)$$

where $1/\tau_f$, $1/\tau_t$ and n_e denote the NGE formation rate, the electron tunneling rate and the photo-excited electron density, respectively. The NGE formation rate $1/\tau_f$ is considered to be proportional to the hole density, so that $1/\tau_f$ is proportional to the excitation density, I_{ex}. On the other hand, $1/\tau_t$ depends on the electric field, but not on the excitation density. Therefore, one obtains

$$I_{PL}^{NGE} \propto \begin{cases} I_{ex} & (1/\tau_t \ll 1/\tau_f) \quad , \qquad (2.\ a) \\ I_{ex}^{2} & (1/\tau_t \gg 1/\tau_f) \quad . \qquad (2.\ b) \end{cases}$$

Intuitive explanation of power dependence is as follows. Supposing the inequality $1/\tau_t \ll 1/\tau_f$ holds, almost all photo-generated carriers form excitons. Therefore, I_{PL}^{NGE} is proportional to the excitation density. On

the contrary, if the inequality $1/\tau_t >> 1/\tau_f$ holds, the photo-generated carriers are likely to go to the tunneling process. Therefore, I_{PL}^{NGE} is proportional to the square of the excitation density. In order to vary $1/\tau_f$ artificially, we changed the overlap of two beams as well as the excitation density.[14] The measurements were performed under three excitation conditions described below.

(1) The excitation pulse repetition frequency is 4MHz, and spot centers of two laser beams are spacially away from each other by about 300μm.

(2) The excitation pulse repetition frequency is 4MHz, and two laser beam spots are completely overlapped.

(3) The excitation pulse repetition frequency is 41MHz, and two laser beam spots are completely overlapped.

In all cases, the spot size was about 150μm in diameter. The spot size and the beam overlap configuration were carefully checked by using the stereomicroscope.

Figures 1 and 2 show the results under the excitation conditions, (1) and (2), respectively. Here, the electric field, F, estimated by the Stark shift of the heavy exciton luminescence peak is shown as the uppermost scale.[2,5] Photoluminescence spectra were the same that already reported in ref 5. The top parts in Figs. 1 and 2 show ω_1 components of I_{PL} and I_{PC} vs. V_{ext}. Two step-like changes are observed in the curves of I_{PL} and I_{PC}. The step-like changes, B (F=28kV/cm) and A (F=8kV/cm), are identified to be electron sequential resonant tunneling and exciton dissociation followed by electron tunneling, respectively.[3,6] Between two step-like changes there

is a plateau. With the increase of the excitation density, I_{PL} increases supralinearly, while I_{PC} increases sublinearly at the plateau region. Here, we note that the nonlinearity for the excitation density is observed in the common electric field. Therefore, the nonlinearity can not be explained in terms of the field screening[10]. If a constant multiplies I_{PL} so as to equalize the I_{PL} maximum value to the I_{PC} maximum value, the sum of both signals is almost independent of V_{ext}, as shown in Figs. 1 and 2. This means that photocurrent behaves as a complement of photoluminescence.[7] Taking account of the absorption and reflection of incident light at the cap layer, the carrier number excited in all the quantum wells is estimated to be 2×10^{13} s^{-1} in the case of right-hand side of Fig. 2. The value corresponds to 3μA. This agrees with the measured I_{PC} maximum within an order of magnitude. This means that almost all the photo-generated carriers contribute to photoluminescence or photocurrent.

The middle parts of Figs. 1 and 2 show the $\omega_1+\omega_2$ component of I_{PL}. Prominent structures C and D are seen in the $\omega_1+\omega_2$ spectra in both Figs. 1 and 2. A structure E is seen in Fig. 2, while not in Fig. 1. In the excitation condition (3), the $\omega_1+\omega_2$ spectra of I_{PL} are almost the same as those in the excitation condition (2). As already reported, the $\omega_1+\omega_2$ component of I_{PC} has almost the same profile with I_{PL}, because the increase of photoluminescence corresponds to decrease of photocurrent in the $\omega_1+\omega_2$ component.[7] By moving the optical delay, we can obtain the temporal information about the $\omega_1+\omega_2$ component. The $\omega_1+\omega_2$ components of I_{PL} and I_{PC} were found to change little within 3ns of the pulse separation.

Excitation density dependences of structures, C, D and E, are different from one another. They depend on the excitation conditions. In the excitation condition (1), the intensity of C was found to be almost proportional to I_{ex}, and that of D was found to be almost proportional to I_{ex}^{2}.[7] Two asymptotic expressions in eq. (2) hold for C and D, respectively. In the excitation condition (2), on the other hand, the excitation density dependences of each structures are more complicated, and do not follow the simple power law. The excitation density dependence of structures, C, D and E, in turn grows stronger. In the excitation condition (3), the intensities of C and D are found to be almost proportional to I_{ex}. The excitation density dependence of E is similar to that in the excitation condition (2).

The electron tunneling rate $1/\tau_t$ is estimated by using double barrier transmission coefficient (T_b) in WKB approximation[15,16]. Here we neglect the hole tunneling, because hole effective mass is much heavier than electron effective mass. We use the formula $1/\tau_t=v_z T_b/2L_z$, where $2L_z/v_z$ corresponds to the classical period of the electron motion in the quantum well, v_z to the z component of the electron velocity and L_z to the well width. The result is shown in the bottom parts of Figs. 1 and 2 for each case. In the calculation, we used the following assumptions. We used the 57:43 band gap split, corresponding to the conduction-band discontinuity of 206meV. We assumed the input electron kinetic energy as 55meV in order to fit the calculated value of resonant electric field to the experimental one.

On the other hand, to estimate the NGE formation rate $1/\tau_f$, we use two-dimensional collision model for rigid disk. An electron tunneling to the

next well moves along the layer, collides with a hole and forms the NGE. In this model the NGE formation rate is expressed by

$$1/\tau_f = 2n_e a_B v_0 \quad ,$$
$$v_0 = v_e - v_h \quad , \qquad (3)$$

where a_B and v_e (v_h) denote the exciton Bohr radius (=13.6nm) and electron (hole) velocity, respectively. In the equation, the hole density is assumed to be equal to the electron density. If the electron-hole system is in thermal equilibrium with lattices, v_i (i=e,h) corresponds to thermal velocity. In the presence of electric field, however, the carrier system is considered to be hot and v_i is assumed to be represented by $(2eFd/m_i)^{1/2}$, where d and m_i (i=e,h) denote one period of superlattices and effective mass ($m_e=0.067m_0$ for an electron and $m_h=0.34m_0$ for a heavy hole), respectively.[9] This assumption is wrong if the NGE formation rate is smaller than hot carrier cooling rate. However, the upper limit of the NGE formation rate is estimated in this way.

In the excitation condition (1), two beams are spacially away from each other, so that the NGE formation rate $1/\tau_f$ is considered to be slower than that in excitation condition (2). In this case, the NGE formation rate observed in the $\omega_1+\omega_2$ component is estimated by using the carrier density at the center position of two beams in the excitation condition (1). We assumed spatial carrier distribution to have a Gaussian profile, because the laser beam has a Gaussian profile.

In the excitation condition (1), the carrier density contributing to the $\omega_1+\omega_2$ component is small enough, so that the NGE formation rate is slower than the tunneling rate, as shown in bottom part of Fig. 1. Then, the eq.(2. b) holds around the structure D. In the excitation condition (2), the carrier density contributing to the $\omega_1+\omega_2$ component is large enough, so that the NGE formation rate is comparable with the tunneling rate under low density excitation and faster than the tunneling rate under high density excitation, except for the case around the resonant tunneling. Then, the eq. (2. b) no longer holds around the structure D. In the resonant tunneling case the NGE is not formed as a result of the resonant enhancement of electron tunneling rate. Therefore the dip between D and E in Fig. 2 arises.

In the excitation condition (3), the carrier density excited by one pulse is smaller than the excitation condition (1) and (2), but temporal as well as spatial overlap of two beams was good, because the excitation pulse repetition rate is more than ten times larger than that in other two conditions. Then, NGE is formed from an electron (a hole) generated by a pulse and a hole (an electron) generated by the next pulse, so that the NGE formation rate $1/\tau_f$ is considered to be faster than electron tunneling rate $1/\tau_t$ when the electric field is below 28kV/cm. Therefore, the intensities of C and D are proportional to I_{ex} in the case of condition (3), following the eq. (2. a).

When the excitation density is high enough, the structure E is observed in the ω_1 and $\omega_1+\omega_2$ components (see the right part of Fig. 2). This means that the NGE formation rate is faster than the tunneling rate at F=42kV/cm, as expected from the calculated results (see the bottom parts of Figs. 1 and 2.). Therefore, some NGE's are formed at F=42kV/cm, and the structure B in

the ω_1 component has a peak shape in the high density excitation. Under low density excitation the NGE formation rate is much slower than the tunneling rate, so that the structure E is not observed.

We note that the NGE formation gives ω_1 and ω_2 components to I_{PL} and I_{PC} [13]. In order to see this feature, we define the critical electric field F_c at which the ω_1 components of I_{PL} and I_{PC} are equal to each other. The critical field F_c depends on the excited carrier density, as shown in Fig. 3. With the increase of the excited carrier density, F_c increases like a step. The ω_1 components of I_{PL} and I_{PC} at F_c were found to be proportional to the excitation density, independent of the excitation conditions.

At the critical field F_c, the electron tunneling process equilibrates with the exciton formation process, so that the ratio of the electron tunneling rate to the exciton formation rate is considered to be constant. Therefore, it is reasonable that ω_1 components of I_{PL} and I_{PC} at F_c are proportional to the excitation density, as is expected from eq. (1). The increase of F_c as well as supralinearity of I_{PL} for the excitation density is explained by the formation of NGE. When the excitation density is low, the NGE formation is small. Then, it is considered that the once formed excitons do not dissociate and go through radiative recombination at about 10kV/cm. On the other hand, the higher the excitation density, the faster the NGE formation. Therefore, the high field is required in order to equalize the carrier number contributing to photocurrent to that contributing to photoluminescence. The reason why the F_c does not increase beyond 20kV/cm is ascribed to the resonant enhancement of $1/\tau_t$.

So far, we have seen the results of population mixing experiment in terms of the NGE model, but another possibility yielding the population mixing component exists. It is the field screening effect by the photo-excited carriers. If the slight electric field difference between under irradiation of two beams and under that of one beam exists, the difference is reflected in the population mixing component as differential form, $\frac{dI_P}{dF}\delta F$ (P=PL,PC). Here, F denotes the electric field and δF denotes the field difference, respectively. The field difference was estimated experimentally and quantitatively. As a result, it was found to be smaller than that of our detection limit which is about 1kV/cm. Thus we omit the possibility. Anyway, it is impossible to explain our results qualitatively and systematically in terms of the field screening.

Figure 4 shows the results of time-resolved heavy exciton photoluminescence.[7] It was obtained in the excitation condition (2). When the electric field F is between 10kV/cm and 29 kV/cm, the temporal change of the heavy exciton luminescence consists of two decay components. The fast one decays in several hundred picosecond, and the slow one in several ten nanosecond, depending on the electric field and excitation density. The slow component is considered to be ascribed to the luminescence of the NGE's formed as a result of the repetitions of exciton dissociation, electron tunneling and exciton formation. In fact, in the flat band condition ($V_{ext}=1.6\pm0.2V$) the slow component is not seen. The results are consistent with those of time resolved population mixing experiment. Because of the slow decay constant of NGE's, population mixing components of I_{PL} and I_{PC} change little within 3ns. At the resonant field of $F_r=2.9\times10^4$V/cm, where the electron sequential resonant tunneling occurs, the slow decay component

diminishes. This is because electron tunneling rate is fast enough not to form NGE as expected from the calculation shown in bottom parts of Figs. 1 and 2. The same phenomena were also observed consistently in the same sample by the time-resolved photocurrent measurement.[8] Above F_r, the single long decay component is observed only under high density excitation. In this condition the NGE luminescence alone is observed, because the NGE formation rate is faster than the tunneling rate. On the other hand, under the low density excitation the exciton luminescence is not seen above F_r. This is because the NGE formation rate is much slower than the tunneling rate. These time-resolved results are consistent with the results obtained by the population mixing spectroscopy.

In summary, we investigated the competition between tunneling and relaxation of photogenerated carriers in GaAs-$Al_{0.29}Ga_{0.71}As$ multi-quantum-wells in a perpendicular electric field by using population mixing and time-correlated single photon counting. We introduce the concept of non-geminate exciton (NGE) to explain the results. The NGE gives the slow decay component to the heavy exciton luminescence. The slow decay component diminishes at the condition of the sequential resonant tunneling because the electron tunneling rate is overwhelmingly faster than the exciton formation rate. The change of population mixing component as a function of the excitation density is explained in terms of the competition between tunneling and relaxation. The time-resolved results are also explained consistently in terms of the competition between tunneling and relaxation.

The authors would like to thank Drs. H. Okamoto and S. Tarucha at Nippon Telegraph and Telephone Corporation for providing high-quality samples. This work was supported by Scientific Research Grant-in-Aid #62460022 from the Ministry of Education, Science and Culture of Japan. It

was also supported by the Mitsubishi Foundation.

References

(1) R. Tsu and L. Esaki, Appl. Phys. Lett. 22, 562 (1973).

(2) G. Bastard, E. E. Mendez, L. L. Chang, and L. Esaki, Phys. Rev. B28, 3241 (1983).

(3) F. Capasso, K. Mohammed, and A. Y. Cho, IEEE J. Quantum. Electron. QE-22, 1853 (1986).

(4) H. -J. Polland, K. Kohler, L. Schultheis, J. Kuhl, O. Gobel, and C. W. Tu, Superlatt. Microstruct. 2, 309 (1986).

(5) Y. Masumoto, S. Tarucha and H. Okamoto, Phys. Rev. B33, 5961 (1986).

(6) Y. Masumoto and F. Sasaki, J. Lumin. 40/41, 709 (1987).

(7) Y. Masumoto and F. Sasaki, J. Lumin. 38, 285 (1987).

(8) S. Tarucha, K. Ploog and K. von Klitzing, Phys. Rev. B36, 4558 (1987).

(9) R. C. Miller, D. A. Kleinman, and A. C. Gossard, Phys. Rev. B29, 7085 (1984).

(10) J.A.Kash, E. E. Mendez and H. Morkoc, Appl. Phys. Lett. 46, 173 (1985).

(11) D. von der Linde, J. Kuhl and E. Rosengart, J. Lumin. 24/25, 675 (1981).

(12) D. Rosen, A. G. Doukas, Y. Budansky, A. Katz and R. R. Alfano, Appl. Phys. Lett. 39, 935 (1981).

(13) Here, we note that the NGE formation gives ω_1 and ω_2 components as well as $\omega_1+\omega_2$ and $\omega_1-\omega_2$ components to photoluminescence and photocurrent. NGE population is represented by the product of electron and hole densities. In our experiment, the electron and hole densities are modulated at frequencies, ω_1 and ω_2. If we take account of up to the second term in Fourier components, the temporal change of both the densities are approximately expressed by $n_1(1+\cos\omega_1 t)+n_2(1+\cos\omega_2 t)$, because the modulation has the form of an on-off wave. Here n_i $(i=1,2)$ represents the carrier density excited

by ω_i light. As a result, the product of electron and hole densities give the ω_1, ω_2, $2\omega_1$, $2\omega_2$, $\omega_1+\omega_2$ and $\omega_1-\omega_2$ components.

(14) Here, we note that $1/\tau_f$ depends on the overlap of two beams and the excitation density, and that the change of the $1/\tau_f$ varies all of the ω_1, ω_2, $\omega_1+\omega_2$, and $\omega_1-\omega_2$ components. The ω_1 and ω_2 components do not seriously depend on the overlap of two beams, while $\omega_1+\omega_2$ and $\omega_1-\omega_2$ components seriously depend on it. This is because the $\omega_1+\omega_2$ and $\omega_1-\omega_2$ components reflect only the NGE that is formed by an electron (a hole) excited by one beam and a hole (an electron) excited by another.

(15) R. H. Davis and H. H. Hosack, J. Appl. Phys. 34, 864 (1963).

(16) D. Bohm, Quantum Theory (Prentice-Hall, Englewood Cliffs, 1951), Chap. 12

Figure Captions

Fig. 1. Heavy exciton luminescence intensity and photocurrent observed in GaAs-$Al_{0.29}Ga_{0.71}As$ superlattices as a function of external electric voltage in the excitation condition (1) (4MHz, bad overlap) described in the text. The upper parts represent ω_1 component of I_{PL} (broken line), I_{PC} (solid line) and $(I_{PL}+I_{PC})/2$ (dotted line). The middle parts represent $\omega_1+\omega_2$ component of I_{PL}. The bottom part is the calculated result of the NGE formation rate $1/\tau_f$ and the tunneling rate $1/\tau_t$. Dotted and broken lines show $1/\tau_f$ at 26mW/cm^2 and 330mW/cm^2 excitation, respectively. The solid line shows $1/\tau_t$.

Fig. 2. Heavy exciton luminescence intensity and photocurrent observed in GaAs-$Al_{0.29}Ga_{0.71}As$ superlattices as a function of external electric voltage in the excitation condition (2) (4MHz, good overlap) described in the text. The upper parts represent ω_1 component of I_{PL} (broken line), I_{PC} (solid line) and $(I_{PL}+I_{PC})/2$ (dotted line). The middle parts represent $\omega_1+\omega_2$ component of I_{PL}. The bottom part is the calculated result of of the NGE formation rate $1/\tau_f$ and the tunneling rate $1/\tau_t$. Dotted and broken lines show $1/\tau_f$ at 7.7mW/cm^2 and 120mW/cm^2 excitation, respectively. The solid line shows $1/\tau_t$.

Fig. 3. Critical field F_c vs. the excited carrier density. Closed circles correspond to the excitation condition (1) (4MHz, bad overlap), open circles

to the excitation condition (2) (4MHz, good overlap), and closed squares to the excitation condition (3) (41MHz, good overlap), respectively.

Fig. 4. Temporal profile of the heavy exciton luminescence obtained by time-correlated single photon counting. The estimated electric fields in the MQW are 0, 22, 28, 42kV/cm for the applied voltages of 1.4, -3.2, -6.1, -8.8V, respectively.

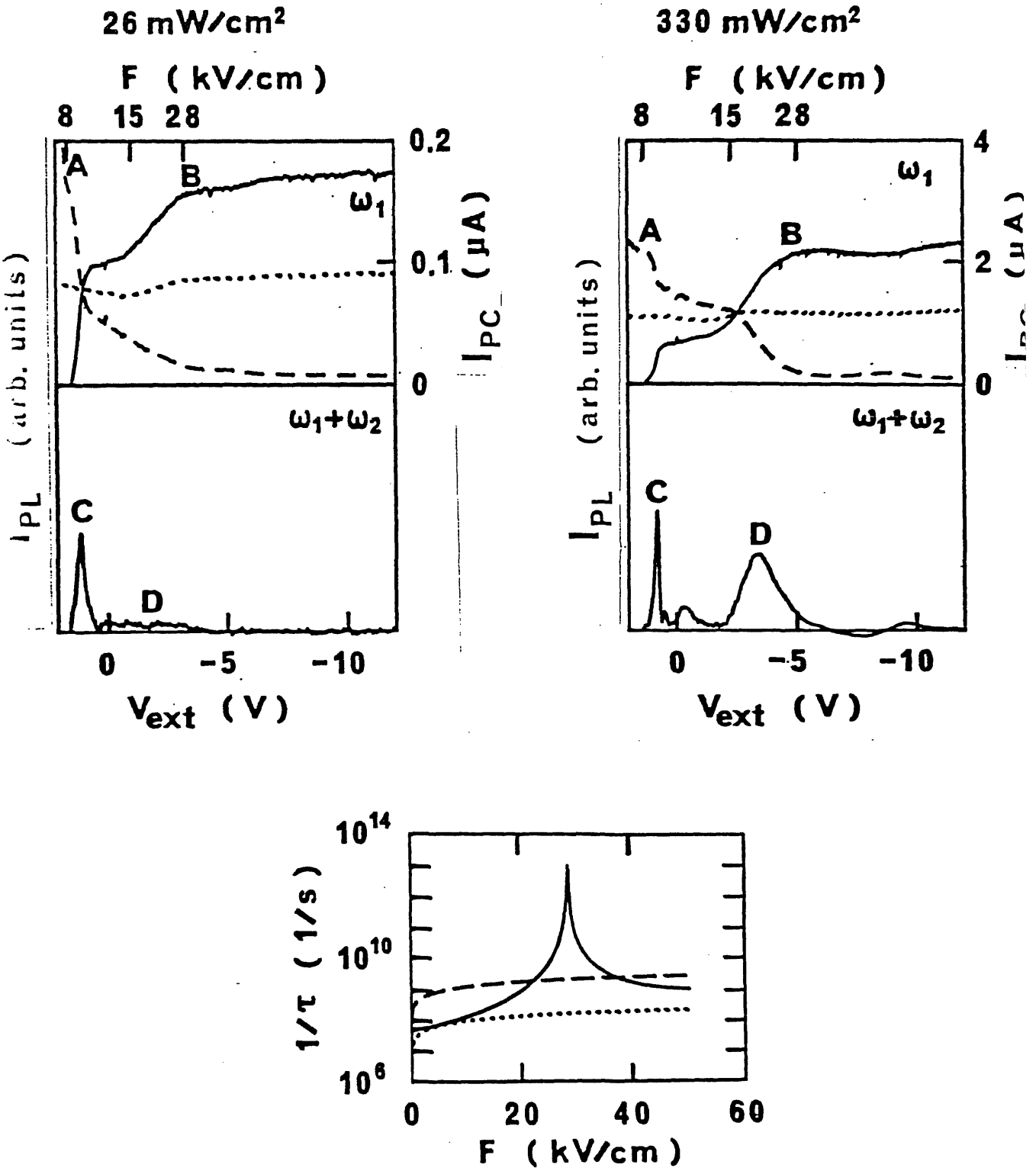
26 mW/cm²
F (kV/cm)
8 15 28
A
B
ω1
0.2
0.1
0
I_PC (μA)
I_PL (arb. units)
ω1+ω2
C
D
0 -5 -10
V_ext (V)
330 mW/cm²
F (kV/cm)
8 15 28
ω1
A
B
4
2
0
I_PC (μA)
I_PL (arb. units)
ω1+ω2
C
D
0 -5 -10
V_ext (V)
10^14
10^10
10^6
1/τ (1/s)
0 20 40 60
F (kV/cm)

Fig - 1

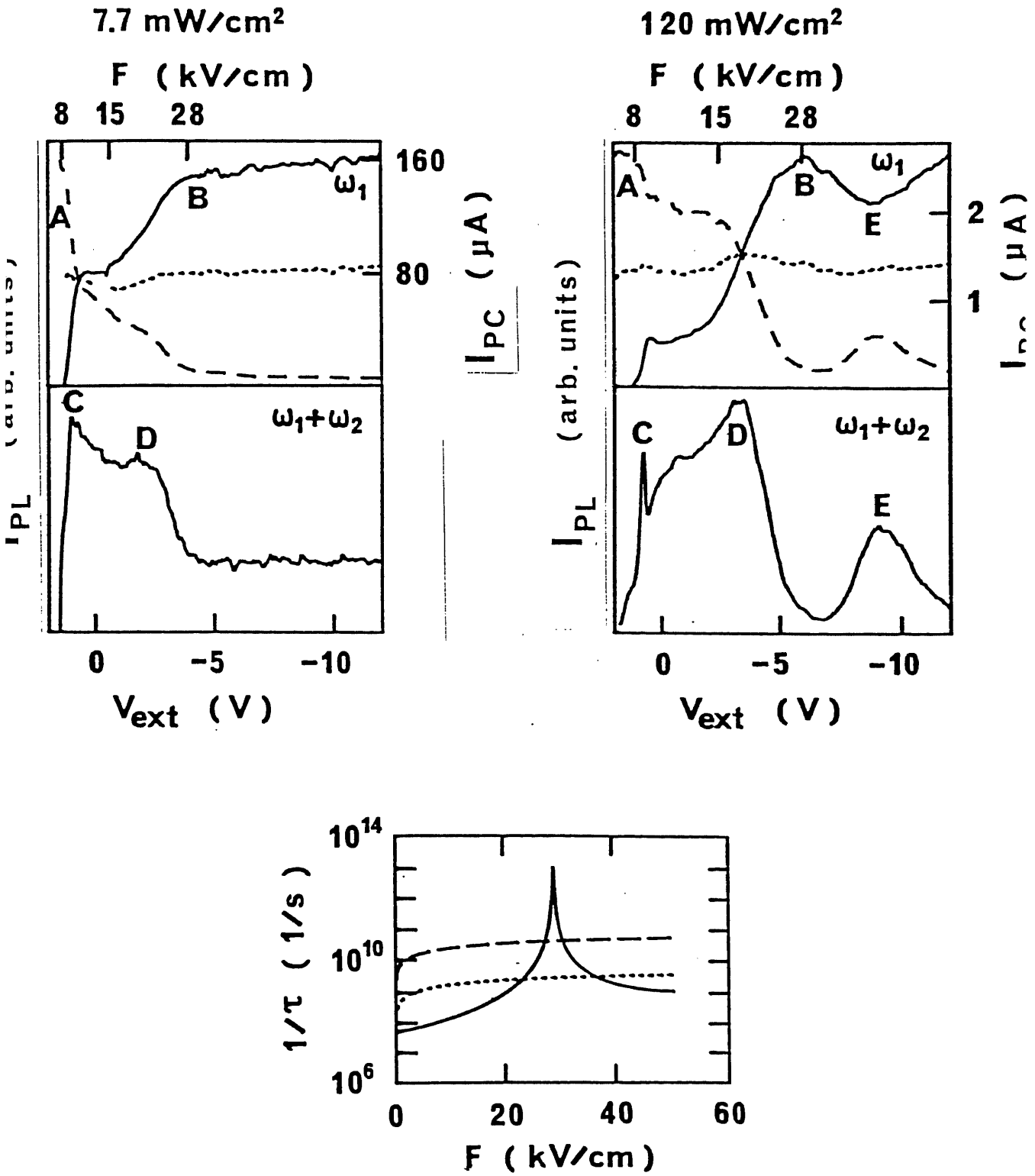
7.7 mW/cm²
F (kV/cm)
8 15 28
A
B
ω1
160
80
I_PC (μA)
C
D
ω1+ω2
I_PL (arb. units)
0 -5 -10
V_ext (V)
120 mW/cm²
F (kV/cm)
8 15 28
A
B
ω1
E
2
1
C
D
ω1+ω2
E
0 -5 -10
V_ext (V)
1/τ (1/s)
10^14
10^10
10^6
0 20 40 60
F (kV/cm)

Fig -3

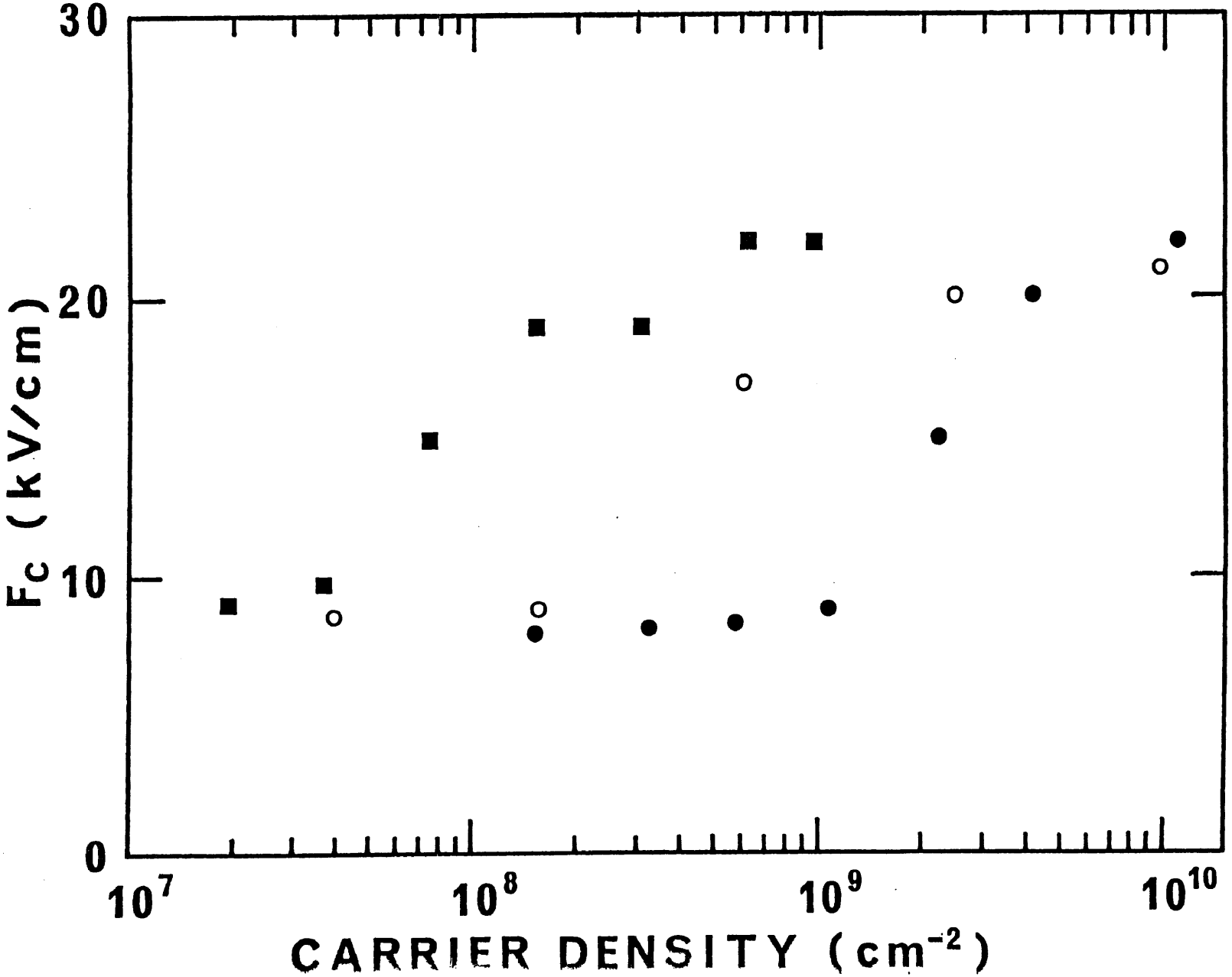

Fig-3

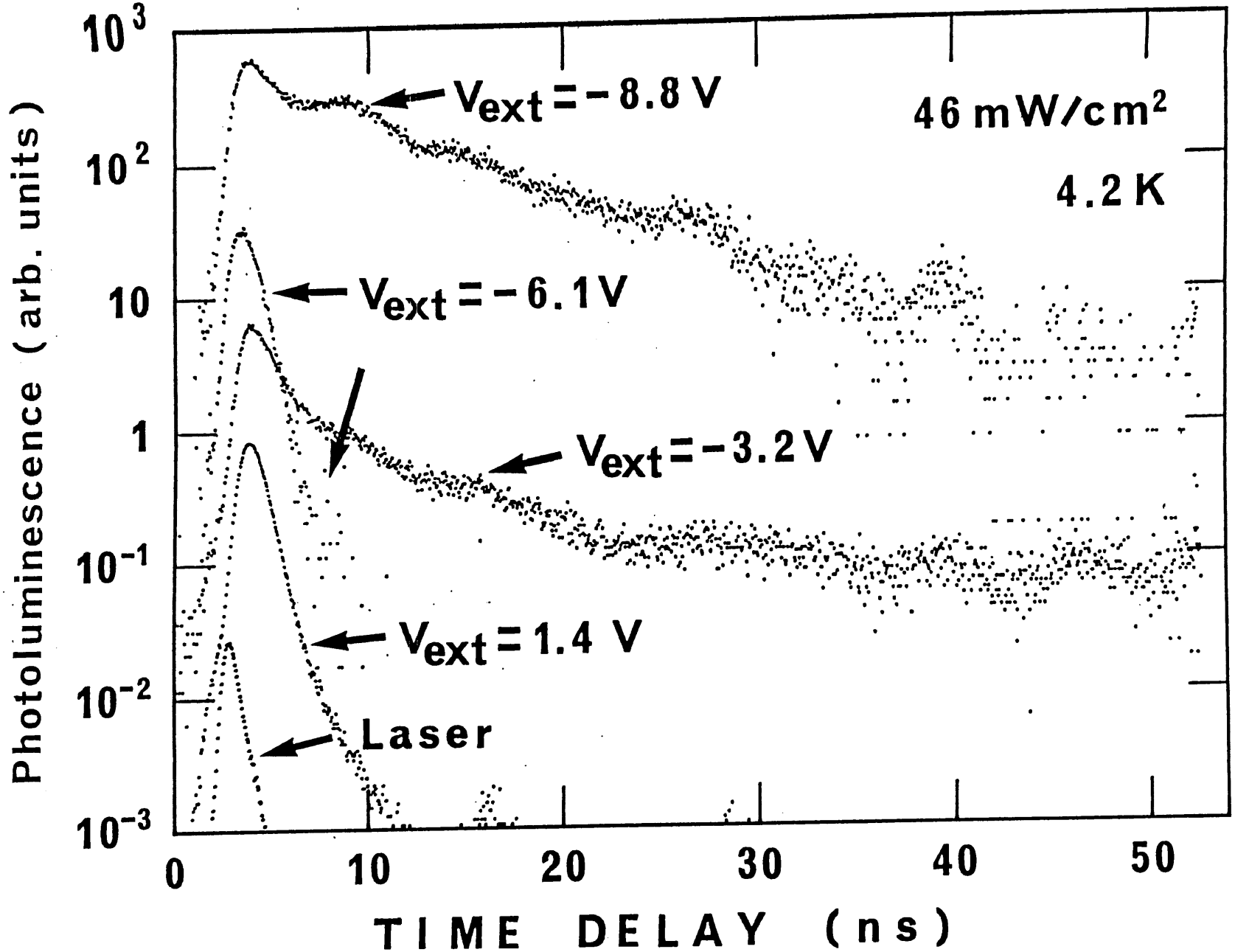
Photoluminescence (arb. units)
10^3
10^2
10
1
10^{-1}
10^{-2}
10^{-3}
$V_{ext} = -8.8$ V
$V_{ext} = -6.1$ V
$V_{ext} = -3.2$ V
$V_{ext} = 1.4$ V
Laser
46 mW/cm^2
4.2 K
0
10
20
30
40
50
TIME DELAY (ns)

Fig.-4

Interlayer Γ-X scattering in staggered-alignment $Al_{0.34}Ga_{0.66}As$-AlAs ternary alloy multi-quantum-well structures

Yasuaki Masumoto, Tomobumi Mishina, Fumio Sasaki and Mitsuhiro Adachi

Institute of Physics, University of Tsukuba, Tsukuba, Ibaraki 305, Japan

Abstract

The interlayer Γ-X scattering rate of photoexcited electrons was measured in staggered-alignment $Al_{0.34}Ga_{0.66}As$-AlAs ternary alloy multi-quantum-well structures for the first time. The scattering process was directly probed by the femtosecond pump-and-probe spectroscopy. The mean Γ-X scattering time of electrons across the interface between $Al_{0.34}Ga_{0.66}As$ layers and AlAs layers at 4.2K is determined to be 1.2 ps, which is 20 times slower than that observed in bulk GaAs at 295K. The slowing mechanism is ascribed to the small penetration of the evanescent Γ electrons into the AlAs barrier layers.

The recent femtosecond spectroscopy has opened the possibility to explore the ultrafast relaxation processes of photoexcited carriers in semiconductors. Especially, ultrafast intervalley scattering of photoexcited electrons in bulk semiconductors, GaAs and $Al_xGa_{1-x}As$, was investigated by the state-of-the-art laser technology.[1-4] One of the next targets of the ultrafast laser technology is to extend its versatility to a variety of materials and to explore new physics. In this work, we investigated the interlayer Γ-X scattering processes of electrons in staggered-alignment $Al_{0.34}Ga_{0.66}As$-AlAs ternary alloy multi-quantum-well structures. In $Al_xGa_{1-x}As$-AlAs ternary alloy multi-quantum-well structures, Γ electron state in the $Al_xGa_{1-x}As$ well layer crosses X electron state in the AlAs layer at a certain value of x.[5-8] When the $Al_xGa_{1-x}As$ layer thickness is 10nm, the crossover was expected to occur at the Al composition of 0.2 and was verified experimentally.[8] Around the Γ-X crossover, the interlayer Γ-X scattering processes are expected to occur. Therefore, we can study dynamically the interlayer Γ-X scattering processes of electrons, by measuring the temporal change of the number of photogenerated Γ-electrons in $Al_xGa_{1-x}As$ layers around Γ-X crossover.

In this work, two samples were investigated. One is 100 alternate layers of 11.8 nm $Al_{0.12}Ga_{0.88}As$ and 4.2 nm AlAs. The other is 100 alternate layers of 9.2 nm $Al_{0.34}Ga_{0.66}As$ and 2.7 nm AlAs. The luminescence and nonlinear absorption study of them were already reported by one of us. The study informed us the band offset ratio and the relevant energy levels for our samples. Energy level diagrams corresponding to two samples are schematically shown in Fig.1. Two samples are representatives situated at both the sides of the interlayer Γ-X crossover. In the sample $Al_{0.12}Ga_{0.88}As$-AlAs, the Γ electron state in the $Al_{0.12}Ga_{0.88}As$ layer is lower than the X, L and Γ electron states in the AlAs

layer. The sample is nested alignment, type I, multi-quantum-well structures. In the $Al_{0.34}Ga_{0.66}As$-AlAs sample, on the other hand, the X electron state in the AlAs layer is lower than the Γ electron state in the $Al_{0.34}Ga_{0.66}As$ layer. The sample is staggered alignment, staggered type II, multi-quantum-well structures. Comparing two samples, the additional relaxation path, the interlayer transfer of Γ electron in the $Al_{0.34}Ga_{0.66}As$ layer to the X state in the AlAs layer, is expected for the electrons at the bottom of the wells in the sample $Al_{0.34}Ga_{0.66}As$-AlAs but not in the sample $Al_{0.12}Ga_{0.88}As$-AlAs. Therefore, our experiments are motivated to clarify the difference in dynamics of photoexcited electrons in two samples and the mechanism of the interlayer Γ-X intervalley scattering.

Samples directly immersed in liquid helium were investigated. The experiment was performed using femtosecond pump and probe spectrometer developed by us. The laser system was composed of a CW mode-locked Nd^{3+}:YAG laser, the first-stage pulse compressor, a second harmonic generator, a synchronously pumped cavity-dumped dye laser, the second-stage pulse compressor and a dye amplifier pumped by a Q-switched Nd^{3+}: YAG laser. The power of the laser pulses (583 nm) was 400 μJ with the pulse duration of 260 fs, which easily generates white continuum pulses. Pump and probe experiments were performed by using 583 nm pump pulses going through an optical delay and the white continuum pulses. Pump pulses (583 nm) hitted the sample with the power density of 700 $\mu J/cm^2$. The white continuum probe pulses transmitted through the center of the pumped region of the sample were spectrally analyzed by a 25 cm monochromator, an optical multi-channel analyzer and a computer. The temporal change of the absorption was observed by the monochromator, a photomultiplier and a Boxcar

integrator with the variation of the optical delay controlled by the computer. In the inset of Figs. 2 and 3, the absorption spectra around the lowest energy exciton resonance (Γ-Γ, n=1) are shown. As is shown, the exciton structure is clearly observed without the pump. However, the structure is bleached under the pump. The temporal change of the absorption coefficient $\Delta\alpha$ around the lowest energy exciton resonance for two samples are plotted in Figs. 2 and 3, respectively. In the sample $Al_{0.12}Ga_{0.88}As$-AlAs, $\Delta\alpha$ decreases at a time constant of 1.7 ps, and then is kept constant. In the sample $Al_{0.34}Ga_{0.66}As$-AlAs, on the other hand, $\Delta\alpha$ drops at a rise time of 1.2 ps, and then increases at a decay time of 1.2 ps with a successive constant tail. The constant tail remains untill 400ps. The fitting is a convoluted result with the convolution of squares of sech functions, where the half width of the convolution is 400 fs. This observation is similar to the results by Becker et al.[4] if the time scale of their result is expanded by about two orders of magnitude.

Here, we must note the mechanism of the exciton bleaching and what the bleaching intensity stands for. In our experimental situation, the band-to-band excitation at 4.2K, the exciton bleaching is considered to occur as a result of the phase-space filling and exchange effects.[9,10] Therefore, the bleaching intensity is mostly proportional to the Γ electron population at the bottom of the well.

In the sample $Al_{0.34}Ga_{0.66}As$-AlAs, the Γ electron state in $Al_{0.34}Ga_{0.66}As$ is higher than the X electron state in AlAs by 100 meV. Therefore the interlayer transfer of the Γ electrons in the $Al_{0.34}Ga_{0.66}As$ layer to the X electron state in the AlAs layer is possible. We estimated the interlayer relaxation rate by the penetration of the Γ electron wavefunction to the AlAs layer and the Γ-X scattering rate of electrons in AlAs, as shown in the next

paragraph. Fortunately, the Γ-X phonon scattering rate of electrons in GaAs has been a current target of the state-of-the-art ultrafast laser spectroscopy.[1-4] The mean Γ-X scattering time of electrons in GaAs was measured to be 55 fs at 295 K by the femtosecond pump and probe spectroscopy.[4] The time almost agrees with the calculated one on the model of the intervalley scattering with the emission and absorption of optical phonons.[1] The scattering rate is governed by the deformation potential. Because the deformation potential of AlAs is not known, the Γ-X scattering rate of electrons in AlAs is assumed to be equal to that in GaAs.[11]

To interprete our observation, we estimated the interlayer Γ-X transfer rate by the simplest method described below. The penetration of the Γ electron wavefunction to the AlAs layer is estimated by the envelope function approximation of Bastard.[12] We solved the effective mass equation

$$[-\hbar^2\nabla^2/2m^*(z)-E-V(z)]F(z)=0,$$

where z is the the direction of superlattice growth, F(z) is the envelope function, V(z) the potential profile and $m^*(z)$ the electron effective mass. The boundary conditions are given by the continuity of both F(z) and $1/m^*(z)(\partial F/\partial z)$. Numerical calculations for $Al_{0.34}Ga_{0.66}As$-AlAs were carried out with the following parameters, the electron effective mass in $Al_{0.34}Ga_{0.66}As$ 0.095 m_0, that in AlAs 0.15 m_0, the potential energy gap 0.783 eV and the well width 9.2 nm.[8,11,13] The potential energy gaps for our samples were determined by the band offset ratio of 0.66:0.34 obtained experimentally.[8] The calculated result is shown in Fig.4. The penetration probability of the Γ electrons, that is the square of the evanescent Γ wavefunction in the AlAs layer is estimated

to be 0.68% of the total. The interlayer Γ-X scattering rate is estimated by the Γ-X scattering rate in AlAs divided by the probability of the Γ electron wavefunction in AlAs. Thus the mean interlayer Γ-X scattering time is estimated to be 4.9 ps by dividing 55 fs by 0.0068 and the ratio of the phonon factor [2N(295)+1]/[2N(4.2)+1] = 1.66, where N(T) is the longitudinal optical phonon occupation number at temperature T. The observed decay time of the exciton population agrees with the estimation within an order of magnitude. Although the envelope function approximation is simplest, we believe that it well discribes the real situation at the interface. The more sophisticated calculation, for example, that on the basis of the interface matrix approach or the interface roughness scattering approach may be useful for the better understanding of the interlayer Γ-X intervalley scattering.[14,15)]

Comparing our results with those by the preceding authors who investigated the ultrafast intervalley scattering[1-4)], we can fully understand the rise as well as decay of the exciton bleaching in two samples. In the sample $Al_{0.12}Ga_{0.88}As$-AlAs, the X and L electron states in $Al_{0.12}Ga_{0.88}As$ are higher than the Γ electron state in $Al_{0.12}Ga_{0.88}As$ by 0.34 eV and 0.21 eV, respectively. The X electron state in AlAs is higher than the Γ electron state in $Al_{0.12}Ga_{0.88}As$ by 0.06 eV. The pump laser energy is 2.12 eV which is higher than the X electron state in $Al_{0.12}Ga_{0.88}As$ by 0.1 eV. Therefore, the electron-electron scattering, Fröhlich-type LO phonon scattering, Γ-X, Γ-L, Γ-X-Γ and Γ-L-Γ intervalley scattering take place frequently in the $Al_{0.12}Ga_{0.88}As$ layer. The intervalley scattering mechanism works to slow down the cooling of Γ electron temperature. Because the exciton bleaching is proportinal to the Γ electron population at the bottom of the well, the rise of the exciton bleaching at a time constant of 1.7 ps is understood consistently with the results by Shah et

al[3]. Then, the electron population slowly decreases as a result of the competiton between the electron cooling and the radiative and nonradiative annihilations. In the sample $Al_{0.34}Ga_{0.66}As$-AlAs, on the other hand, the X electron state in AlAs is lower than the Γ electron state in $Al_{0.34}Ga_{0.66}As$ by 0.12 eV. The X and L electron states in the $Al_{0.34}Ga_{0.66}As$ layer is higher than the Γ electron state in the $Al_{0.34}Ga_{0.66}As$ layer by 0.111 eV and 0.078 eV, respectively. The pump laser is higher than the Γ, L and X states in $Al_{0.34}Ga_{0.66}As$ layer. Therefore the intervalley scattering also works. However, the additional decay channel of the electron population, interlayer Γ-X scattering, arises. This additional decay process contributes the 1.2 ps decay of the electron population at the bottom of the well. The slow tail part comes from the cooling of electron system.

In summary, we observed the interlayer Γ-X scattering of electrons for the first time. The interlayer Γ-X scattering time was determined to be 1.2 ps by the femtosecond pump and probe experiments. The scattering rate is explained by taking account of the Γ-X intervalley scattering rate and the penetration of the Γ electron wavefunction into AlAs layers.

Authors wish to thank Dr. H. Okamoto at the Furukawa Electric Co., Ltd and Dr. H. Iwamura at Nippon Telegraph and Telephone Corporation for providing high-quality samples. They also wish to thank Prof. M. Matuura at Yamaguchi University for valuable comments on the manuscript. This work was in part supported by the Scientific Research Grant-in-Aid #62460022, #62104001 and Grant-in-Aid #63604511 for the Scientific Research on Priority Areas, New Functionality Materials - Design, Preparation and Control - by the Ministry of Education, Science and Culture of Japan. It was also supported by the

Mitsubishi Foundation.

References

1) A.J. Taylor, D.J. Erskin and C.L. Tang: J. Opt. Soc. Am. B 2 663 (1985).

2) R.W. Schoenlein, W.Z. Lin, E.P. Ippen and J.G. Fujimoto: Appl. Phys. Lett. 51 1442 (1987).

3) J. Shah, B. Deveaud, T.C. Damen, W.T. Tsang, A.C. Gossard and P. Lugli: Phys. Rev. Lett. 59 2222 (1987) .

4) P.C. Becker, H.L. Fragnito, C.H. Brito Cruz, J. Shah, R.L. Fork, J.E. Cunningham, J.E. Henry and C.V. Shank: Appl. Phys. Lett. 53 2089 (1988).

5) B.A. Wilson, P. Dawson, C.W. Tu and R.C. Miller: J. Vac. Sci. Technol. B4 1037 (1986).

6) P. Dawson, B.A. Wilson, C.W. Tu and R.C. Miller: Appl. Phys. Lett. 48 541 (1986).

7) For the review of the staggered-alignment multi-quantum-well structures, see B.A. Wilson: IEEE J. Quantum Electron. 24 1763 (1988).

8) Y. Masumoto and T. Tsuchiya: J. Phys. Soc. Jpn. 57 4403 (1988).

9) W.H. Knox, C. Hirlimann, D.A.B. Miller, J, Shah, D.S. Chemla and C.V. Shank: Phys. Rev. Letters 56 1191 (1986).

10) D.S. Chemla, D.A.B. Miller and S. Schmitt-Rink: in Optical Nonlinearities in Semiconductors ed. by H. Haug (Academic, 1988) Chap.4.

11) S. Adachi: J. Appl. Phys. 58 R1 (1985).

12) G. Bastard: Phys. Rev. B24 5693 (1981).

13) H.C. Casey, Jr. and M.B. Panish: Heterostructure Lasers (Academic Press, 1978), Chap.4.

14) T. Ando and H. Akera: Proc. 19th Int. Conf. Phys. Semicond. (1988).

15) E. Finkman, M.D. Sturge, M.H. Meynadier, R.E. Nahory, M.C. Tamargo, D.M. Hwang and C.C. Chang: J. Lumines. 39 57 (1987).

Figure Captions

Fig.1 Schematic energy diagrams for two samples, type I $Al_{0.12}Ga_{0.88}As$-AlAs and staggered type II $Al_{0.34}Ga_{0.66}As$-AlAs.

Fig.2 Temporal change of the absorption change of the lowest heavy excitons denoted by an arrow in the $Al_{0.12}Ga_{0.88}As$-AlAs sample. The dashed line shows the fitting by $1 - \exp(-t/\tau_r)$ convoluted by the convolution of the laser pulse shape, where τ_r = 1.7 ps. In the inset the absorption spectra with and without pump pulses are shown, by dashed and solid lines, respectively.

Fig.3 Temporal change of the absorption change of the lowest heavy excitons denoted by an arrow in the $Al_{0.34}Ga_{0.66}As$-AlAs sample. The dashed line shows the fitting by $[1 - \exp(-t/\tau_r)]\cdot[\exp(-t/\tau_d) + c]$ convoluted by the convolution of the laser pulse shape, where τ_r = 1.2 ps, τ_d = 1.2 ps and c = 0.29. In the inset the absorption spectra with and without pump pulses are shown, by dashed and solid lines.

Fig.4 Square of the Γ electron wavefunction in $Al_{0.34}Ga_{0.66}As$-AlAs calculated by the envelope function approximation.

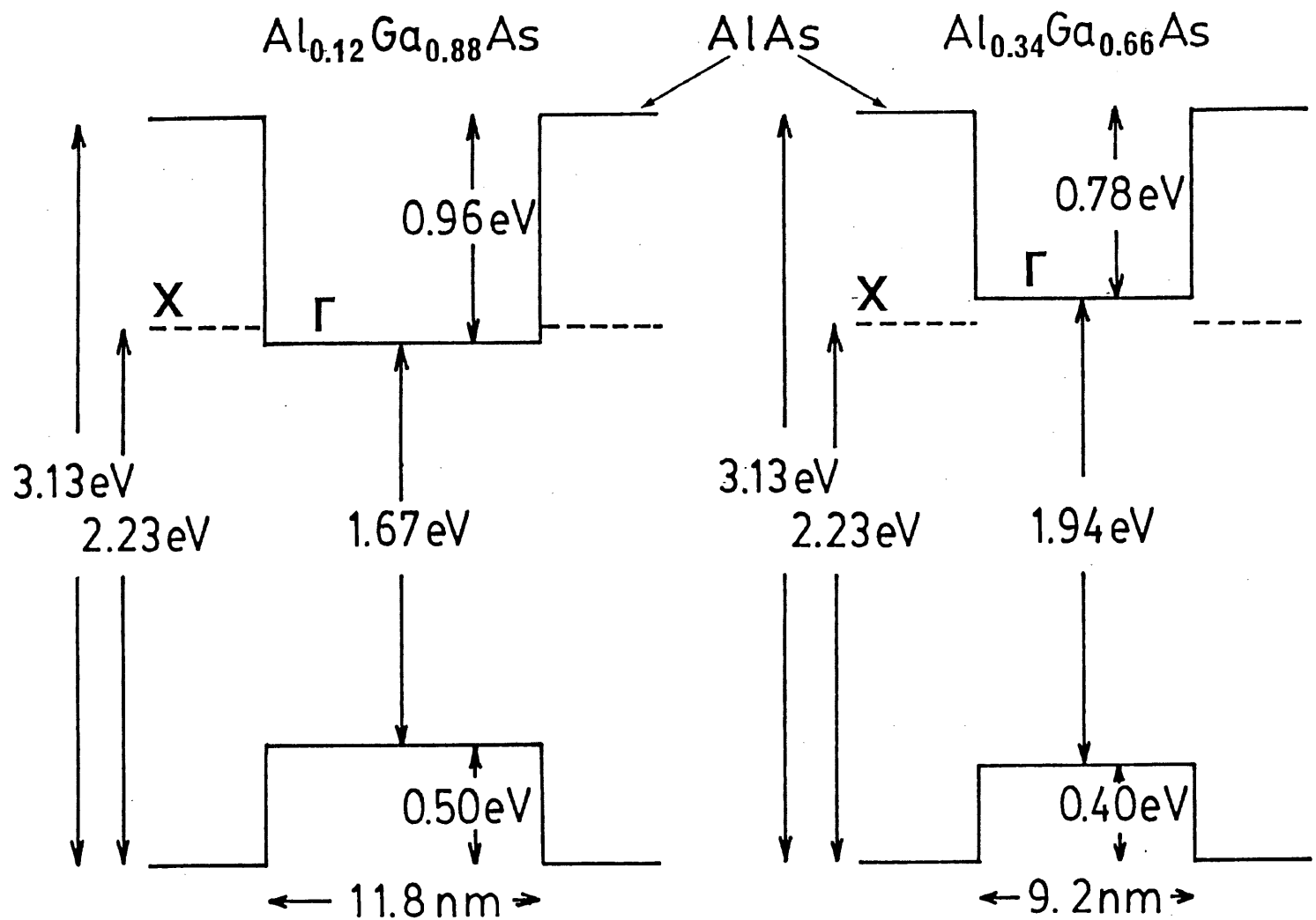
$Al_{0.12}Ga_{0.88}As$
AlAs
$Al_{0.34}Ga_{0.66}As$
0.96eV
0.78eV
X
Γ
X
Γ
3.13eV
2.23eV
1.67eV
3.13eV
2.23eV
1.94eV
0.50eV
0.40eV
11.8nm
9.2nm

Fig. 1

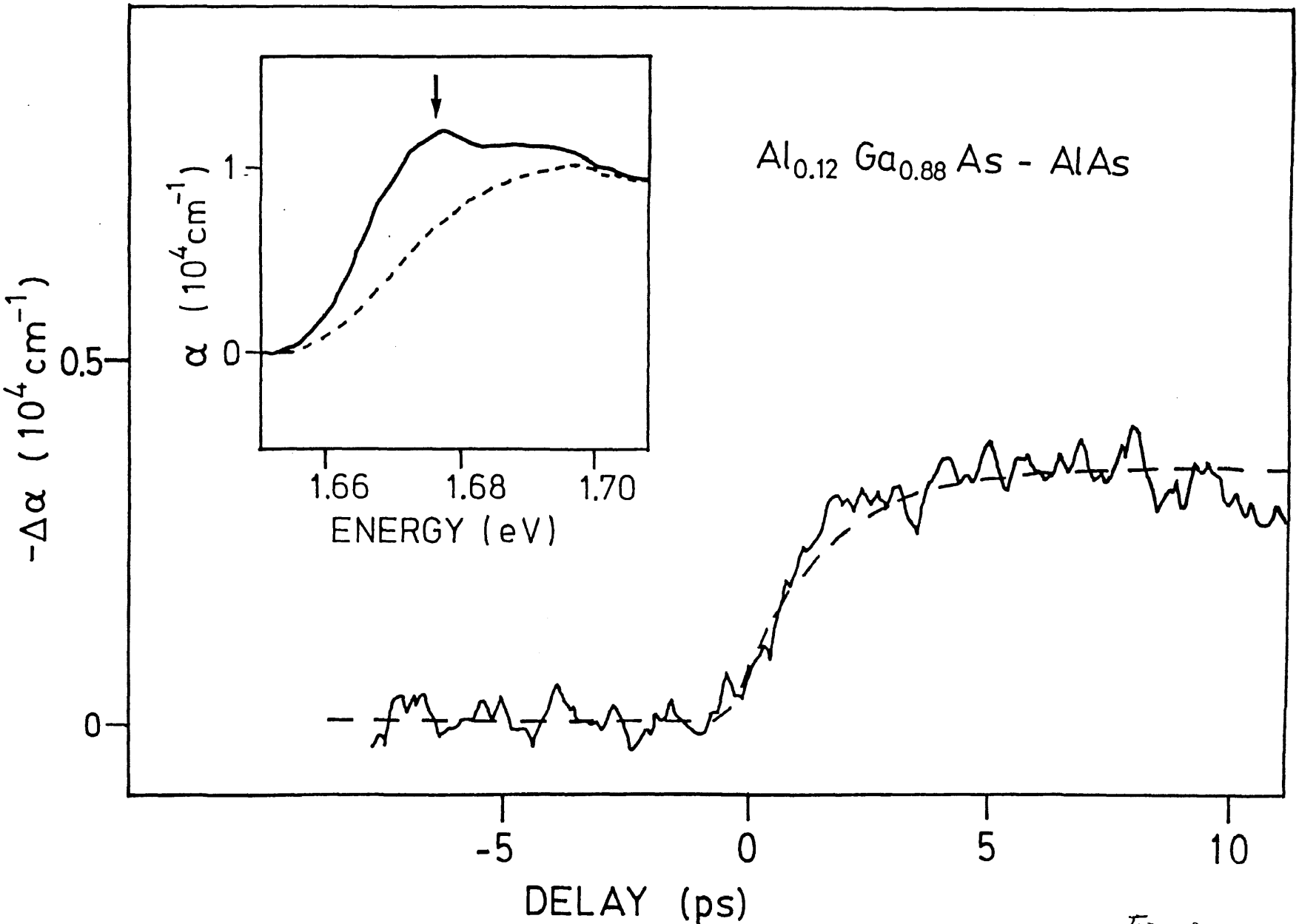
$Al_{0.12}\ Ga_{0.88}\ As$ - AlAs
$-\Delta\alpha\ (10^4 cm^{-1})$
0.5
0
-5
0
5
10
DELAY (ps)
$\alpha\ (10^4 cm^{-1})$
1
0
1.66
1.68
1.70
ENERGY (eV)

Fig. 2

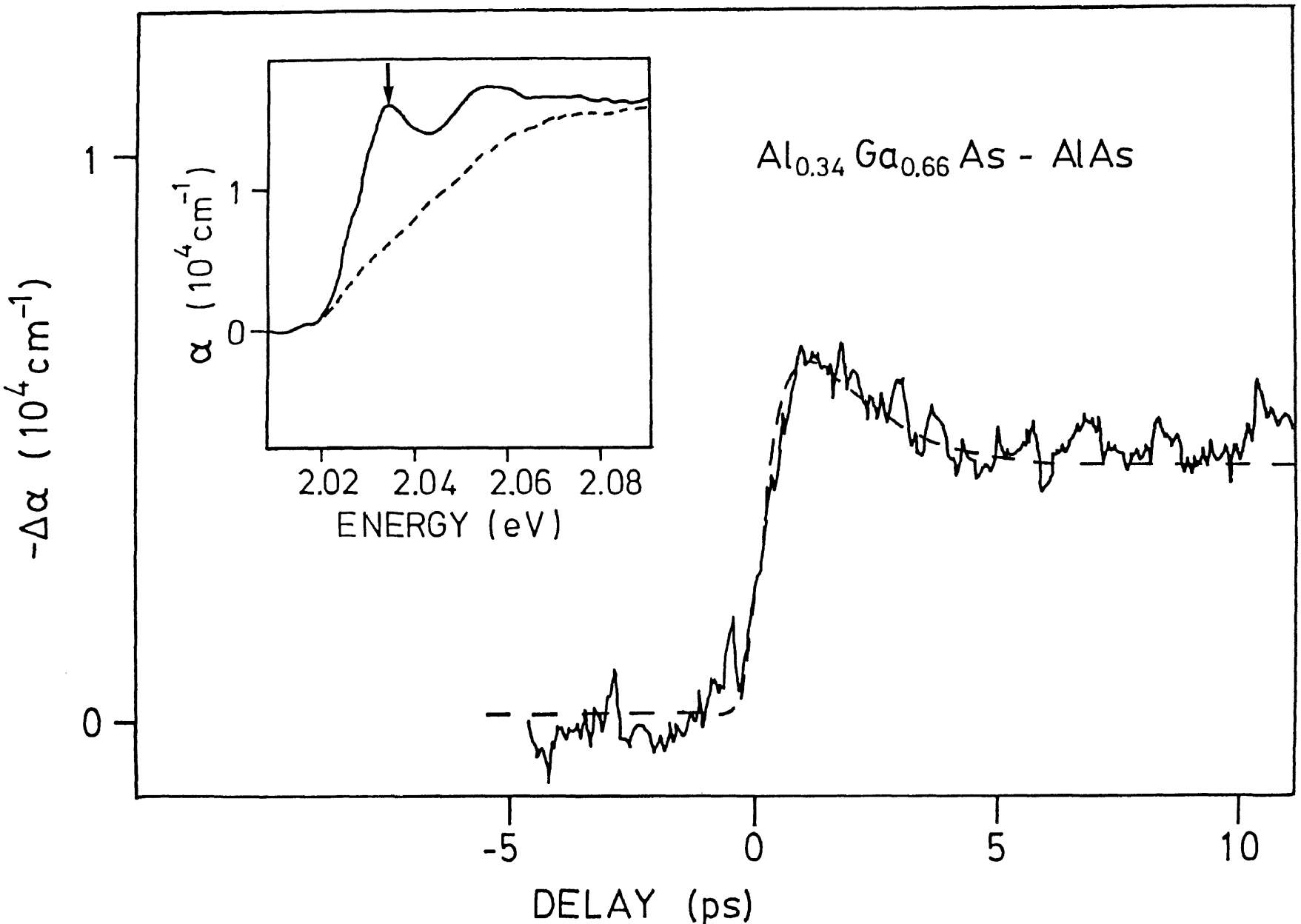
$Al_{0.34}Ga_{0.66}As$ - AlAs
$-\Delta\alpha$ ($10^4 cm^{-1}$)
1
0
-5
0
5
10
DELAY (ps)
α ($10^4 cm^{-1}$)
1
0
2.02
2.04
2.06
2.08
ENERGY (eV)

Fig. 3

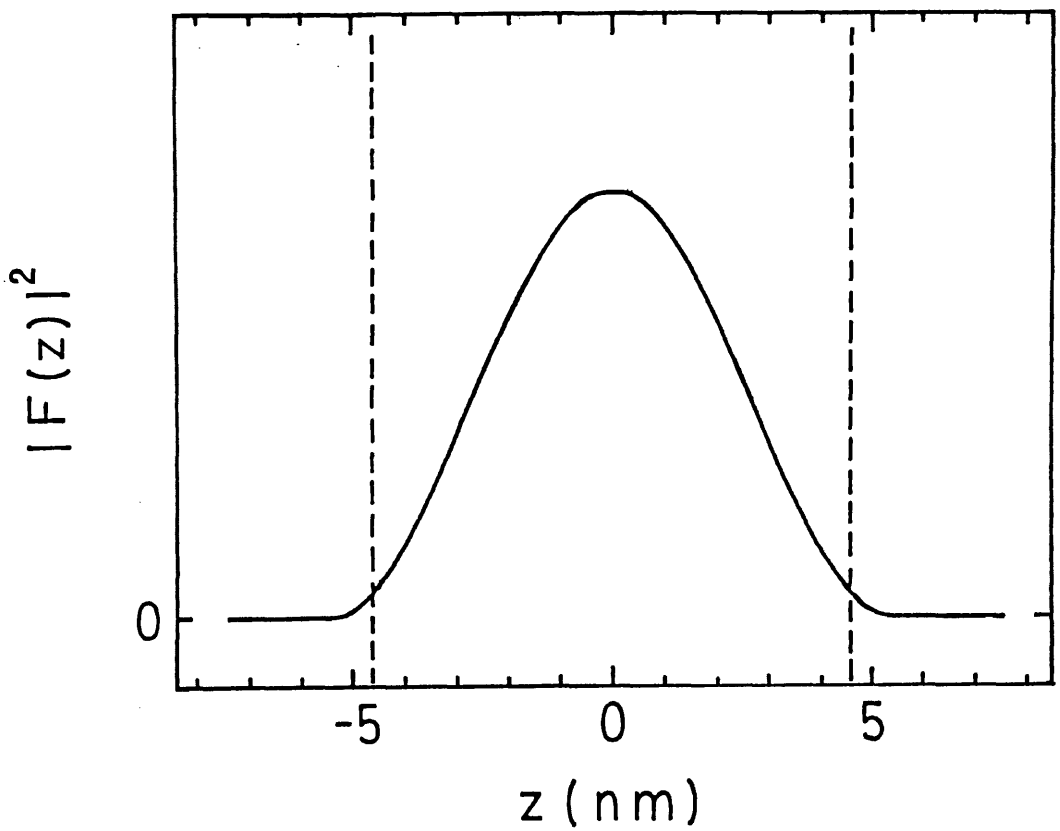

Fig. 4

Pulse distortion in GaAs quantum wells studied by light gating technique

Mitsuhiro Adachi and Yasuaki Masumoto

Institute of Physics, University of Tsukuba
Tsukuba, Ibaraki 305, Japan

Abstract

The pulse distortion in GaAs quantum wells was studied by means of light gating technique. In the experiment, we used the incoherent picosecond pulse to observe accurately the changes of the coherent spike and its surrounding envelope. The experimental results clearly showed that the pulse is not anomalously delayed but is strongly distorted around the exciton resonance. We also compared the results with the computational simulation based on the absorption saturation mechanism: The simulated results well agreed with experimental results. The simulation showed that the recovery time of the exciton saturation is 90 ps around the tail part of the exciton absorption. We also observed the reduction of the coherent spike around the exciton resonance. Theoretical calculation indicates that the coherent propagation effect in the linear absorber causes the reduction of the coherent spike.

§ 1. Introduction

There are many interesting phenomena in the physics of pulse propagation in the condensed matter. Especially, associated with the excitons in semiconductors, pulse distortion is expected to occur as a result of the exciton polariton effect or the nonlinear optical effect such as the hole burning. In the case of bulk semiconductors, time-of-flight measurements have shown large pulse delay due to the polariton effect[1,2]. On the other hand in the case of the two-dimensional GaAs multi-quantum-wells, excitons is spatially confined in a direction perpendicular to the layers, and the wavevector normal to the layers is quantized. Therefore it is not possible to expect polariton effect in a direction perpendicular to the layers. Instead, the nonlinear optical effect is important in excitons in semiconductor quantum wells. Hegarty investigated the phenomena, but only crudely[3].

In this study, we used the incoherent picosecond pulse to observe the pulse propagation in GaAs quantum wells around the exciton resonance. The propagated pulses were measured by correlating with incident pulses in the nonlinear crystal. The experiment clearly demonstrates the distortion of both the pulse shape and the coherent spike. We discuss pulse distortion due to the absorption saturation and reduction of the coherent spike due to the coherent propagation effect in sections 2 and 3, respectively.

§ 2. Experimental procedures

The sample applied in this experiment was grown by the molecular beam epitaxy (MBE) on a GaAs substrate and consists of 200 alternate periods of the GaAs layer 43 Å thick and the AlAs layer 62 Å thick. A window was etched in the GaAs substrate to allow passage of the laser beam. The 4 MHz laser pulses were obtained from a cavity dumped LD700 dye laser synchronously pumped by a mode-locked Kr^+ laser. In order to generate optimum incoherent laser pulses, the real time autocorrelator was used to monitor the laser pulses.

The weak-limit absorption spectrum of the sample at 2.1K and three laser spectra used are shown in Fig.1. The absorption peak at low energy part shows the lowest 1s heavy exciton, and that at high energy part represents 1s light exciton. The absorption spectrum of the heavy exciton is centered at 1.683 eV and has an inhomogeneous linewidth of 10 meV due to the fluctuations of the layer thickness. The spectral width of laser pulses were 2.9 meV.

The schematic experimental diagram is shown in Fig.2. The output laser beam was separated into two beams by a 50%-50% beam splitter. One beam passed through an optical delay was continuously attenuated by a neutral density filter and was focused on the sample in the cryostat. The spot size of the laser beam on the sample surface was about 150 μm in diameter. The power density of the laser was continuously varied by the variable neutral density filter. Another beam was bent by the mirrors to be mixed with the beam propagated through the sample in an RDP crystal. The correlation profile between these two beams was observed by the noncollinear second-harmonic generation. The second-harmonic light was detected by a photomultiplier associated with the monochromator whose resolution is adjusted to be 1 Å. The signal was amplified by a lock-in amplifier and processed by a computer. The optical delay was controlled with an accuracy of 10 μm by the same computer. Thus the intensity of the second harmonic light was measured as a function of the delay time. For the purpose to measure the coherent spike

with the uppermost time resolution, we adopted the electronic micrometer (Feinprüf Millitron 1202IC and 1300) for the control of the optical delay. The computer synchronized the pulse motor stepping with the output of the electronic micrometer which can detect the spatial separation down to 0.2 μm. Thus, the intensity of the coherent spike was investigated as a function of the optical delay with the enough time resolution and accuracy.

§ 3. Effect of absorption saturation

The autocorrelation traces of the laser pulse, represented by the dashed lines in Fig.3, consist of the sharp central component, that is a so-called coherent spike whose correlation width is 520 fs, and a symmetrically broad correlation background envelope whose correlation width is 19 ps. The incoherent laser pulses which give the autocorrelation traces in Fig.3 are easily generated by adjusting a dye laser cavity. The broad correlation envelope is close to a Lorentzian function.

The crosscorrelation traces of the laser pulses, represented by solid lines in Fig.3, consist of the broad asymmetric correlation envelope and the coherent spike. The crosscorrelation shows pulse distortion. The leading edge of the pulses was strongly absorbed, while the trailing edge was absorbed little. The pulse distortion decreases when the excitation power density decreases to $\sim 10^{-8}$ J/cm^2·pulse (Fig.3(c)) or increases to $\sim 10^{-6}$ J/cm^2·pulse (Fig.3(a)) or when the excitation photon energy increases. The pulse distortion completely disappeared when the excitation photon energy of the laser is located at the transparent energy region below the exciton resonance. These experimental results are understood in terms of the absorption saturation of exciton states in GaAs

quantum wells, as described below.

The shift of the coherent spike is constant to be 30 fs and does not depend on both the excitation photon energy and the excitation power density. The shift of the coherent spike comes from the linear refractive index of the sample 2.1 μm thick and the thin epoxy layer. The fact indicates that there is not any detectable anomalous dispersion due to exciton. Therefore the coherent spike is regarded as the zero time standard so that the peak delay of the base correlation trace could be accurately decided regardless of the long term drift. Crosscorrelation traces in Fig.3 are displayed by setting the coherent spike to the zero time standard. Further, for the reliable determination of the peak delay, the base correlation trace was fitted by an asymmetric Lorentzian function $f(t)$ in the way of least-squares

$$f(t) = \frac{at + c}{bt^2 + c}, \tag{1}$$

where a,b and c are fitting parameters. The peak delay relative to the coherent spike is plotted in Fig.4 as a function of the excitation power density. Note that the delay is at its maximum at a certain excitation power density. The maximum shifts toward the high excitation power density together with the increase of the excitation photon energy.

Selden have presented an equation which describes the delay of pulses propagating through saturable absorber[4].

$$\frac{d \ln T}{dt'} + \ln T = 2\beta g(t')(1-T) + \ln T_0, \tag{2}$$

$$t' = \frac{t}{\tau_s},$$

where T is the transmittance at time t', T_0 is the initial transmittance at the weak limit intensity, β is the ratio of the peak incident intensity to the saturation intensity, $g(t')$ is the normalized input pulse function, and t' is dimensionless time in units of τ_s, the relaxation time for excited state of the

absorber.

On the basis of this model, the peak shift of the correlation trace was calculated. The function of the crosscorrelation traces in disregard of the coherent spike $S(\tau)$ are expressed by the convolution

$$S(\tau) = \int_{-\infty}^{\infty} dt\ g(t/\tau_s - \tau)T(t/\tau_s)g(t/\tau_s). \qquad (3)$$

The temporal change of $T(t/\tau_s)$ with a certain τ_s is given by solving eq.(2). The pulse function $g(t/\tau_s)$ used is a Lorentzian function because the convolution of Lorentzian functions is also a Lorentzian function. In Fig.4 the calculated result for the excitation photon energy of 1.6766 eV is plotted as a function of the excitation power density by the solid line.

This calculated result is in good agreement with the experimental one when the relaxation time is τ_s = 90 ps. The calculations qualitatively describes the experimental feature. In particular, the calculations well describes that the delay is at its maximum at a certain excitation power density. By the further calculation for 1.6791 eV and 1.6862 eV, the relaxation time τ_s was found to decrease together with the increase of the excitation photon energy in agreement with the previous study[5]. The obtained relaxation times for 1.6791 eV and 1.6862 eV are 60 ps and 40 ps, respectively.

Hegarty treated the pulse delay observed in the pulse propagation in GaAs quantum wells as follows. When the pulse passes through the material, the early part of the pulse burns a hole and is strongly attenuated. The burned hole, which can be viewed as a negative absorption sitting on top of a much broader resonance, gives rise to its own anomalous dispersion which can alter the group velocity of the remainder of the pulse. However our experiment shows that the early part of the pulse is strongly attenuated, but there is no evidence of the pulse delay due to anomalous dispersion. Therefore, we believe that the phenomena are mostly explained by the Selden's model. There is another default in Hegarty's model.

Hegarty's-model cannot explain that the peak delay attains its maximum at the certain excitation density, but Selden's model can. Nevertheless the calculated delay based on the Selden's equation is not fully consistent with the experiment one because the clear derivation is observed at the high excitation level. Selden described the saturation phenomenon as a process involving two levels. In order to improve the consistence between the experimental result and calculated one, eq.(2) may be necessary to be extended to the inhomogeneously broadened excited states.

§ 4. Coherent propagation effect of incoherent light

The observed coherent spike showed a small but remarkable change of amplitude with the variation of the excitation photon energy. Figure 5 shows two coherent spike profiles corresponding to cases that the sample is absent or present. Here, the base correlation trace is normalized to be unity. The excitation photon energy hits the low energy tail part of the 1s heavy exciton absorption. In the transparent photon energy region the ratio of the coherent spike to the base correlation trace does not depend on whether the sample is absent or present.

The peak amplitude ratio of the coherent spike to the base correlation trace is plotted in the absorption spectrum in Fig.6. It is shown that the ratio decreases to be its minimum when the incident photon energy hits the low energy tail part of the exciton absorption. The ratio was found to be independent of the excitation power density, as shown in Fig.7. This means that the effect is not the nonlinear but linear optical effect. In order to simulate the result, a simple theoretical analysis was performed as follows.

The coherent spike is represented by a squared function of the field

correlation profile,

$$| \langle \tilde{E}^*(t)\tilde{E}(t+\tau) \rangle |^2, \tag{4}$$

where $\tilde{E}(t)$ represents amplitude of the complex light field and $\langle\ \rangle$ means the statistical average. Moreover the width of the coherent spike (520 fs) is comparable to the reciprocal of the laser spectrum width and the correlation time t_c of the field. The maximum power density used is 3.0×10^{-6} J/cm^2·pulse. This corresponds to the Rabi frequency Ω_R of 2.3×10^{10} rad/s for 1s heavy exciton in the sample. We evaluated Ω_R, using the relation,

$$\Omega_R = \frac{\mu_{1h}}{\hbar} | \tilde{E}(t) | = e\sqrt{\frac{f_{1h}}{2m_0\hbar\omega}} | \tilde{E}(t) | ,$$

where μ_{1h} represents the electric dipole matrix element of the 1s heavy exciton, $f_{1h} = 4.2\times10^{-3}$ is the experimentally measured oscillation strength of the 1s heavy exciton[6], e is electron charge and m_0 is electron mass. Then $\Omega_R\times t_c$, which corresponds to an area of pulse during the correlation time, becomes $\pi/260$.

Because $\tilde{E}(t)$ is incoherent, $\tilde{E}(t)$ changes its phase in random way between 0 and 2π in the duration of the correlation time t_c. Therefore it is reasonable that the optical field envelope satisfies the following condition because the time integrals of the electric field whose phase is randomly modulated are cancelled each other.

$$\left| \frac{\mu_{1h}}{\hbar}\int_{-\infty}^{t} dt'\, \tilde{E}(t') \right| \ll 1, \tag{5}$$

for any t. The condition (5) means that the area of a pulse is very small. Then, it is possible to apply the linear-dispersion theory developed by Crisp to the present pulse-propagation phenomenon[7]. The electric field envelope which Crisp presented is given by

$$\tilde{E}(z,t) = \frac{1}{2\pi}\int_{-\infty}^{\infty} d\omega \int_{-\infty}^{\infty} dt'\, \tilde{E}(0,t') \exp\{i\omega(t'-t)\} \exp\{-\tilde{A}(\omega)z\}, \tag{6}$$

where $\tilde{A}(\omega)$ and z represent the amplitude modulation factor in the medium and the

propagation length in the medium, respectively. The amplitude modulation factor $\bar{A}(\omega)$ is written by the absorption coefficient $\alpha(\omega)$ and the refractive index $n(\omega)$ of the sample as follows,

$$\bar{A}(\omega) = \alpha(\omega) - in(\omega)\frac{\omega}{c}. \tag{7}$$

$\bar{E}(0,t)$ means the envelope of an incident pulse at the front face of the sample. Replacing the variable $t'-t$ to s in eq.(6), $\bar{E}(z,t)$ is rewritten as

$$\bar{E}(z,t) = \int_{-\infty}^{\infty} ds\ \bar{E}(0,s+t)\bar{F}(z,s), \tag{8}$$

$$\bar{F}(z,s) = \frac{1}{2\pi}\int_{-\infty}^{\infty} d\omega \exp\{i\omega s - \bar{A}(\omega)z\}. \tag{9}$$

In ref.[7], $\bar{E}(0,t)$ was given by a short coherent pulse with small amplitude. In the present case, however, $\bar{E}(0,t)$ is not a coherent pulse but an incoherent one. Morita et al. reported the calculation of an incoherent pulse propagation in the study of the pulse propagation in an Na-vapor cell[8]. Their calculation has an assumption as follows,

$$\bar{E}(0,t) = V(t)R(t), \tag{10}$$

where $R(t)$ is the Gaussian-distributed random variable of zero mean and $V(t)$ is the slowly varying envelope function. $R(t)$ in eq.(10) reflects the characteristic feature of the coherent spike. We also adopt the same assumption. Then, the crosscorrelation trace $J(\tau)$ is given by[9]

$$\begin{aligned} J(\tau) &\propto \int_{-\infty}^{\infty} dt\ \bar{E}^*(d,t)\bar{E}(d,t)\bar{E}^*(0,t-\tau)\bar{E}(0,t-\tau) \\ &\propto \int_{-\infty}^{\infty} dt\ |V(t)|^2 |V(t-\tau)|^2 K(\tau), \end{aligned} \tag{11}$$

$$\begin{aligned} K(\tau) = \int_{-\infty}^{\infty} ds' \int_{-\infty}^{\infty} ds''\, \bar{F}^*(d,s')\bar{F}(d,s'') \\ \times \langle R^*(s'+t)R(s''+t)R^*(t-\tau)R(t-\tau)\rangle , \end{aligned} \tag{12}$$

where d is the sample thickness. The autocorrelation function of $R(t)$, which represents the coherent spike, is given by

$$h(\tau) = \langle R^*(t)R(t+\tau)\rangle . \tag{13}$$

It is a Fourier transform of the laser spectrum $P(\omega)$

$$h(\tau) = \frac{1}{2\pi}\int_{-\infty}^{\infty} d\omega P(\omega) \exp(-i\omega\tau). \tag{14}$$

By using eq.(12) and the fractorization property in higher-order moments of Gaussian random variables, eq.(12) is reduced to two parts[10].

$$K(\tau) = \left| \int_{-\infty}^{\infty} ds\, \bar{F}(d,s)h(\tau+s) \right|^2 + \int_{-\infty}^{\infty} ds' \int_{-\infty}^{\infty} ds'' \, \bar{F}^*(d,s')\bar{F}(d,s'')h(s''-s')h(0). \quad (15)$$

Another form of $K(\tau)$ is obtained by substituting eqs.(9),(14) into eq.(15).

$$K(\tau) = \left(\frac{1}{2\pi}\right)^2 \left| \int_{-\infty}^{\infty} d\omega\, P(\omega) \exp\{-\tilde{A}(\omega)d - i\omega\tau\} \right|^2 + \left(\frac{1}{2\pi}\right)^2 \int_{-\infty}^{\infty} d\omega P(\omega) \exp\left[-2Re\{\tilde{A}(\omega)\}d\right] \int_{-\infty}^{\infty} d\omega' P(\omega'), \quad (16)$$

By substituting eq.(7) into eq.(6), we can obtain

$$K(\tau) = \left(\frac{1}{2\pi}\right)^2 \left| \int_{-\infty}^{\infty} d\omega\, P(\omega) \exp\{-\alpha(\omega)d\} \cos\left[\omega\left\{\tau + \frac{n(\omega)}{c}\right]\right\} \right|^2 + \left(\frac{1}{2\pi}\right)^2 \left| \int_{-\infty}^{\infty} d\omega\, P(\omega) \exp\{-\alpha(\omega)d\} \sin\left[\omega\left\{\tau + \frac{n(\omega)}{c}\right]\right\} \right|^2 + \left(\frac{1}{2\pi}\right)^2 \int_{-\infty}^{\infty} d\omega P(\omega) \exp\{-2\alpha(\omega)d\} \int_{-\infty}^{\infty} d\omega' P(\omega'). \quad (17)$$

For the simple calculation, we assume $\alpha(\omega)$ and $n(\omega)$ as follows based on the Lorentz model.

$$\alpha(\omega) \sim \frac{4\pi\alpha_0\omega_0\Gamma/4}{(\omega_0-\omega)^2 + (\Gamma/2)^2}, \quad (18)$$

$$n(\omega) \sim \frac{4\pi\alpha_0\omega_0(\omega_0-\omega)/2}{(\omega_0-\omega)^2 + (\Gamma/2)^2} + 1, \quad (19)$$

where α_0 represents the exciton-phonon coupling strength. The value is adjusted to describe approximately the absorption spectrum in Fig.1. They also satisfy Kramers-Kronig relations. Since $|V(t-\tau)|^2$ is a slowly varying function of τ compared with $K(\tau)$, $K(\tau)$ represents the coherent spike profile. The amplitude ratio of the coherent spike to the base correlation trace is obtained by comparing $K(0)$ with the wing of the $K(\tau)$ profile.

In order to clarify which dominates the reduction of the coherent spike, $n(\omega)$ or $\alpha(\omega)$, we calculated $K(\tau)$ by artificially setting one of $n(\omega)$ and $\alpha(\omega)$ to zero. Figure 8 shows the calculated ratio, corresponding the cases of $\{n(\omega) = 0, \alpha(\omega) \neq 0\}$ and $\{n(\omega) \neq 0, \alpha(\omega) = 0\}$, when the laser spectrum $P(\omega)$ has a Gaussian profile. In the case of $\{n(\omega) \neq 0, \alpha(\omega) = 0\}$, the calculated result does not show the reduction of coherent spike. On the other hand in the case of $\{n(\omega) = 0, \alpha(\omega) \neq 0\}$, it is satisfactory to account for the experimental feature in Fig.6. The calculation clearly indicates that the absorption $\alpha(\omega)$ causes the reduction of coherent spike but the refractive index $n(\omega)$ dose not. The present work presents the first observation of the coherent propagation effect of incoherent light in semiconductors due to the absorption $\alpha(\omega)$.

§ 5. Conclusions

The remarkable pulse distortion in GaAs quantum wells was observed around the exciton resonance by means of light gating technique. We demonstrated the usefulness of the incoherent pulses to observe the distortion of both the pulse envelope and the coherent spike. The pulse was strongly distorted, but was not anomalously delayed. The pulse distortion in GaAs quantum wells around the exciton resonance is well understood by taking account of the absorption saturation. The relaxation time τ_s = 90 ps obtained by our experiments is comparable to the result of pump and probe experiment previously presented. The SHG crosscorrelation technique is conventional technique to know the ultrafast temporal change of the absorption saturation under the certain conditions. The reduction of the coherent spike observed experimentally was explained by taking account of the coherent propagation effect in the linear absorber. The effect

was observed in semiconductors for the first time in the present experiment.

Acknowledgements

Authors wish to thank Dr. M. Tanaka at National Research Laboratory of Metrology for the useful technical advice on the time-resolved measurement with high precision. This work was in part supported by Grant-in-Aid #63604511 for Scientific Research on Priority Areas, New Functionality Materials-Design, Preparation and Control-by the Ministry of Education, Science and Culture of Japan.

References

[1] Y. Masumoto, Y. Unuma, Y. Tanaka and S. Shionoya: *J. Phys. Soc. Jpn.* 47, 1844 (1979).

[2] R.G. Ulbrich and G.W. Fehrenbach: *Phys. Rev. Lett.* 43 963 (1979).

[3] J. Hegarty: *Phys. Rev. B* 25 4324 (1982).

[4] A.C. Selden: *J. Phys. D* 3 1935 (1970).

[5] J. Hegarty and M.D. Sturge: *J. Opt. Soc. Am. B* 2 1143 (1985).

[6] Y. Masumoto, M. Matsuura, S. Tarucha and H. Okamoto: *Phys. Rev. B* 32 4725 (1985).

[7] M.D. Crisp: *Phys. Rev. A* 1 1604 (1970).

[8] N. Morita, K. Torizuka, and T. Yajima: *J. Opt. Soc. Am. B* 3 548 (1986).

[9] E. P. Ippen and C. V. Shank: in *Ultrashort Light Pulses* ed. by S. L. Shapiro (Springer,1977) Chap.3.

[10] R. Loudon: *The quantum theory of light* (Oxford, 1978) Chap.5.

Figure Captions

Fig.1 Absorption spectrum of the sample and three excitation laser spectra.

Fig.2 Schematic diagram of experimental system. The magnified inset shows the detail of the sample surroundings.

Fig.3 SHG correlation traces. In the each figure, solid lines and dashed lines correspond to cases that sample is present or absent, respectively. The excitation power densities corresponding to Fig.3(a), Fig.3(b) and Fig.3(c) are 2×10^{-6} J/cm^2·pulse, 4×10^{-7} J/cm^2·pulse and 5×10^{-8} J/cm^2·pulse, respectively. Note that the crosscorrelation traces are shift by 30 fs so as to set the coherent spikes to the zero time standard.

Fig.4 Peak delay of the base correlation envelopes relative to the coherent spike as a function of the excitation power density. Experimental results are shown by symbols together with the calculated result for 1.6766 eV denoted by the solid line.

Fig.5 The typical coherent spikes corresponding to cases that the sample is present or absent are shown. SHG intensity is normalized by the peak amplitude of the base correlation trace.

Fig.6 The peak amplitude ratio of the coherent spike to the base correlation trace as a function of the excitation photon energy (symbols). The solid line

shows the absorption spectrum.

Fig.7 The peak amplitude ratio of the coherent spike to the base correlation trace as a function of the excitation power density. The incident photon energy is 1.6796 eV.

Fig.8 The calculated result of the peak amplitude ratio of the coherent spike to the base correlation trace as a function of the excitation photon energy. Circles and crosses correspond the cases of $\{n(\omega) = 0, \alpha(\omega) \neq 0\}$ and $\{n(\omega) \neq 0, \alpha(\omega) = 0\}$, respectively. Here $n(\omega)$ and $\alpha(\omega)$ are the refractive index and the absorption coefficient, respectively. The solid line and the dashed line represent the model absorption spectrum and the corresponding refraction spectrum, respectively.

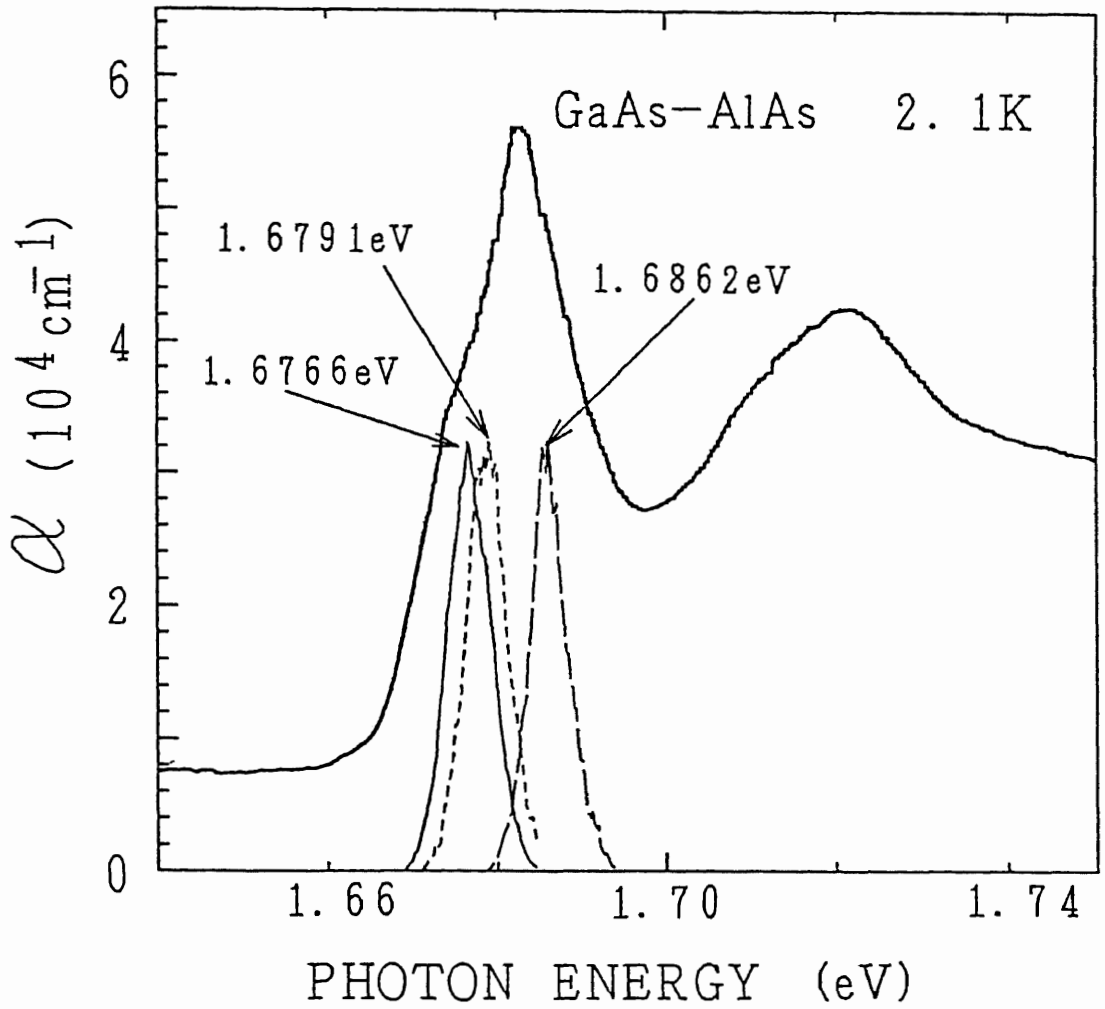
GaAs—AlAs 2. 1K
1. 6791eV
1. 6862eV
1. 6766eV
α (10⁴cm⁻¹)
0
2
4
6
1. 66
1. 70
1. 74
PHOTON ENERGY (eV)

Fig. 1

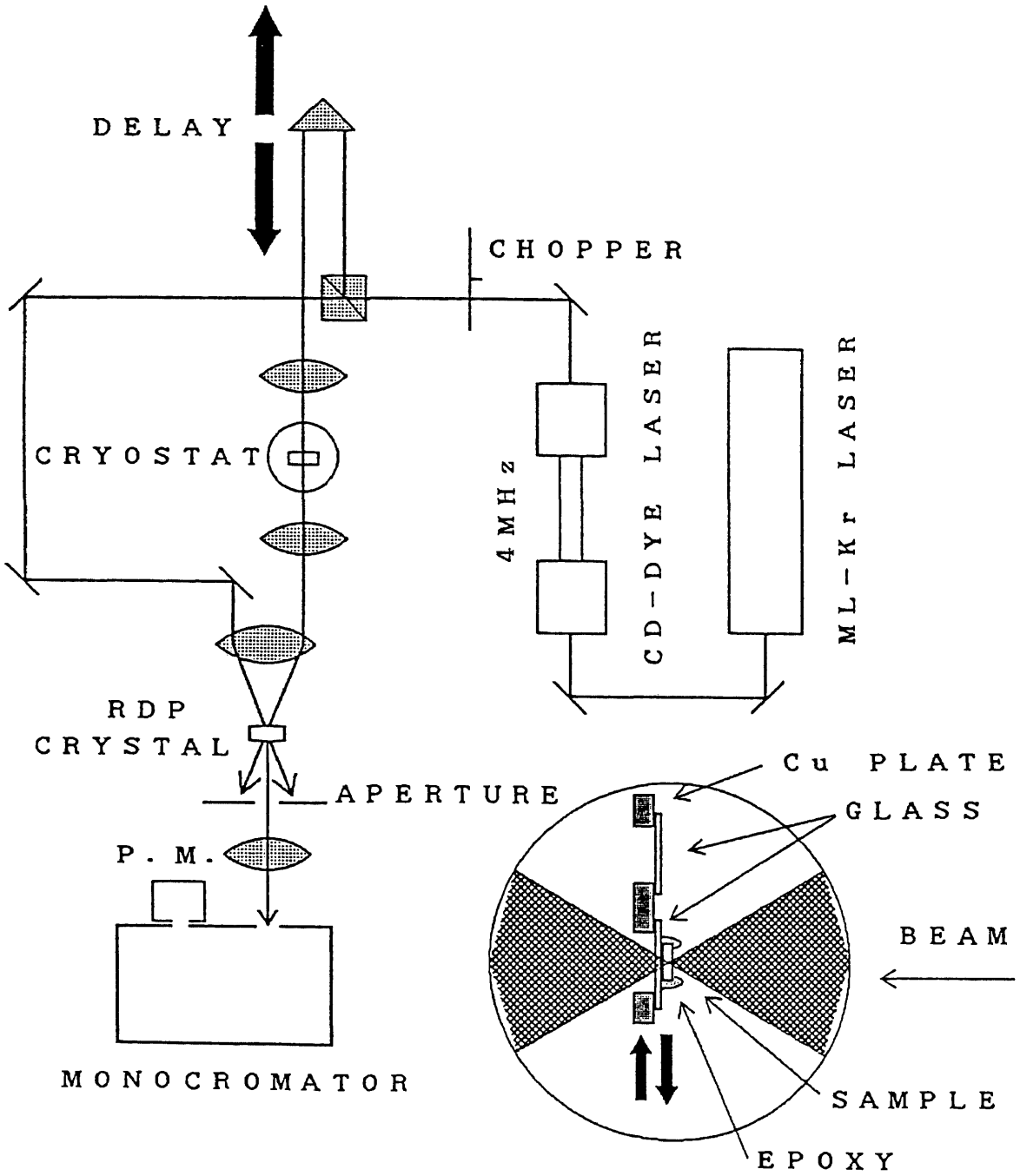
DELAY
CHOPPER
CRYOSTAT
4 MHz
CD-DYE LASER
ML-Kr LASER
RDP
CRYSTAL
APERTURE
P. M.
MONOCROMATOR
Cu PLATE
GLASS
BEAM
SAMPLE
EPOXY

Fig. 2

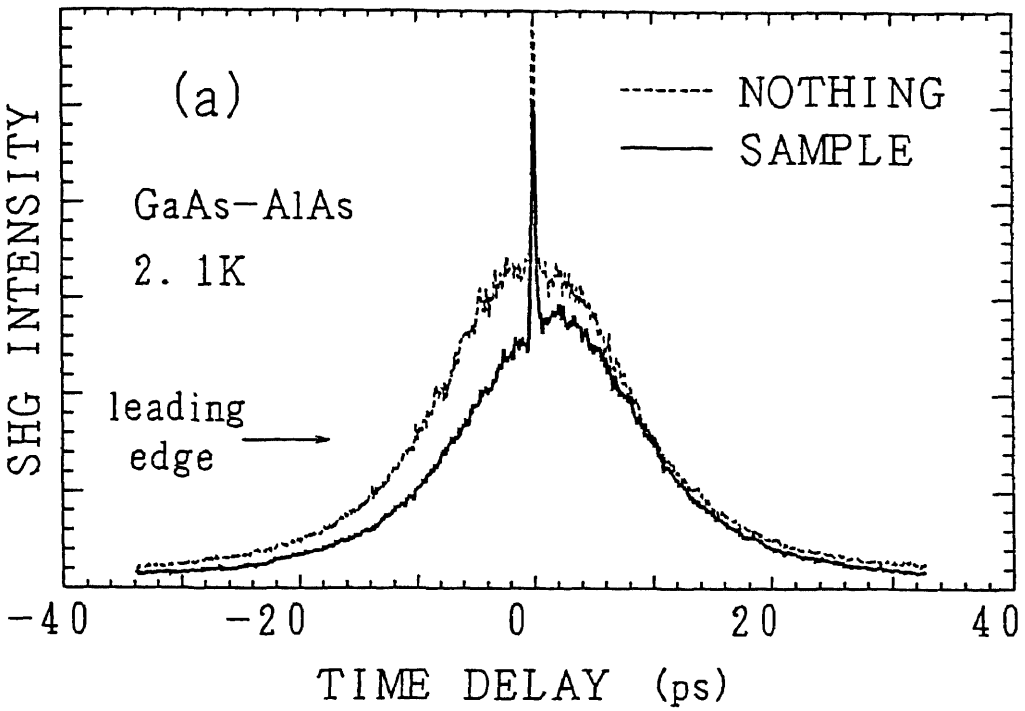
(a)
GaAs-AlAs
2. 1K
leading
edge
NOTHING
SAMPLE
SHG INTENSITY
-40
-20
0
20
40
TIME DELAY (ps)

Fig. 3 (a)

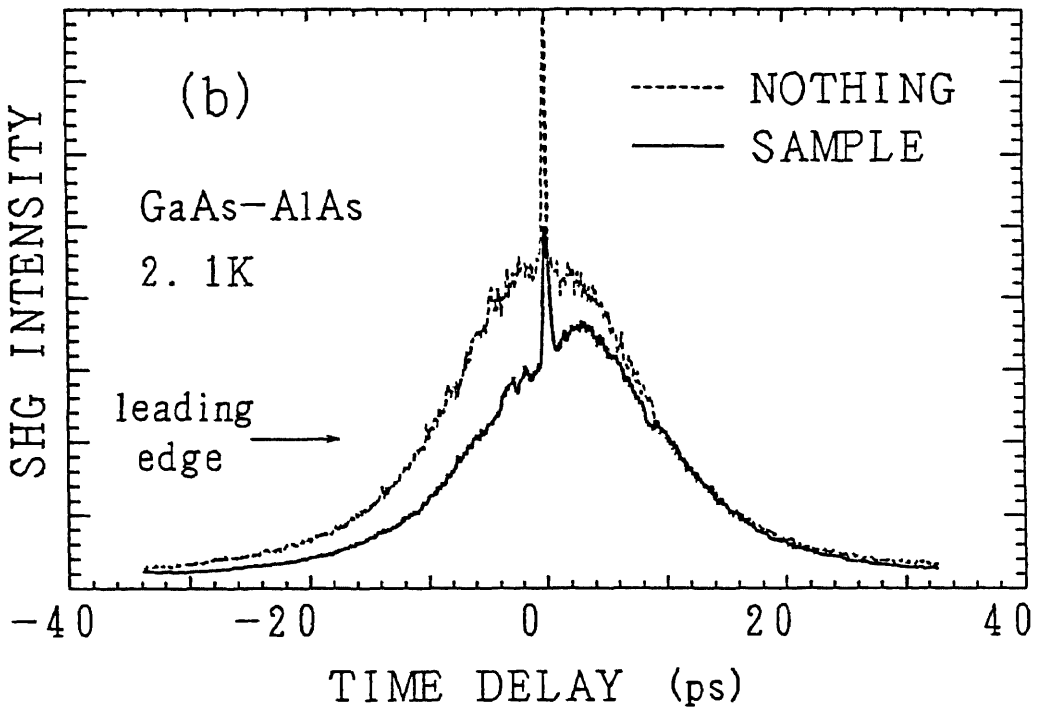
(b)
GaAs-AlAs
2. 1K
leading
edge
NOTHING
SAMPLE
SHG INTENSITY
-40
-20
0
20
40
TIME DELAY (ps)

Fig. 3(b)

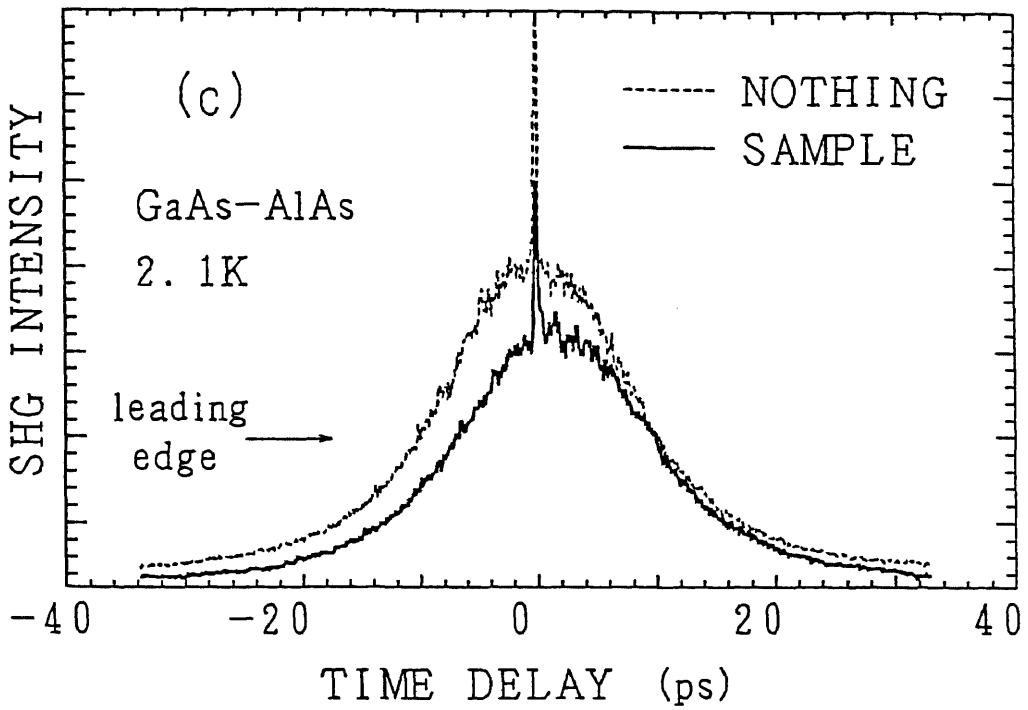
(c)
GaAs-AlAs
2. 1K
leading
edge
NOTHING
SAMPLE
SHG INTENSITY
-40
-20
0
20
40
TIME DELAY (ps)

Fig. 3 (c)

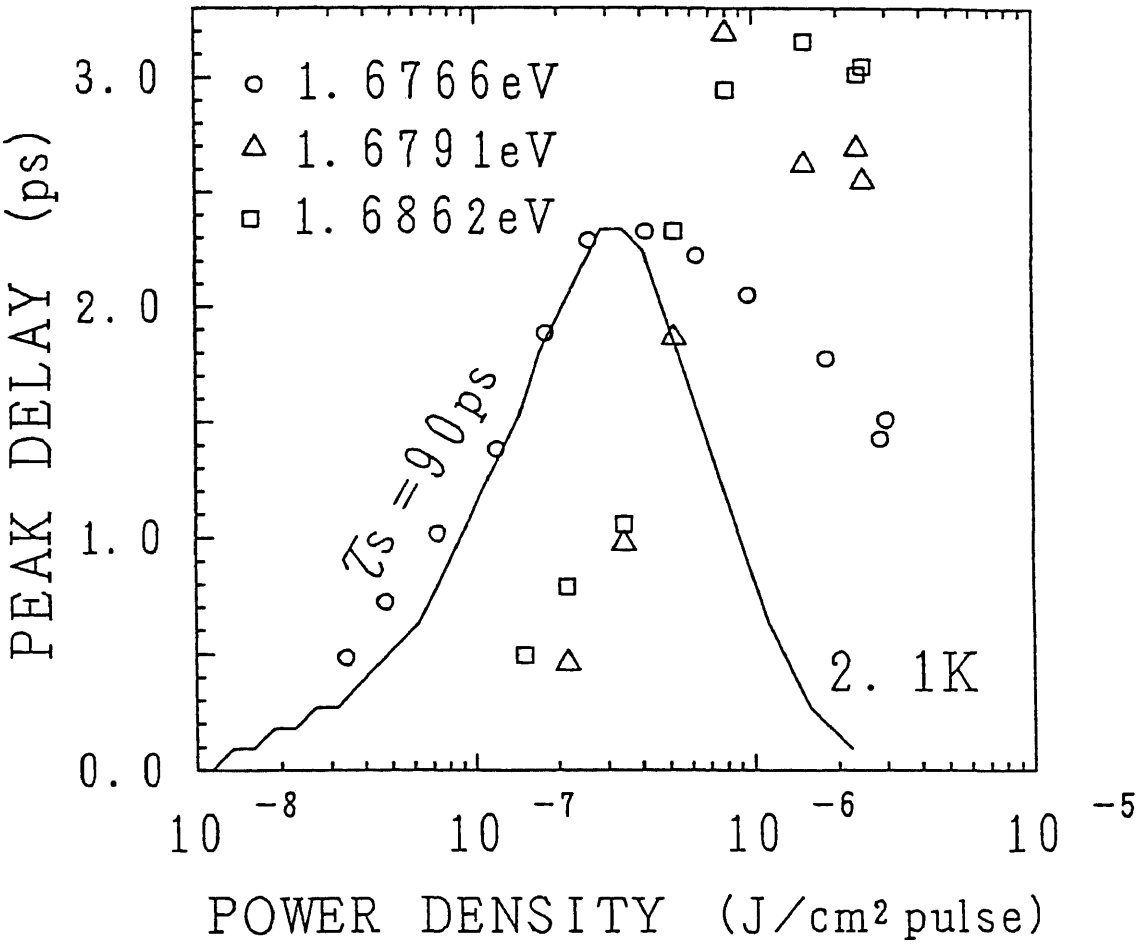
3.0
2.0
1.0
0.0
PEAK DELAY (ps)
1.6766eV
1.6791eV
1.6862eV
τs = 90ps
2.1K
10 -8
10 -7
10 -6
10 -5
POWER DENSITY (J/cm² pulse)

Fig. 4

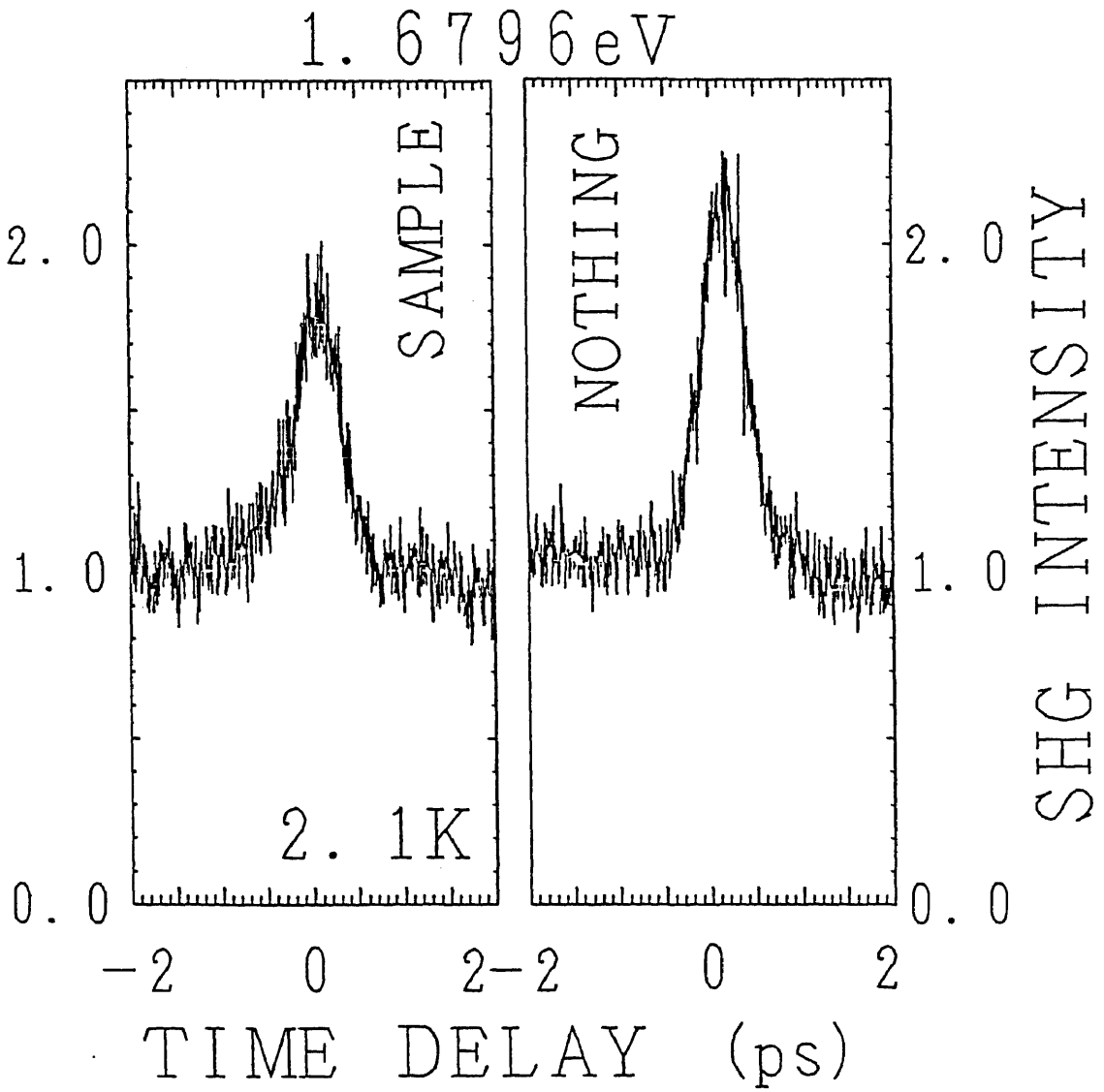
1.6796eV
SAMPLE
NOTHING
2.1K
2.0
1.0
0.0
SHG INTENSITY
-2
0
2
TIME DELAY (ps)

Fig. 5

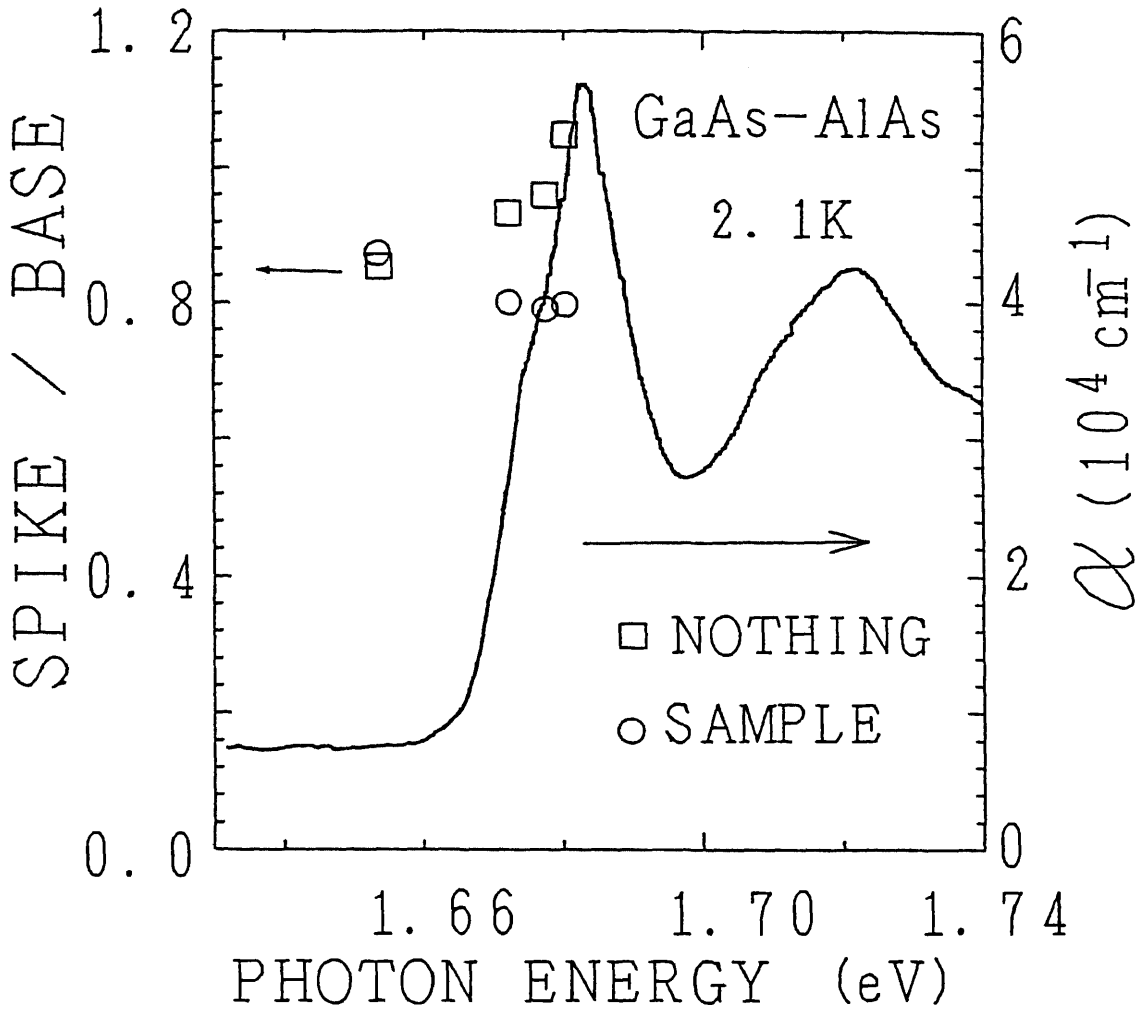
1.2
0.8
0.4
0.0
SPIKE / BASE
6
4
2
0
α (10⁴ cm⁻¹)
GaAs-AlAs
2.1K
NOTHING
SAMPLE
1.66
1.70
1.74
PHOTON ENERGY (eV)

Fig. 6

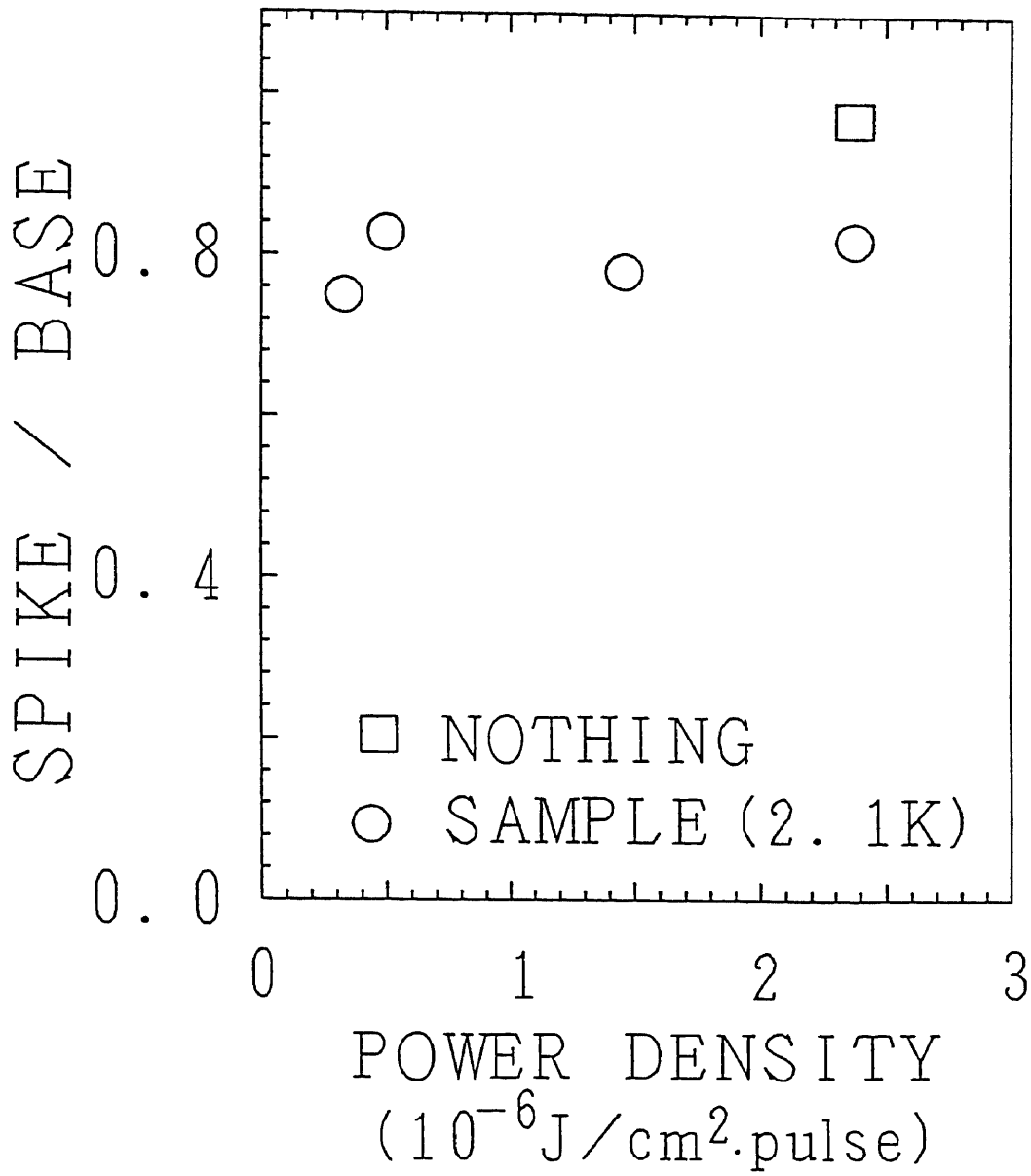
SPIKE / BASE
0.8
0.4
0.0
NOTHING
SAMPLE (2.1K)
0
1
2
3
POWER DENSITY
(10⁻⁶J/cm².pulse)

Fig. 7

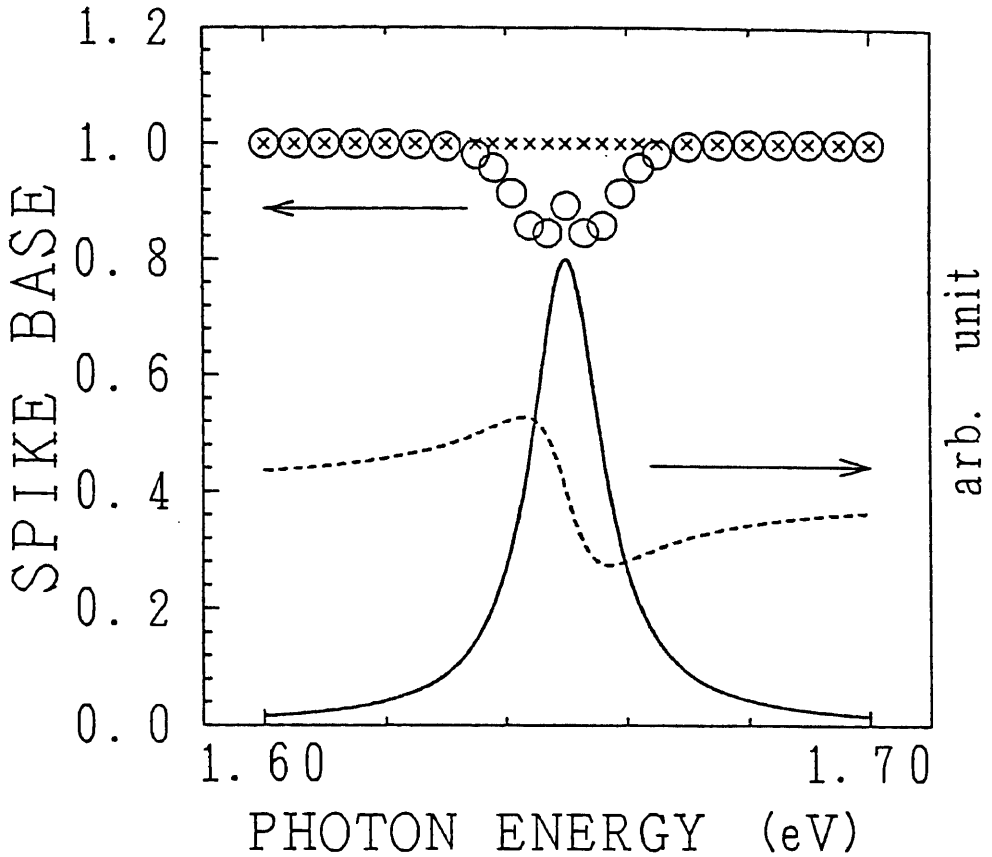
1.2
1.0
0.8
0.6
0.4
0.2
0.0
SPIKE BASE
arb. unit
1.60
1.70
PHOTON ENERGY (eV)

Fig. 8

Homogeneous width of exciton absorption spectra in CuCl microcrystals

Yasuaki Masumoto, Tetsuro Wamura and Atsushi Iwaki

Institute of Physics, University of Tsukuba, Tsukuba, Ibaraki 305, Japan

Abstract

Homogeneous width of Z_3 exciton absorption spectra in CuCl microcrystals was measured for the first time. It was determined to be 0.15 meV at 77K by the laser saturation spectroscopy. The temperature dependence of the Z_3 exciton absorption linewidth also supported the result. The measurements of the saturation density, the homogeneous linewidth and the lifetime of Z_3 excitons informed us the transition dipole moment for a CuCl microcrystal. The obtained transition dipole moment for a CuCl microcrystal is 16 times of that for an unit cell in bulk CuCl.

Recently nonlinear optical properties of semiconductor microcrystals have attracted much interest. Especially, CuCl microcrystals, giving the typical example of the exciton quantization[1], are expected to show the large optical nonlinearity[2,3]. In our previous paper, we demonstrated the optical nonlinearity of Z_3 excitons in CuCl microcrystals in NaCl host crystals by the laser saturation spectroscopy[4]. However, the basic optical character of CuCl microcrystals, such as the homogeneous width of Z_3 excitons, their transition dipole moment and so on, are not yet known. Homogeneous width is masked by the inhomogeneous broadening due to the size distribution of CuCl microcrystals. Homogeneous width is one of the most important parameters characterizing the linear and nonlinar optical properties of excitons, because it determines the coherent length which dominates the exciton lifetime and the transition dipole moment for a microcrystal. This is because the transition dipole moment of excitons in the coherent volume are superposed to be enhanced one[5-7]. In this work, we investigated the homogeneous width of the Z_3 exciton absorption spectra in CuCl microcrystals by the laser saturation spectroscopy. Simultaneously we observed the temperature dependence of the absorption linewidth of Z_3 excitons to clarify the mechanism of the homogeneous broadening as well as to ascertain the homogeneous width obtained by the laser saturation spectroscopy. We also measured the lifetime of Z_3 excitons. The saturation density, the homogeneous linewidth and the lifetime of excitons informed us the transition dipole moment of excitons for a CuCl microcrystal, which the current theory refered to[2,3].

Samples of CuCl microcrystals in NaCl host crystals were grown by the transverse Bridgman method followed by heat treatment[4]. The size of the CuCl microcrystals was determined by the absorption peak energy of Z_3 excitons at 77K following the method established by Itoh[8]. In this study, we used a typical

sample 0.035 cm thick containing CuCl microcrystals whose mean radius is 6.1 nm. The CuCl molar fraction in the sample is determined to be 0.16% by the plasma emission spectroscopy[4].

To obtain the temperature dependence of the absorption spectra, we used a temperature variable cryostat. We also used an incandescent lamp, a monochromator, a photomultiplier and a lock-in amplifier. For the laser saturation spectroscopy, we used a dye laser pumped by a nitrogen laser. The sample was directly immersed in liquid nitrogen. The dye laser is composed of an output mirror, a dye cell filled with BBQ in dioxane, a beam expander made of two prisms and an echelle grating (316 grooves/mm). Selecting the order of the grating and adjusting the beam expander, we could easily change the linewidth of the laser output quasi-continuously. The peak photon energy of the laser light was set to be 3.223 eV (384.58 nm) which corresponds to the Z_3 exciton absorption peak of the sample at 77 K. The pulse duration was 3.6 ns and the pulse power was measured by using a pyroelectric energy detector. The size of the excitation spot was measured under a microscope. The transmitted laser light was detected directly by a photomultiplier with a calibrated set of neutral density filters. The signal was averaged by using a Boxcar integrator.

In Fig.1, temperature dependence of the absorption spectra of CuCl microcrystals is shown. At low temperatures, spectra are composed of sharp Z_3 and $Z_{1,2}$ exciton absorption lines. With the rise of temperature, the exciton structure broadens together with the blue shift. At elevated temperatures, exciton absorption spectra have the Lorentzian shape. The linewidth of the Z_3 exciton absorption is plotted as a function of temperature in Fig.2.

As is shown, the linewidth changes little below 70K. The size distribution

of CuCl microcrystals causes the inhomogeneous broadening of the exciton absorption. The linewidth below 70K almost comes from the inhomogeneous linewidth. The temperature dependence of the linewidth of the Z_3 exciton absorption $\Gamma(T)$ is well expressed by the equation[9)]

$$\Gamma(T) = \Gamma_{inh} + A\,/[\exp(B/k_BT) - 1] \quad , \qquad (1)$$

where Γ_{inh} = 8.0 meV is the inhomogeneous broadening. The best fitting is obtained with parameters A = 474 meV and B = 55.7 meV, as is shown in Fig.2. Fitting is satisfactory. Fitting is not good, if we use the fitting function $\Gamma(T) = \Gamma_{inh} + CT^2$, where C is a fitting parameter. So far, the expression has been used to explain the temperature dependence of the Z_3 exciton linewidth in CuCl[10)]. In this case the line broadening is due to interactions of excitons with long-wavelength acoustic phonons[11)].

Instead, the validity of eq.(1) implies that the line broadening is due to interactions of Z_3 excitons with optical phonons. Energies of longitudinal optical (LO) phonon and transverse optical (TO) phonon at the Γ point in CuCl are 25.6 meV and 20.0 meV, respectively[12)]. The absorption of one optical phonon can not explain eq.(1), because the value of B is about twice of the LO phonon energy. Succesive absorption of two LO phonons can explain eq.(1), because $nn' = [\exp(\hbar\omega_{LO}/k_BT)-1]^{-1}[\exp(\hbar\omega'_{LO}/k_BT)-1]^{-1} \simeq \{\exp[(-(\hbar\omega_{LO} + \hbar\omega'_{LO})/k_BT]-1\}^{-1}$ holds when $\hbar\omega_{LO}, \hbar\omega'_{LO} > k_BT$. Here n(n') and $\hbar\omega_{LO}(\hbar\omega'_{LO})$ are the phonon occupation number and the LO phonon energy, respectively. Therefore, a possible broadening mechanism for the Z_3 excitons at elevated temperatures is the scattering of the Z_3 excitons to the $Z_{1,2}$ excitons as a result of the succesive absorption of two LO phonons, because the $Z_{1,2}$ exciton state is higher than the Z_3 exciton state by 70 meV. Exciton thermal ionization can not be

taken into account in contrast to the case of GaAs quantum wells[9], because the binding energy of the Z_3 excitons is 213 meV, which is much larger than the value of B. The large binding energy and the 70 meV energy splitting of Z_3 and $Z_{1,2}$ excitons may cause the peculiar thermal broadening mechanism of Z_3 excitons. Our experimental observation about the phonon broadening of the Z_3 exciton absorption is limited to the elevated temperatures, because the inhomogeneous broadening dominates the broadening at low temperatures. Therefore we can not infer the phonon broadening mechanism at low temperatures.

Next, homogeneous width of the Z_3 exciton absorption was studied by the laser saturation spectroscopy[13]. On the basis of the laser saturation spectroscopy, the saturation density I_s is expressed by

$$I_s = \varepsilon_0 c\hbar^2/(2|\mu|^2 T_1 T_2) \quad , \quad (2)$$

where ε_0 is the dielectric constant in vacuum, c the light velocity in vacuum, the transition dipole moment, T_1 the longitudinal relaxation time and T_2 the transverse relaxation time. This equation holds when the laser linewidth is sufficiently narrower than the homogeneous width, $\Gamma_h = \hbar/T_2$. When the laser linewidth Γ_l is comparable to or larger than the homogeneous width Γ_h, eq.(2) is rewritten as[14]

$$I_s = \varepsilon_0 c\hbar \Gamma_{eff}/(2|\mu|^2 T_1) \quad , \quad (3)$$

$$\Gamma_{eff} = \Gamma_h + \Gamma_l \quad .$$

Here Γ_{eff} is the effective linewidth which is the convoluted result of the homogeneous linewidth and the laser linewidth. We assumed the laser spectra to be Lorentzian for simplicity. The homogeneous width Γ_h is obtained, if I_s is

investigated as a function of Γ_1. Figure 3 shows the fitting of the experimental result of the intensity-dependent absorption coefficient by the expression $\alpha = \alpha_1/(1+I/I_s) + \alpha_2$, where α is the absorption coefficient, I is the laser intensity and α_1 and α_2 are fitting parameters. The obtained saturation density I_s is shown by arrows in Fig.3. The saturation densities thus obtained are plotted as a function of the laser linewidth I_1 in Fig.4. The saturation density increases with the increase of the laser linewidth, as expected. By fitting eq.(3) to the experimental results, we obtained the homogeneous linewidth of the Z_3 exciton in CuCl at 77K. It is 0.15 meV.

We can easily obtain the homogeneous broadening at elevated temperatures, because the phonon broadening is dominant. Reversely, we must estimate the homogeneous broadening at low temperatures by extraporating the phonon broadening contribution. The calculation based on the eq.(1) gives 0.1 meV to the homogeneous width of the Z_3 excitons at 77 K in fairly well agreement with the result of the laser saturation spectroscopy. Therefore the experiments on the temperature dependence of the linewidth supports our dicision on the homogeneous width. At low temperatures, the homogeneous width is expected to decrease much more, because the phonon broadening is reduced. Experimental demonstration that the saturation density depends on eq.(3) suggests that it decreases much more at low temperatures.

Equation (2) informs us that the transition dipole moment $|\mu|$ is determined, if we obtain I_s, $\hbar/T_2$ and T_1. The luminescence lifetime of Z_3 excitons was measured to be 610 ps at 77K under the band-to-band excitation by using the ultraviolet picosecond pulses (3.42 eV) and a synchroscan streak camera. Using the values of I_s = 4.5 $\mu J/cm^2$, $\hbar/T_2$ = 0.15 meV and T_1= 610 ps, we can obtain

the value of $|\mu|$ to be 6.3×10^{-18} esu cm (6.3 Debye) for a CuCl microcrystal. The oscillator strength f for a unit cell in bulk CuCl is 5.8×10^{-3}. This corresponds to the dipole moment of 0.40×10^{-18} esu cm (0.40 Debye), because the transition dipole moment $|\mu|$ and the oscillator strength f is related to each other by the equation, $f = 2m_0\hbar\omega(|\mu|/e\hbar)^2$, where m_0 is the electron mass and e is the electron charge. Therefore the transition dipole moment for a CuCl microcrystal is enhanced by 16. The coherent volume in a CuCl microcrystal is 250 times of the unit cell but is not extented for the whole microcrystal volume as theory expected[2,3]. In fact, the whole microcrystal is considered to be coherent, because the energy split between the first and second quantum levels in a CuCl microcrystal whose radius is 6.1 nm is 15 meV and is larger than Γ_h = 0.15 meV. We can not explain this discrepancy. We may have to measure T_1 under the resonant excitation of the Z_3 excitons.

In summary, homogeneous width of Z_3 exciton absorption spectra in CuCl microcrystals was measured by using the laser saturation spectroscopy for the first time. It was 0.15 meV at 77K for CuCl microcrystals whose mean radius is 6.1 nm. The extraporation of the temperature broadening of the Z_3 exciton absorption linewidth to 77 K also supported the result. The laser saturation spectroscopy also informed us the transition dipole moment for a CuCl microcrystal to be 16 times of that for an unit cell in bulk CuCl.

The authors would like to express their sincere thanks to Prof. E. Hanamura at the University of Tokyo for the critical reading of the manuscript and enlightening discussions. They indebted to Mr. H. Tanaka and Mr. Y. Yamada for the sample preparation and the lifetime measurement. This work was in part supported by Grant-in-Aid #63604511 for Scientific Research on Priority Areas, New Functionality Materials - Design, Preparation and Control - by the Ministry

of Education, Science and Culture of Japan.

Figure captions

Fig.1. Absorption spectra of CuCl microcrystals in NaCl at various temperatures. The mean radius of the CuCl microcrystals is 6.1 nm.

Fig.2. Temperature dependence of the linewidth of the Z_3 exciton absorption. The fitting is shown by the solid line described by eq.(1) in the text.

Fig.3. Laser intensity dependence of the absorption coefficient at the Z_3 exciton resonance at 77K. Experimental points are shown by various symbols corresponding to the laser linewidth Γ_l (meV). The least-squares fitted results are shown by solid lines.

Fig.4. The saturation density as a function of the laser linewidth. The solid line is the fitted result based on eq.(3) in the text.

References

1) A.I.Ekimov, Al.L.Efros and A.A.Onushchenko, Solid State Commun. 56, 921 (1985).

2) E.Hanamura, Solid State Commun. 62, 465 (1987).

3) E.Hanamura, Phys. Rev. B 37, 1273 (1988).

4) Y.Masumoto, M.Yamazaki and H.Sugawara, Appl. Phys. Lett. 53, 1527 (1988).

5) J.Feldmann, G.Peter, E.O.Göbel, P.Dawson, K.Moore, C.Foxon and R.J.Elliott, Phys. Rev. Lett. 59, 2337 (1987).

6) E.Hanamura, Phys. Rev. B 38, 1228 (1988).

7) E.Hanamura, To be published in Proc. of the NATO workshop on optical switching in low-dimensional systems, (Plenum, 1989).

8) T.Itoh, Y.Iwabuchi, and M.Kataoka, Phys. Status Solidi (b) 145, 567 (1988).

9) D.A.B.Miller, D.S.Chemla, D.J.Eilenberger, P.W.Smith, A.C.Gossard and W.T.Tsang, Appl. Phys. Lett. 41, 679 (1982).

10) Y.Kaifu and T.Komatsu, Phys. Status Solidi (b) 48, K125 (1971).

11) Y.Toyozawa, Progr. Theor. Phys. 27, 89 (1962).

12) in Landolt-Börnstein - Numerical Data and Functional Relationships in Science and Technology, vol.17b (Semiconductors - Physics of II-VI and I-VII Compounds, Semimagnetic Semiconductors) ed. by O. Madelung (Springer, 1982) p.255.

13) K.Shimoda, Introduction to Laser Physics (Springer, 1986) Chap.8.

14) J.Hegarty and M.D.Sturge, J. Opt. Soc. Am. B 2, 1143 (1985).

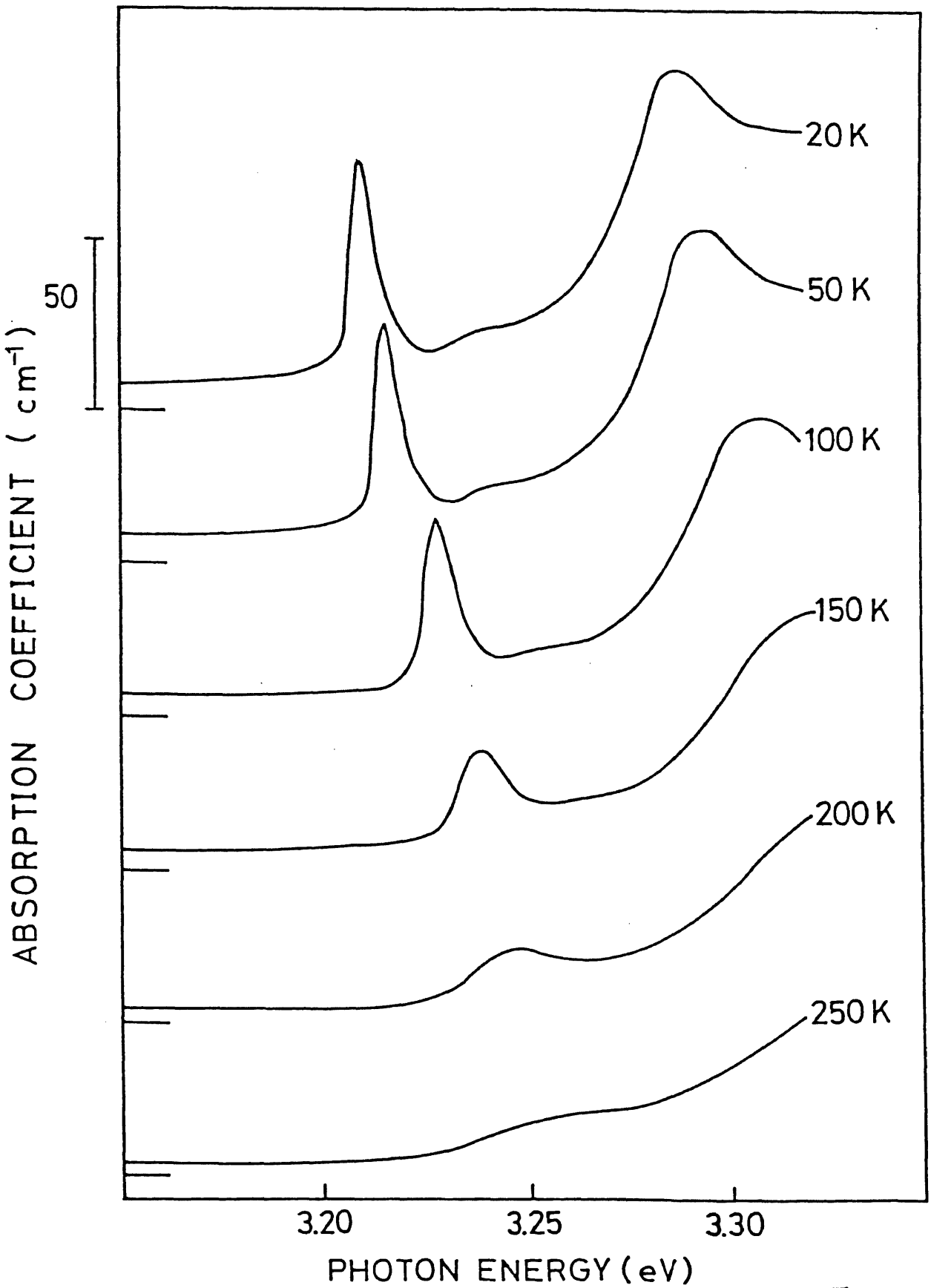
20 K
50 K
100 K
150 K
200 K
250 K
50
ABSORPTION COEFFICIENT (cm^{-1})
3.20
3.25
3.30
PHOTON ENERGY (eV)

Fig. 1

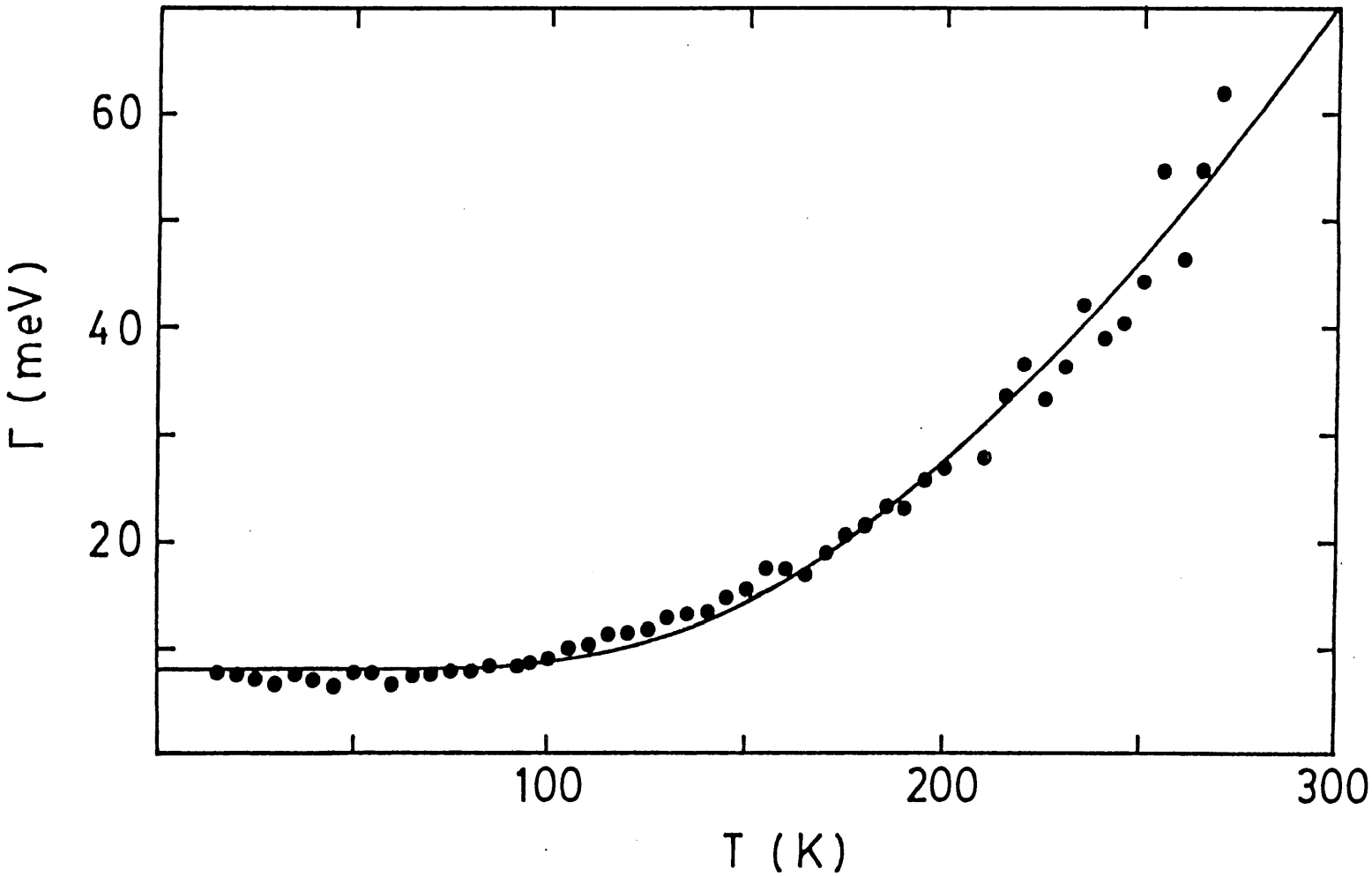

Fig. 2

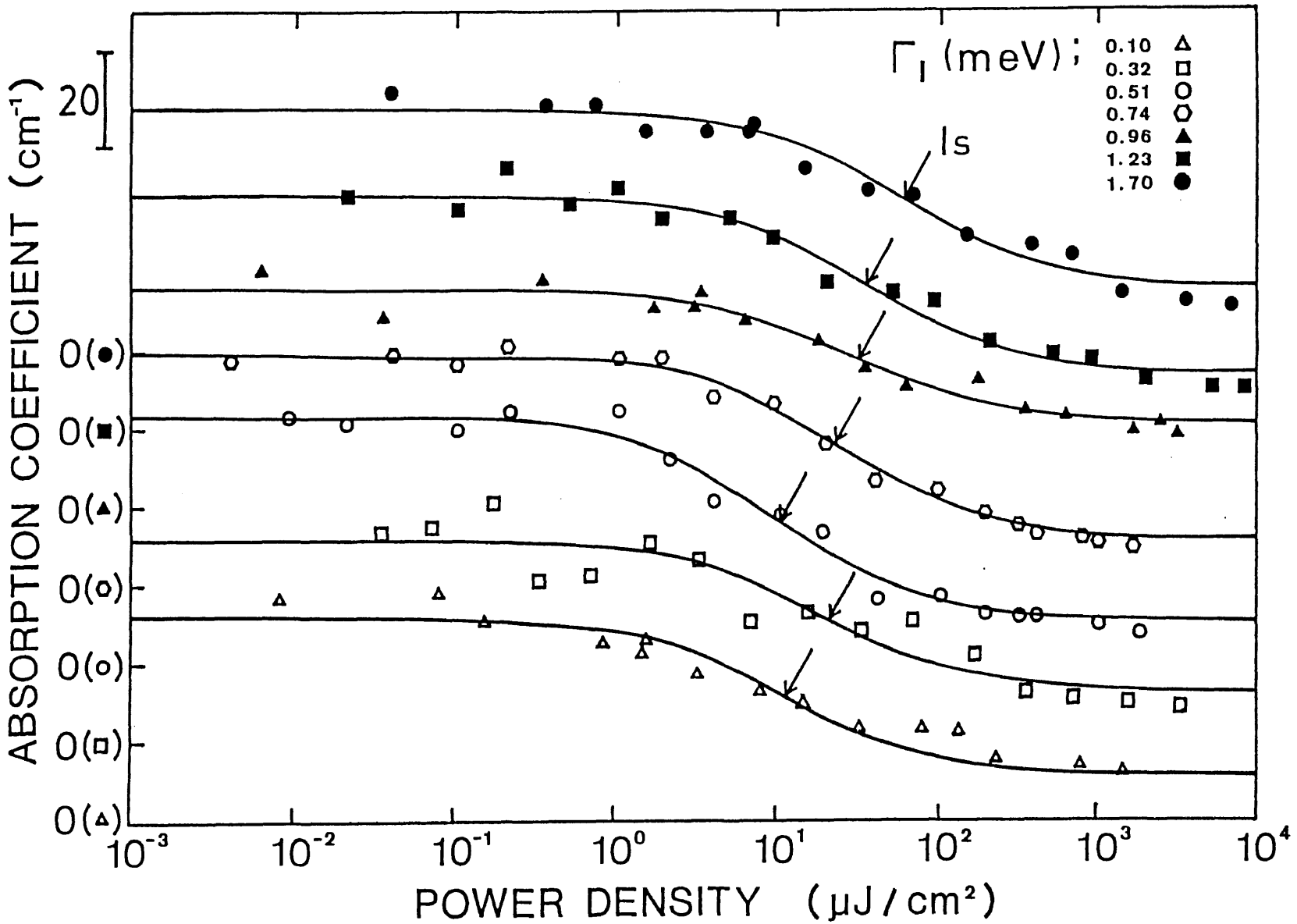
ABSORPTION COEFFICIENT (cm⁻¹)
20
0(●)
0(■)
0(▲)
0(○)
0(○)
0(□)
0(△)
Γ1 (meV);
0.10
0.32
0.51
0.74
0.96
1.23
1.70
Is
10⁻³
10⁻²
10⁻¹
10⁰
10¹
10²
10³
10⁴
POWER DENSITY (μJ/cm²)

Fig. 3

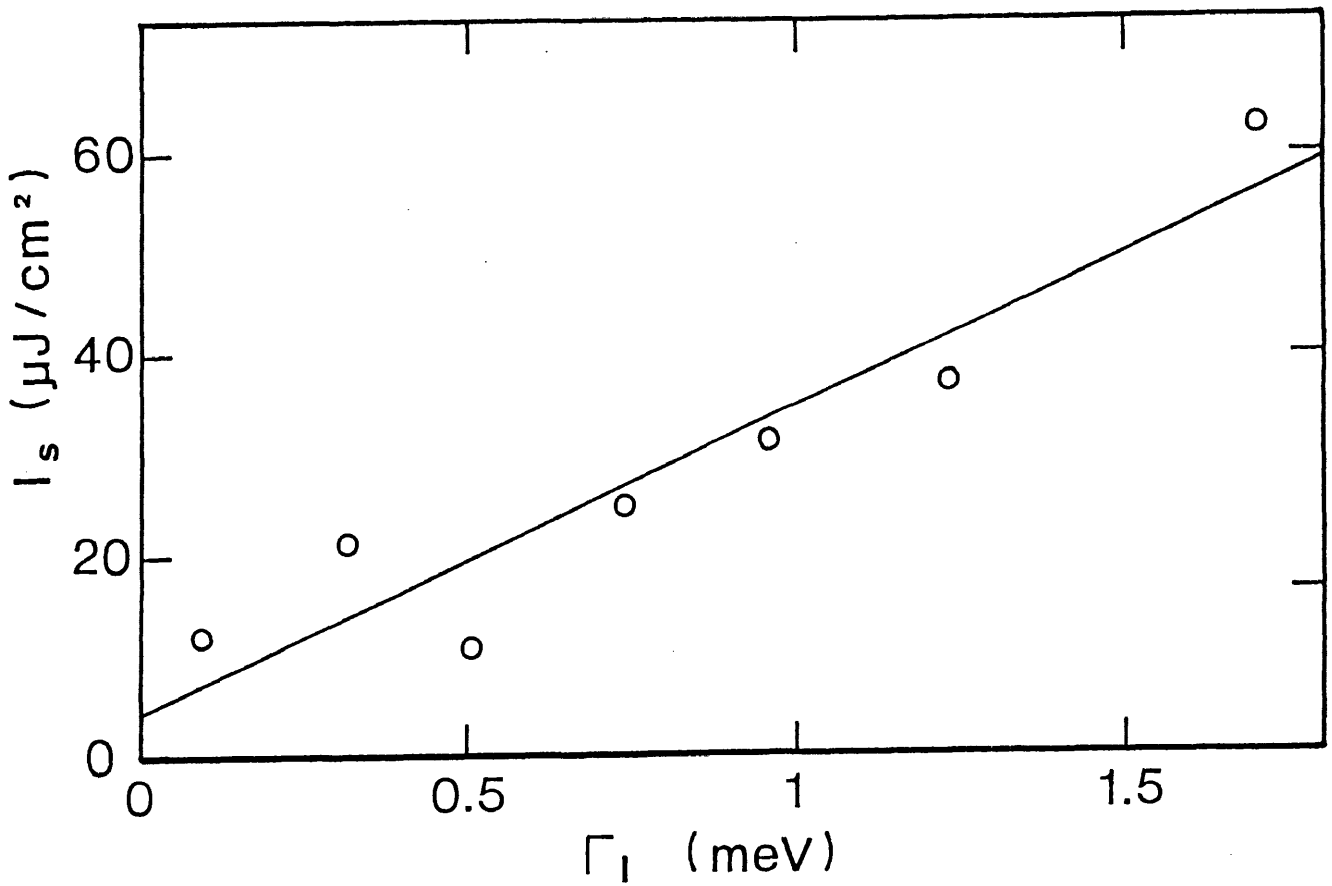

Fig. 4